University of Brasília
Department of Aerospace Engineering

Comparison of Operational Modal Analysis Methods for Aerospace Structures

By

Hugo Eduardo García Sosa

Advisor: Prof. Dr. Sergio Henrique da Silva Carneiro

A dissertation submitted to the University of Brasília in accordance with the requirements of the degree of Bachellor in Aerospace Engineering in the Faculty of Gama.

August 2024

Abstract

Structures engineered by professionals must endure various loads contingent upon operational requirements. Among these, dynamic loads like vibrations pose a significant challenge due to their potential to induce undesired behavior, leading to damage, operational impracticality, and even structural failure. Therefore, comprehending how structures respond to vibrations is paramount for ensuring integrity and safety. Operational Modal Analysis (OMA) emerges as a crucial tool in this pursuit. OMA serves as a potent technique for assessing modal parameters dictating structural dynamical behavior, encompassing natural frequencies, damping ratios, and mode shapes. The OMA process involves measuring structure responses to assumed white-noise input, generating correlation functions in the time-domain, and subsequently deriving auto-power and cross-power spectra families. What sets OMA apart from other methods like experimental modal analysis (EMA) is its utilization of real boundary conditions and operational inputs, enabling analysis without interrupting structure operations. This paper focuses on applying OMA to various structures, comparing established modal extraction methods from literature, specifically the Numerical Algorithm for Subspace Identification (N4SID), and the Stochastic Subspace Identification methods (SSI): SSI-COV and SSI-DATA. Initially, the OMA method is validated on a steel cantilever beam, where modal parameters estimated by these methods are compared with theoretical data derived from modal simulations using the Finite Element Method, ensuring the accuracy of OMA results. Subsequently, a wing from an aircraft and a drone structure are subjected to testing to estimate their modal parameters for operational safety assurance. Results indicate a good correlation between theoretical and experimental modal parameters across all tests, affirming the efficacy of the OMA approach. Overall, this paper explores the application of three OMA methods across diverse structures pertinent to the aerospace industry, aiming to unveil their dynamic characteristics.

Key-words: OMA, aerospace, modal parameters, N4SID, SSI.

Resumo

Estruturas projetadas por profissionais devem suportar diversas cargas dependendo dos requisitos operacionais. Dentre elas, cargas dinâmicas como vibrações representam um desafio significativo devido ao seu potencial de induzir comportamentos indesejados, levando a danos, impraticabilidade operacional e até mesmo falhas estruturais. Dessa forma, saber como as estruturas irão responder às vibrações é fundamental para a integridade e segurança do projeto. A Análise Modal Operacional (OMA) surge como uma ferramenta crucial nesta busca como uma técnica potente para avaliar parâmetros modais que ditam o comportamento dinâmico estrutural, abrangendo frequências naturais, taxas de amortecimento e modos de vibração. O processo OMA envolve medir as respostas da estrutura à entrada que é assumida em forma de ruído branco, para gerar funções de correlação no domínio do tempo e, subsequentemente, derivando famílias de espectros de potência automática e de potência cruzada. O que diferencia o OMA de outros métodos, como a análise modal experimental (EMA) é a utilização de condições de contorno reais e entradas operacionais, permitindo a análise sem interromper as operações da estrutura. Este artigo se concentra na aplicação da OMA a várias estruturas, comparando métodos de extração modal estabelecidos na literatura: o Algoritmo Numérico para Identificação de Subespaço (N4SID) e os Métodos de Identificação Estocástica de Subespaços (SSI): SSI-COV e SSI-DATA. Inicialmente, o método OMA é validado em uma viga cantiléver de aço, onde os parâmetros modais são estimados por estes métodos e comparados com dados teóricos derivados uma análise teórica e de simulações modais usando o método de elementos finitos (FEM) garantindo a precisão dos resultados do OMA. Posteriormente, as estruturas de um aerodesign e um drone são submetidas a testes para estimar seus parâmetros modais utilizando os métodos OMA previamente validados. Os resultados obtidos indicam uma boa correlação entre os parâmetros modais teóricos e experimentais em todos os testes, demonstrando a eficácia da abordagem OMA. No geral, este artigo explora a aplicação de três métodos OMA em diversas estruturas pertinentes à indústria aeroespacial, com o objetivo de determinar as suas características dinâmicas.

Palavras chave: OMA, aerospace, modal parameters, N4SID, SSI.

Dedication and acknowledgements

This work represents the culmination of a dream that started in 2016, when I decided that I wanted to study aerospace engineering, and as fate would have it, I had the luck of studying in the Faculty of Gama in the University of Brasilia. The journey has not always been easy, there were times in which I wanted to quit, in which I was unsure if this was really my dream, but alas with dedication and specially with the support of the people around me this dream is finally reaching a conclusion and a new chapter is about to begin.

I do not want to end this journey without acknowledging and especially thanking everyone who has helped me during these years. I want to start by acknowledging my parents, who despite knowing that this journey would have us physically separated by thousands of kilometers, never hesitated in supporting me both emotionally and financially.

To my sister, whom I admire and whose dedication and effort always inspire me to give the best of me. To my cousins, uncles and nephews who are always present in my life and who give me their support every time we have the time to talk in this fast-pacing life.

To my friends, both in home country Guatemala and in this wonderful second home called Brazil that have accompanied me during this journey and made it much brighter and special with their presence.

To my advisor, whom with his constant dedication, corrections and especially patience have helped me during this phase of the university and have helped me become a better person and a better future professional.

And finally, I would like to dedicate this work to the entire community of the Faculty of Gama, from the professors to the administrative personnel, the cleaning and the cafeteria staff and even my other colleagues who have been a fundamental part of my developing from a shy foreign student to a much more mature future engineer.

"Luck is what happens when preparation meets opportunity"

-Seneca The Younger, Roman Philosopher

DISSERTATION APPROVAL

HUGO EDUARDO GARCÍA SOSA

Comparison of Operational Modal Analysis Methods for Aerospace Structures

Dissertation submitted to the undergraduate course in *Aerospace Engineering* from the University of Brasília, as a partial requirement to obtain the Title Bachelor's degree in **Aerospace Engineering**.

Approved Work. Brasília, August 6^{th}, 2024

Prof. Dr. Sergio Henrique Carneiro da Silva
Advisor

Prof. Dr. Polliana Candida Oliveira Martins
Evaluation Panel Member

Prof. Dr. Maria Alzira de Araujo Nunes
Evaluation Panel Member

Brasília, DF 2024

TABLE OF CONTENTS

Page

List of Tables **xiii**

List of Figures **xv**

Latin Symbols **xxi**

Greek Symbols **xxiii**

Acronyms **xxv**

1 Introduction **1**

1.1 Motivation 5

1.2 Objectives 6

1.2.1 Main Objective 6

1.2.2 Specific Objectives 6

1.3 Dissertation Layout 6

2 OMA State of the Art **9**

2.1 OMA in Civil Engineering 9

2.2 OMA in Aeronautic and Aerospace Engineering 11

2.3 OMA in the Next Future 13

3 Theoretical Framework **15**

3.1 Operational Modal Analysis 15

3.2 Historical Background 16

3.3 Reasons to Use OMA 17

3.3.1 Real world operational conditions differ significantly from laboratory conditions: 17

3.3.2 Practical / Size Limitations: . . . 18
3.3.3 Ongoing Health Monitoring / Damage Detection . . . 18
3.3.4 Cost of Analysis . . . 18
3.4 OMA Main Theory . . . 19
3.4.1 OMA Techniques . . . 23
3.4.2 Techniques Used in This Work . . . 25
3.4.3 OMA Techniques Overview . . . 33
3.4.4 OMA Limitations . . . 34
3.5 EMA vs OMA . . . 35
3.6 Modal Assurance Criterion (MAC) Matrix . . . 36

4 Methodology **39**
4.1 OMA Validation . . . 39
4.1.1 Theoretical Analysis . . . 41
4.1.2 ANSYS® Modal Analysis . . . 42
4.1.3 OMA with ANSYS® Transient Simulations . . . 43
4.1.4 OMA on the Steel Cantilever Beam . . . 45
4.2 OMA on Different Structures . . . 48
4.2.1 Case Study - Aluminum Cantilever Beam **(ACB)** . . . 49
4.2.2 Case Study - Steel Free-Free Beam **(SFFB)** . . . 50
4.2.3 Case Study - Mamutes' Barbie Aerodesign **(BARBIE)** . . . 51
4.2.4 Case Study - EDRA's Hyarra Drone **(HYARRA)** . . . 53

5 Results **55**
5.1 OMA Validation . . . 55
5.1.1 Analytical Modes . . . 55
5.1.2 Simulated Modal Analysis . . . 57
5.1.3 ANSYS® TRANSIENT SIMULATIONS . . . 59
5.1.4 OMA Performed on the SCB . . . 71
5.1.5 Final Remarks of the OMA Validation Process . . . 82
5.2 OMA Tests . . . 84
5.2.1 Case Study: Aluminum Cantilever Beam (ACB) . . . 84
5.2.2 Case Study: Steel Free-Free Beam (SFFB) . . . 88
5.2.3 Case Study: Mamutes' Barbie Aerodesign (BARBIE) . . . 94
5.2.4 Case Study: Hyarra's Drone Structure (HYARRA) . . . 99

6 Conclusions **103**
6.1 Future Works . . . 105

Bibliography **107**

A Appendix A: Steel Cantilever Beam Creation **111**

B Appendix B: Impulse Simulation 4096 Hz Code **115**

C Appendix C: MATLAB® Output-Only Modal Analysis Toolbox Guide **121**
C.1 OoMA and MAC Installation . . . 121
C.2 OoMA Script and Simulation/Experiment Parameters . . . 122
C.2.1 Transient Impulse Simulation (4096 Hz) . . . 123
C.3 Output-Matrix Import . . . 123
C.3.1 Transient Impulse Simulation (4096 Hz) . . . 123
C.4 Time Signals and PSDs Plot . . . 124
C.4.1 Transient Impulse Simulation (4096 Hz) . . . 124
C.5 OMA Methods . . . 126
C.5.1 N4SID . . . 126
C.5.2 SSI-COV . . . 128
C.5.3 SSI-DATA . . . 130
C.6 Modal Assurance Criterion (MAC) . . . 131
C.6.1 Auto-MAC . . . 131
C.6.2 Cross-MAC . . . 132

D Appendix D: Siemens® Simcenter Testlab 2306® - Guide **135**
D.1 1. Initial Setting . . . 136
D.2 2. Geometry Creation . . . 137
D.3 3. Data Import . . . 140
D.4 4. Data Selection . . . 141
D.5 5. Data Validation . . . 147
D.6 6. Operational PolyMAX . . . 149
D.7 7. Cross-MAC . . . 149

E Appendix E: Complete Set of Mode Shapes **151**
E.1 MATLAB® OoMA Toolbox - Mode Shapes . . . 151
E.1.1 Impulse Simulations . . . 151

E.1.2 White Noise Simulations 156

List of Tables

Table **Page**

2.1 Comparison of natural frequencies and MAC matrices for different modes of the HCT building. 11

3.1 OMA Methods 33
3.1 OMA Methods 34
3.2 EMA vs OMA. 35

4.1 SCB Parameters 40
4.2 ACB parameters used. 49

5.1 Analytical Bending Modes of the SCB 56
5.2 ANSYS® Modal Parameters 57
5.3 f_n Differences between Analytical and Simulated Modal Analysis 59
5.4 Modal parameters for the Impulse Transient Simulations obtained with the MATLAB® OoMA Toolbox. 60
5.5 Analytical vs Impulse Transient Simulations MATLAB OoMA Toolbox Modal Parameters 61
5.5 Analytical vs Impulse Transient Simulations MATLAB OoMA Toolbox Modal Parameters 62
5.6 Aliasing Effect in Natural Frequency - Impulse Simulations 62
5.7 Modal parameters for the White Noise Transient Simulation obtained with MATLAB® OoMA Toolbox. 65
5.7 Modal parameters for the White Noise Transient Simulation obtained with MATLAB® OoMA Toolbox. 66
5.8 Analytical vs White Noise Transient Simulations in MATLAB OoMA Toolbox Modal Parameters 66

5.8 Analytical vs White Noise Transient Simulations in MATLAB OoMA Toolbox Modal Parameters 67
5.9 Aliasing Effect in the White Noise Transient Simulations 67
5.10 Modal Parameters obtained from the Transient Simulations with SIEMENS Simcenter Testlab 2306 70
5.11 Modal parameters from the OMA test performed on the SCB in 14/05/2024. . 72
5.12 Modal parameters from the OMA test performed on the SCB in 12/06/2024 in the 1st run and 1st filtering process. 74
5.13 Modal parameters from the OMA test performed on the SCB in 12/06/2024 in the 1st run and 2nd filtering process. 76
5.14 Modal parameters from the OMA test performed on the SCB in 12/06/2024 in the 2nd run and 1st filtering process. 78
5.15 Modal parameters from the OMA test performed on the SCB in 12/06/2024 in the 2nd run and 2nd filtering process. 80
5.16 OMA validation process results comparison. 83
5.17 Aluminum cantilever beam properties. 84
5.18 ACB - Analytical Modal Parameters 85
5.19 ACB - OMA Modal Parameters 86
5.20 SFFB - Analytical Modal Parameters 89
5.21 SFFB Test - OMA Modal Parameters 91
5.22 Mamutes' Barbie Aerodesign - Modal parameters 94
5.23 EDRA's Hyarra Drone - Modal Parameters with Simcenter and Op. PolyMAX 100

List of Figures

Figure **Page**

1.1 The Millennium Bridge at the City of London. 2
1.2 Stonecutters Bridge in Hong Kong, China 4
1.3 Dissertation Layout 7

2.1 Bridges with continuous dynamic monitoring systems. 10
2.2 HCT Building Model 11
2.3 COSDYNA control surface being tested and the accelerometers placement. . 12
2.4 Mode found during the COSDYNA-OMA test using the narrow-band technique. 12
2.5 VEGA 13
2.6 OMA performed on a container vessel. 14

3.1 Gaussian white noise assumption needed for OMA 20
3.2 Autocorrelation Function (ACF) Process 21
3.3 EMA vs OMA Summary. 36
3.4 MAC matrices comparison. 37

4.1 Steel Cantilever Model (SCB) used for the OMA validation. 40
4.2 OMA Validation Process 41
4.3 Beam Element Model (BEM) of the SCB 43
4.4 Example of a Response Matrix $\mathbf{Y}$ in Excel® 44
4.5 Geometry of the SCB created on Siemens® Simcenter Testlab 2306. 45
4.6 SCB Measurement points 46
4.7 OMA Acquisition Equipment 46
4.8 OMA Test Performed on the SCB 47
4.9 OMA Tests on Different Structures 48
4.10 Aluminum Cantilever Beam (ACB) 49
4.11 Steel Free-Free Beam 50

4.12 Mamutes' Barbie AeroDesign 51
4.13 Barbie boundary conditions. 52
4.14 EDRA's Structure 53
4.15 OMA testing of the EDRA's Hyarra Drone. 54

5.1 Analytical Mode Shapes 56
5.1 Analytical Mode Shapes 57
5.2 ANSYS® Bending Mode Shapes. 58
5.3 Aliasing effect in PSD for the Impulse Simulations. 63
5.4 Impulse Transient Simulations Mode Shapes - MATLAB OoMA Toolbox . . . 63
5.4 Impulse Transient Simulations Mode Shapes - MATLAB OoMA Toolbox . . . 64
5.5 Alasing effect in the PSD for the White Noise Simulations. 68
5.6 White Noise Transient Simulations Mode Shapes - MATLAB OoMA Toolbox. 68
5.6 White Noise Transient Simulations Mode Shapes - MATLAB OoMA Toolbox. 69
5.7 SIEMENS Simcenter Testlab - Impulse Simulation 8192 Hz - Mode Shapes. . 71
5.8 SIEMENS Simcenter Testlab - **White Noise** Simulation 8192 Hz - Mode Shapes. 71
5.9 SCB Test 14/05/2024 - Mode Shapes obtained with the OoMA Toolbox. 73
5.10 SCB Test 14/05/2024 - Mode Shapes obtained with the OoMA Toolbox. 73
5.11 SCB Test 12/06/2024 Run 1 Filter 1 - Mode Shapes obtained with the OoMA Toolbox. 75
5.12 SCB Test 12/06/2024 Run 1 Filter 1 - Mode Shapes obtained with the OoMA Toolbox. 75
5.12 SCB Test 12/06/2024 Run 1 Filter 1 - Mode Shapes obtained with the Simcenter Testlab 2306. 76
5.13 SCB Test 12/06/2024 Run 1 Filter 2 - Mode Shapes obtained with the OoMA Toolbox. 77
5.14 SCB Test 12/06/2024 Run 1 Filter 2 - Mode Shapes obtained with Simcenter Testlab 2306. 77
5.14 SCB Test 12/06/2024 Run 1 Filter 2 - Mode Shapes obtained with Simcenter Testlab 2306. 78
5.15 SCB Test 12/06/2024 Run 2 Filter 1 - Mode Shapes obtained with the OoMA Toolbox. 79
5.16 SCB Test 12/06/2024 Run 2 Filter 1 - Mode Shapes obtained with Simcenter Testlab 2306. 79

5.16 SCB Test 12/06/2024 Run 2 Filter 1 - Mode Shapes obtained with Simcenter Testlab 2306. 80
5.17 SCB Test 12/06/2024 Run 2 Filter 2 - Mode Shapes obtained with the OoMA Toolbox. 81
5.18 SCB Test 12/06/2024 Run 2 Filter 2 - Mode Shapes obtained with Simcenter Testlab 2306. 81
5.18 SCB Test 12/06/2024 Run 2 Filter 2 - Mode Shapes obtained with Simcenter Testlab 2306. 82
5.19 Aluminum Cantilever Beam - Analytical Mode Shapes 85
5.20 Mode shapes of the ACB obtained with the OoMA Toolbox. 87
5.21 Mode shapes of the ACB obtained with the Simcenter Testlab 2306 software. 87
5.21 Mode shapes of the ACB obtained with the Simcenter Testlab 2306 software. 88
5.22 SFFB - Analytical mode shapes. 89
5.22 SFFB - Analytical mode shapes. 90
5.23 SFFB - Geometry created in Simcenter Testlab 2306 90
5.24 SFFB - Mode shapes obtained with the OoMA Toolbox. 91
5.25 SFFB Mode shapes obtained with the Simcenter Testlab 2306 software. . . . 92
5.26 SFFB - MAC Matrices 93
5.27 Mode shapes obtained from the simulated modal analysis of the Barbie aerodesign provided by the team. Source: Mamutes do Cerrado Aerodesign 96
5.28 Barbie Mode Shapes obtained with Simcenter Testlab 2306 - OMA Analysis . 96
5.28 Barbie mode shapes obtained with Simcenter Testlab 2306 software with the OMA and Operational PolyMAX add-ins. 97
5.29 Barbie - OMA analysis Auto-MAC 97
5.30 Barbie - Operational PolyMAX analysis Auto-MAC 98
5.31 Barbie Cross-Power Spectra 99
5.32 Mode shapes from the simulated modal analysis of the EDRA's Hyarra drone structure provided by the team. Source: Equipe de Robótica Aérea - EDRA . . 101
5.33 Hyarra mode shapes obtained with Simcenter Testlab 2306 software. 101
5.34 Hyarra mode shapes obtained with Simcenter Testlab 2306 software. 102

A.1 SCB technical drawings. 112
A.2 SCB components. 112
A.3 The creation of the main channel was the most complicated part of the manufacturing process as a mistake in this stage would have caused the entire main plate to be unusable. 113

A.4 In the second part of the work both EMA and OMA will be performed on the beam to asses the accuracy of the OMA methods. 113

C.1 OoMA Toolbox download page 122
C.2 Response Matrix 124
C.2 Response Matrix 124
C.3 Time Signals and PSD Functions from the Impulse 4096 Hz simulation. . . . 126
C.4 Impulse Simulation 4096 Hz Mode Shapes obtained with the N4SID method. 127
C.5 The natural frequencies and damping ratios obtained with the N4SID method can be found in the workspace environment under the names fn_n4 and $zeta\_n4$ from which the values can be extracted. 128
C.6 In the stabilization diagram for the SSI-COV method in, it is possible to see that a model order of 14 is the minimal that yields a row with a stable pole in each one of the suspected modes of the system. 129
C.7 SSI-COV mode shapes obtained for the Impulse Simulation 4096 Hz. 130
C.8 The modal parameter values can be accessed in the same way done for the N4SID method. The only difference is that in the SSI-COV method it will be necessary to find the vector that corresponds to the minimal model order found. 131
C.9 Auto-MACs created for *Impulse Simulation 4096 Hz*. 132
C.10 Cross-MACs created for the *Impulse Simulation 4096 Hz*. 133

D.1 Simcenter Testlab 2306® *Navigator* window. 136
D.2 Add-Ins configuration. 136
D.3 Geometry creation - Components 137
D.4 Geometry creation - Nodes 138
D.5 Geometry creation - Lines 138
D.6 Geometry creation - Surface Creation 139
D.7 Geometry creation - Component color 139
D.8 Data Import - Select Block 140
D.9 Data Import - Data Block Editor 140
D.10 Data Import - Time-signal imported 141
D.11 Input Basket Transfer 142
D.12 Operational Data Collection 143
D.13 Operational Data Selection 143
D.14 Op. Time MDOF - Frequency band selection. 144
D.15 Op. Time MDOF - Stabilization diagram. 145

D.16 Op. Time MDOF - Stabilization diagram pole selection. 145
D.17 Op. Time MDOF - Modal parameters verification. 146
D.18 Curve adjustment. 147
D.19 OMA validation window. 147
D.20 OMA validation visualization options. 148
D.21 OMA validation mode shapes display. 148
D.22 Operational PolyMAX Analysis. 149
D.23 Cross-MAC analysis. 150

E.1 Impulse Simulations 1024 Hz - Mode Shapes 151
E.1 Impulse Simulations 1024 Hz - Mode Shapes 152
E.2 Impulse Simulations 2048 Hz - Mode Shapes 152
E.2 Impulse Simulations 2048 Hz - Mode Shapes 153
E.3 Impulse Simulations 4096 Hz - Mode Shapes 153
E.3 Impulse Simulations 4096 Hz - Mode Shapes 154
E.4 Impulse Simulations 8192 Hz - Mode Shapes 154
E.4 Impulse Simulations 8192 Hz - Mode Shapes 155
E.5 White Noise 1024 Hz - Mode Shapes 156
E.6 White Noise 2048 Hz - Mode Shapes 157
E.7 White Noise 4096 Hz - Mode Shapes 158
E.8 White Noise 8192 Hz - Mode Shapes 159

LATIN SYMBOLS

A,B,C	State space matrices.
A_c	System matrix in continuous time.
A_d	System matrix in discrete time.
f(t)	Force vector.
$[G_{xx}(j\omega)$]	PSD matrix of the input.
$[G_{yy}(j\omega)$]	PSD matrix of the output.
$H(j\omega)$	Frequency response function (FRF) matrix.
Hz	Hertz.
N	Number of data points.
M	Number of measurement channels.
M,D,K	Mass, damping and stiffness matrices.
O	Projection matrix.
R_k	Covariance matrix at time lag k.
$\mathbf{U}_i$	Eigenvectors of $[G_{yy}(j\omega)]$
X_0	Kalman State matrix.
x(t)	State vector.
Y	System response matrix.
Y_h	Block Hankel matrix.

Y_{hp},Y_{hf} Past and future half part of Block Hankel matrix.

y_k System response in discrete time.

y(t) System response in continuous time.

Greek Symbols

Γ_s Observability matrix.

$[\lambda_i$,$\Phi]$ Poles and eigenvectors of 2^{nd} order differential equation.

$[\mu_i$,$\Psi]$ Poles and eigenvectors of discrete system matrix.

ζ Damping ratio.

ω Angular frequency in rad/s.

φ Mode shapes.

ω_n Natural frequency in rad/s.

Acronyms

ACB	Aluminum Cantilever Beam
ACF	Auto-Correlation Function
AVT	Ambient Vibration Test
BEM	Beam Element Model
CCF	Cross-Correlation Test
COSDYNA	Control Surface Dynamics Project
DFT	Discrete Fourier Transform
DLR	German Aerospace Center
EFDD	Enhanced Frequency Domain Decomposition
EMA	Experimental Modal Analysis
FDD	Frequency Domain Decomposition
FEM	Finite Element Model
FFT	Fast Fourier Transform
FRF	Frequency Response Function
FVT	Forced Vibration Test
GVT	Ground Vibration Test
IFT	Inverse Fourier Transform
IOMAC	International Operational Modal Analysis Conference

MAC	Modal Assurance Criterion
MDOF	Multiple-Degree-Of-Freedom
N4SID	Numerical Algorithms for Subspace Identification
OMA	Operational Modal Analysis
OMAX	Combined Experimental-Operational Modal Analysis
ONERA	French Aeronautics, Space and Defense Research Lab
OoMA	Output-Only Modal Analysis
PP	Peak Picking
PSD	Power Spectra Density
SCB	Steel Cantilever Beam
SDOF	Single-Degree-Of-Freedom
SFFB	Steel Free-Free Beam
SHM	Structural Health Monitoring
SSI	Stochastic Subspace Identification
SVD	Singular Value Decomposition
TDD	Time Domain Decomposition
VEGA	European Vector of Advanced Generation

CHAPTER 1

INTRODUCTION

On June 10th, 2000, the City of London opened to the public a new footbridge crossing the river Thames linking Bankside with the City of London, the bridge is officially named the London Millennium Footbridge but is mostly simply known as the Millennium Bridge and is one of the most famous bridges in the world (fig. 1.1). However, only two days after its initial opening, the bridge was forced to close due to an extremely worrying wobbling movement whenever pedestrians crossed it. This wobbling movement concerned engineers who, altogether with city officials, decided to close the bridge for safety reasons. In the posterior days after the closure, the engineers of the bridge tried some minor modifications to alleviate the movements suffered by the bridge, but after only another couple of days it was obvious that the problem was far more complex than originally expected. This attracted the attention of engineers and physicists around the world that were curious about why the bridge behaved in that way.

Research conducted by an inter-university team, which included an experimental modal analysis (EMA) of the whole structure, concluded that the reason for the wobbling movement that the bridge experienced was caused by a type of resonance called synchronous lateral excitation, created by the pedestrians when they crossed the bridge as they, unknowingly, walked with a lateral frequency (≈0,9 Hz) very close to the natural frequency of the bridge (≈0,8 Hz) (Manchester, 2018). Finally, in 2002 and after further research and modifications to the bridge, which included the installation of new tuned dampeners, the bridge reopened to the public. But one question remained, how did the engineers that designed the bridge fail to anticipate this phenomenon? To answer this

Figure 1.1: The Millennium Bridge at the City of London. Source: New Civil Engineer, available at: https://www.newcivilengineer.com/latest/new-study-uncovers-real-reason-behind-millennium-bridge-wobble-15-12-2021/

question, it is necessary to better understand some basic principles about the dynamics to which the bridge, and other structures, are subjected to.

When designing a bridge, or any structure, it is very important to determine the type of loads to which it will be subjected. These loads can be of a great variety of natures, but two usually are the most present: static loads, like weight, and dynamic loads that can vary in repetitive or random motion like wind hitting the structure. In the case of the Millennium Bridge considerations for people crossing the street and interactions with the wind were of concern.

However, if engineers knew that people crossing the bridge would influence the structure, why did the bridge still undergo the wobbling movement? The answer lies in the fact that real life structures vary from models created by engineers and that the operational conditions of the bridge were not completely anticipated.

In general, every structure in the world will suffer from some sort of motion, wanted or unwanted, and will react to it. According to (AVITABILE, 2018) from the University of Massachusetts, these wanted or unwanted excitations to which structures of all kinds are subjected when in operation are called operational conditions. These operational conditions can be caused by the structures themselves, like the vibration on the structure of a car caused by its engine, or could come from external sources, like the movement

caused on a building due to an earthquake. These operating conditions need to be very well understood, as they could cause reactions in the structure that may not be acceptable for their intended purpose. This doesn't necessarily mean that they could damage or destroy the structure, but rather are just not suitable for its purpose. In the case of the Millennium Bridge, the wobbling movement caused by pedestrians didn't compromise the structural integrity of the bridge, but the lateral movement was uncomfortable for anyone crossing it and raised safety concerns, so it was not acceptable at all.

With all this known, then the next question to be asked is how it is possible then to understand the behavior of structures when subjected to dynamic loads? The answer relies on two disciplines: structural dynamics and modal analysis. For the purposes of this work, only modal analysis will be discussed. Modal analysis is, according to Avitabile (2018) a technique used to determine the dynamic characteristics of a structure independent from loads applied. To put it in simple terms, it is a technique used to determine how a structure will react when excited by any given force in terms of its dynamic characteristics: its natural frequency, damping ratio, and mode shapes.

There are two main techniques for achieving this, Experimental Modal Analysis (EMA) and Operational Modal Analysis (OMA). EMA is a highly controlled technique in which both the input force and the reactions of the structure are measured. From there, a mathematical model of the structure is constructed to determine its dynamic characteristics. This is the most used method as it is the oldest one, simple to understand and very reliable, but despite this, it won't always be the best solution when analyzing a structure. There are times at which conducting an EMA will not be possible, this could be due to size limitations as sometimes structures are too big to fit into a laboratory or the impossibility of recreating realistic excitation forces. Additionally, to perform an EMA, it is necessary to stop the operation of the structure being analyzed, and the costs to perform the tests are sometimes too expensive to be carried by small businesses.

Therefore, OMA is an alternative solution. OMA, as its name implies, is a modal technique that is conducted with the structure being analyzed in its operational conditions, this means that the structure of interest is already in the place where it will be installed and will be subjected to the expected operational conditions or "real conditions".

Due to these factors, OMA has been of great interest to civil engineering, in which it has been consolidated. Civil engineering structures tend to be too large to perform an EMA adequately, and whenever an EMA is performed it means that the structure will have to be shut down until the EMA is concluded, which in addition with the cost of the shakers used to excite the structure being analyzed, performing an EMA can become

very expensive. However, installing a series of accelerators across the structure and using the natural excitations to which the structure is subjected to in its daily operation is a much cheaper and faster option. Additionally, OMA techniques are also useful for the dynamic monitoring of the structures, which according to (MAGALHãES, 2010) has led to the installation of accelerometers in several civil engineering structures like the Stonecutters Bridge in Hong Kong seen in figure 1.2, which has 58 accelerometers to constantly monitor the dynamic behavior of the bridge.

Figure 1.2: The Stonecutters Bridge in Hong Kong. Source: Research Gate, available at: https://www.researchgate.netpublication/335228501 _Flexural_analysis_and_design_of_stainless_steel _reinforced_concrete_beams/figures?lo=1

However, in recent years there has been an increasing interest in OMA in aerospace and aeronautic engineering. In the aerospace engineering for example trying to perform an EMA in a rocket would be practically impossible due to size limitations and recreation of the excitation conditions, however installing a series of accelerometers in the rocket structure to perform an OMA is a much more feasible task. Additionally, in recent years there has been an interest in the aeronautic industry to automatize the OMA process for in-flight real-time data, allowing the engineers to better understand the aircraft structural response to the several flying conditions that can occur during a flight, and to monitor the integrity of the structure as OMA allows for the implementation of structural health monitoring (SHM) techniques.

Although both EMA and OMA are modal techniques which aim to obtain the same results, the ideal would be to perform both in combination to finite element models (FEM) to confirm that the data being obtained is accurate. Both EMA and OMA have their own

advantages and disadvantages, so it is necessary for any engineer to understand both when deciding which one to choose when, due to limitations of time or money, it is not possible to apply both. This dissertation will focus on OMA, describing the underlying theory behind it, its advantages, disadvantages and when to use it.

As it is the first time this technique is being applied using the Siemens® software Simcenter Testlab 2306®, in the University of Brasilia, this work will be divided into two main parts, the first one to validate the OMA process and results obtained through this software using a steel cantilever beam as the structure for analysis, due to the simplicity of its geometry and the well consolidated theory behind its dynamic behavior. And the second part of this work will be dedicated to the application of the OMA techniques to different structures to asses their dynamic characteristics.

1.1 Motivation

As part of the tasks in the EDRA's competition team, one of the most important parts of any project for a competition is the design and construction of the drone structure. This process can take up to several months to complete, due to the immense number of requirements from each individual competition and the requirements from other areas of the team. Modal analysis is one key element during this process as it is necessary to guarantee that the structure of the drone will not enter in resonance during operation, causing it to become unstable and in the worst-case scenario, causing it to crash due to the uncontrollable vibration.

However, although in recent years efforts have been made to make this modal analysis in a more representative way, substantial differences between the model simulated and the actual drone always exist, due to the presence of electronic components, fastening mechanism and manufacturing defects. This way, the best way of obtaining the modal parameters from the drone itself would be to perform the modal analysis during the operation of the drone itself, in other words, through an operational modal analysis (OMA) as it is the only way of guarantee that the excitation forces and boundary conditions will be trustworthy.

As such, this work serves as a first approach to OMA in which the theory behind this modal analysis technique and different OMA methodologies will be explored with the objective of assessing the modal parameters from the EDRA's drone structure, as well as from other structures of interest to the aerospace and aeronautics industries, such as the Mamutes' Barbie Aerodesign. Afterwards, evaluations of the results and

recommendations for future works will be presented to guarantee that this technique can be correctly implemented in future works, allowing for a more diversified repertoire of modal analysis techniques available at the University of Brasilia.

1.2 Objectives

1.2.1 Main Objective

Apply various Operational Modal Analysis (OMA) techniques to assess the modal parameters of structures relevant to the aerospace and aeronautic industries. First on a steel cantilever beam (SCB) to validate the methodology followed during the work, afterwards the OMA analysis would be performed on an aero model and a drone structure through a series of tests using the MATLAB® OoMA Toolbox and Siemens® Simcenter Testlab® 2306 software.

1.2.2 Specific Objectives

1. Evaluate the software Output-Only Modal Analysis (OoMA) Toolbox using the OMA techniques N4SID, SSI-COV and SSI-DATA through a series of tests performed on a steel cantilever beam system to guarantee that the methodology followed yielded good results for the OMA techniques.

2. Evaluate the results from the OMA and Operational PolyMAX add-ins from the Siemens® Simcenter Testlab 2306® software through a series of tests performed on a model of a steel cantilever beam, an aero-design and a drone structure.

3. Document all relevant data about the use of all the OMA techniques and software applied during this work, relating the problems found during the test, possible solutions and recommendations for future works.

1.3 Dissertation Layout

This dissertation starts introducing the concept of Operational Modal Analysis (OMA) giving a brief historical background as to when OMA started being developed. Afterwards it delves into the basic theory behind OMA, showing some of the more commonly used methods, making emphasis into the methods used in this work.

Then it describes the methodology followed for this work, which is divided into two main parts. The first part consists of the validation of the OMA process, through simulations and experimentation with a steel cantilever beam (SCB) system to guarantee fidelity in the results; and the second part consists in the implementation of the OMA process in more complex structures, being the EDRA's drone Hyarra and the Mamutes' aerodesign Barbie.

Afterward, the results from all the tests are presented and evaluated, giving detailed explanations of the modal parameters obtained for natural frequencies, damping ratios and mode shapes obtained. Finally, the conclusions are presented in which a final review of the results is made altogether with recommendations for future works. A complete layout can be seen below in figure 1.3.

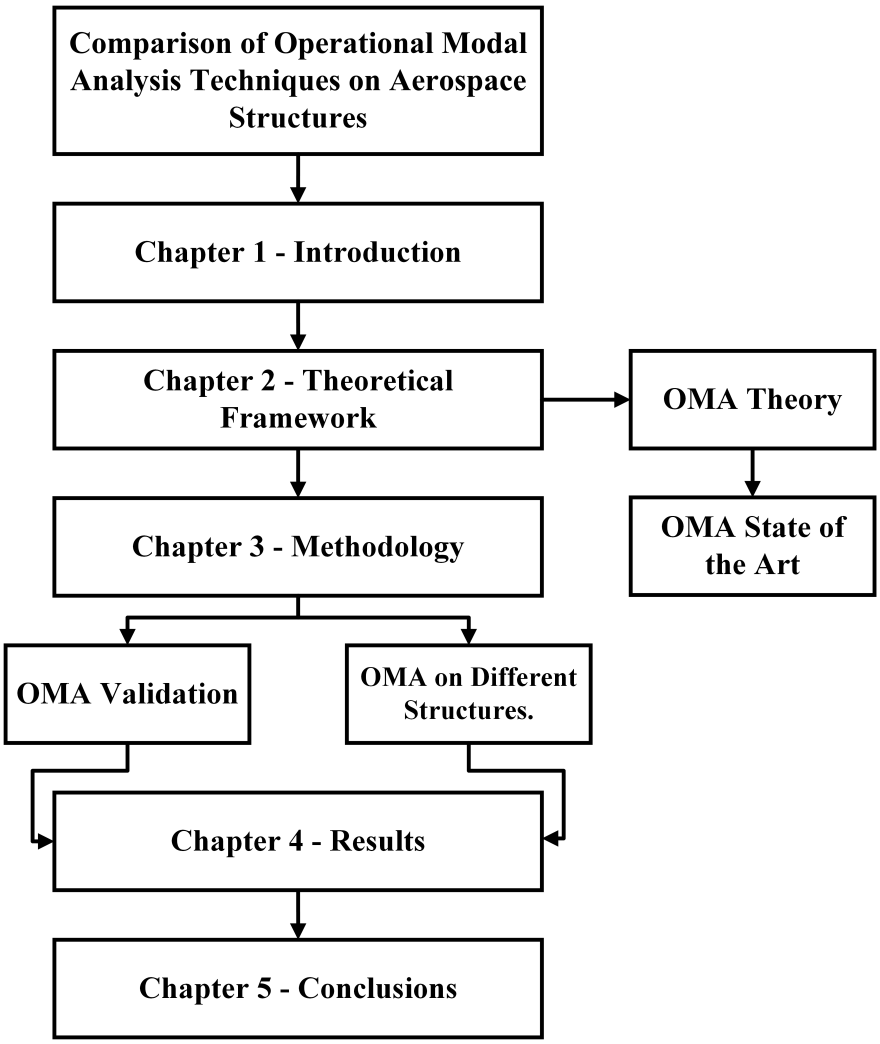

Figure 1.3: Dissertation Layout

CHAPTER 2

OMA State of the Art

Despite being considerably younger than its sibling (EMA), OMA has established itself as a reliable technique to study the dynamic characteristics of all kinds of structures, varying from small equipments like computers to massive ones like bridges.

According to (BRINCKER; VENTURA, 2015) part of the reasons why OMA has gained so much popularity in recent years is that it can be used for all applications in which EMA is commonly used with the addition of a new range of applications in which EMA can hardly compete with OMA. This new range of applications include the continuous monitoring of structures, estimation of loads, vibration levels and fatigue, etc.

2.1 OMA in Civil Engineering

The main area in which OMA has been consolidated is in civil engineering, due to the fact that more often than not, civil engineering structures are too big to be properly studied using the traditional EMA techniques. Furthermore, performing an EMA would require the structures to be closed during the analysis, it would require very big and expensive equipment to perform the *forced vibration tests - FVT* and there is not a possibility of continuous monitoring of the structure.

On the contrary, OMA suits civil engineering structures extremely well as it doesn't require the structures to be shot down for the analysis, on the contrary, it takes advantage of the excitations produced during the operation of the structure itself. Measurement

(a) Oresund Bridge in Denmark, with 22 tri-axial accelerometers.

(b) Samcheonpo Bridge in South Korea with 50 accelerom-eters.

(c) Stonecutters Bridge in Hong Kong (China) with 58 accelerometers im-bued in the structure.

Figure 2.1: Bridges with continuous dynamic monitoring systems.

equipments for OMA are also relatively cheap when compared to EMA equipments and in recent years, improvements in both the equipments and techniques had allowed engineers to perform OMA while also implementing a continuous monitoring of the structures being analyzed.

According to (MAGALHãES, 2010) an example of the continuous monitoring of civil engineering structures through the use of OMA techniques can be seen in the Oresund Bridge in Denmark, the Samcheonpo Bridge in Korea and the Sontecutters Bridge in Hong Kong as seen in figure 2.1, where a series of accelerometers were installed in the bridges for a continuous monitoring of their dynamic characteristics over time.

Other form in which OMA has been used in civil engineering is in the validation of FEM models from structures already built, such as the case of the HCT building presented by (BRINCKER; VENTURA, 2015). For this building, a FEM was created using the theoretical data available from the building plans and the modal parameters were extracted through a simulated modal analysis.

However, after performing an OMA on the building, it was possible to discover that the modal parameters were slightly different from those calculated in the simulations. After performing multiple OMAs and confirming that the values were consistent in every test, the engineers were able to confirm that these were the actual modal parameters from the building, which allowed them to update the FEM model, as seen in figure 2.2 and table 2.1.

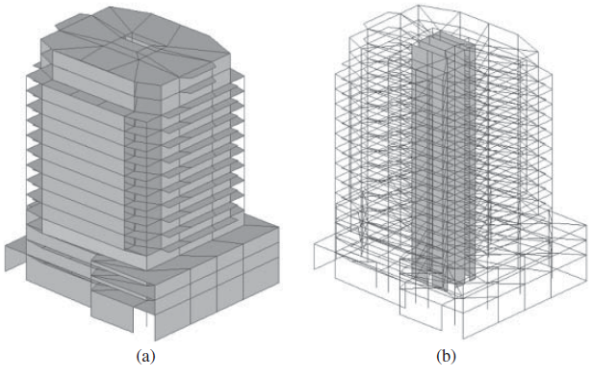

Source: (BRINCKER; VENTURA, 2015)

Figure 2.2: HCT building model. (a) Complete Model. (b) Details of the Model.

Table 2.1: Comparison of natural frequencies and MAC matrices for different modes of the HCT building.

Mode No.	OMA		FEM before		FEM updated
	Frequency (Hz)	Frequency (Hz)	MAC (%)	Frequency (Hz)	MAC (%)
1	1.23	1.33	79	1.20	83
2	1.27	1.74	60	1.40	82
3	1.44	2.07	57	1.63	85
4	3.87	4.08	79	3.88	84
5	4.25	4.38	55	4.25	73
6	5.35	5.66	64	5.62	81

Source: (BRINCKER; VENTURA, 2015)

2.2 OMA in Aeronautic and Aerospace Engineering

In aeronautics, OMA is a tool used to assess the modal parameters of new or modified aircraft with the advantage of doing so using actual in-flight data. Traditionally, as part of the airworthiness certification process that aircraft must endure, a Ground Vibration Test (GVT) needs to be performed by engineers to assess the modal parameters from the aircraft structure. However, these tests use artificial excitations to do so, which limits the type of loads that can be applied in the aircraft structure, with the addition of the impact that the boundary conditions may have on the results obtained.

On the other hand, OMA allows engineers to measure the response on the aircraft during in-flight operation, allowing to calculate the modal parameters form the aircraft taking into consideration all the aerodynamic effects that the airplane suffer and that are

not possible to recreate during the GVT, which in recent years have become even more important as the incidence of clear-weather turbulence have been steadily increasing during the last 40 years.

In addition to the GVT, other test required for the airworthiness certifications is the wind-tunnel test, in which models of the aircraft being studied or specific components are put in a wind tunnel, recreating different flying and atmospheric conditions to study the aero-dynamic effects on the structure. As presented by (ZHANG et al., 2024), an OMA was simultaneously performed during one of these tests, specifically during the Control-Surface Dynamics (COSDYNA) project (fig. 2.3), performed jointly by the German Aerospace Center (DLR) and the French aeronautics, Space and Defense Research Lab (ONERA) which had the purpose of investigating the aeroelastic impact of the control-surface to relevant unsteady air loads of an aircraft wing.

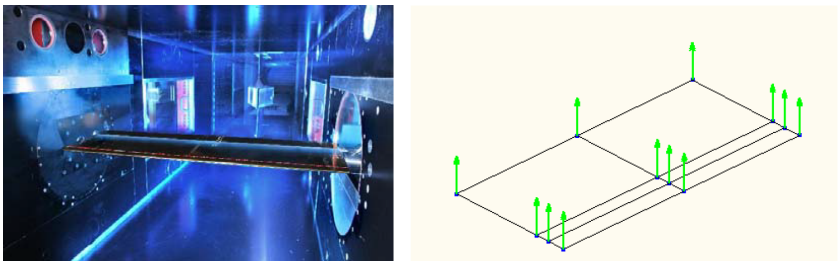

Source: (ZHANG et al., 2024)

Figure 2.3: COSDYNA control surface being tested and the accelerometers placement.

During the test OMA allowed to not only calculate the modal frequency and damping ratios of the structure itself, but also the aerodynamic stiffness and aerodynamic damping coming from the airflow, aiding the team during its research, and further proving the adaptability and usefulness of the technique. One of the modes found during this test can be seen below in figure 2.4.

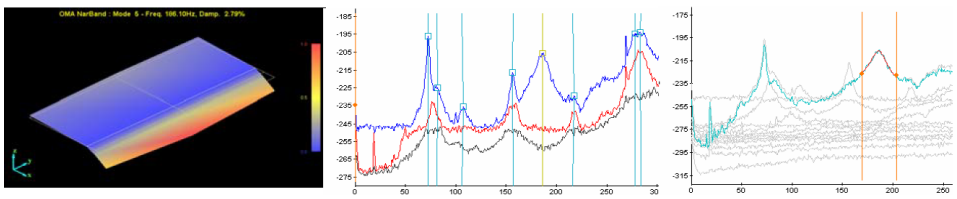

Source: (ZHANG et al., 2024)

Figure 2.4: Mode found during the COSDYNA-OMA test using the narrow-band technique.

Another very important conclusions observed during the test was that "modal parameter changes, especially modal damping and frequencies, are clearly observed between wind-on and wind-off cases" (ZHANG et al., 2024).

In the aerospace industry, OMA has also been used in recent years to understand the dynamic characteristics of several components, like rockets, payload, etc. as normal tests are not capable of recreating all the conditions caused by the combustion of the propellants, the effects produced during the separation of the stages nor the aerodynamic effects produced during the atmospheric flight of rockets. One example in which OMA was used was during the construction of the European launch vehicle Vector of Advanced Generation (VEGA) (fig. 2.5a) in which an OMA was performed using measurements obtained during a static firing test (fig. 2.5b) to validate the FEM already created.

(a) VEGA before liftoff (b) VEGA firing test

Source: (FRANSEN et al., 2024)

Figure 2.5: An OMA was performed during the construction of the VEGA carrier.

2.3 OMA in the Next Future

With the advent of new more sophisticated technologies, like wireless accelerometers and better data acquisition equipment, and with new techniques being developed every year that are allowing easier, better and automatized OMA techniques, is expected that OMA will be gain even greater relevance in the following years, not only in the civil, aeronautic or aerospace industries, but in all engineering areas as OMA has shown to be reliable, easy to implement and adequate to a gigantic amount of different conditions. As a final example of the application of an OMA, (BRINCKER; VENTURA, 2015) also

shows the study of a container ship (fig. 2.6) which further demonstrates that the areas in which OMA can be applied are wide and are only expected to grow.

(a) Container Vessel studied with an OMA

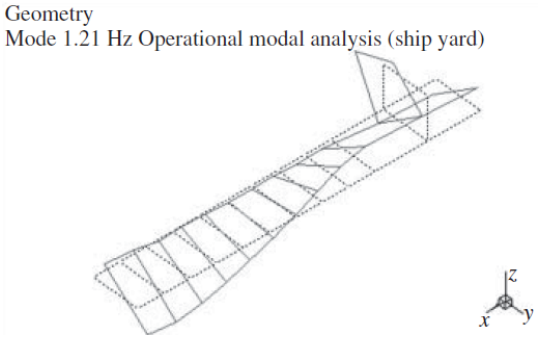

(b) One of the modes found on the contianer vessel studied.

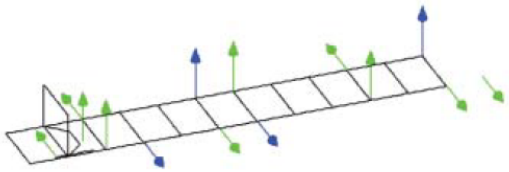

(c) Accelerometer placement.

Source: (BRINCKER; VENTURA, 2015)

Figure 2.6: OMA performed on a container vessel.

CHAPTER 3

THEORETICAL FRAMEWORK

The theoretical framework is divided into two main parts. The first part contains the information related to the theory behind OMA, starting with some historical background explaining the evolution of the method over the years. Additionally, information regarding the reasons why to use OMA is also presented. Then, the main theory explaining what OMA is and how it works is shown, followed by the main techniques used, explaining in further detail the three techniques used in this dissertation. Additionally, some limitations of the technique are presented, followed lastly by a comparison between OMA with the well consolidated Experimental Modal Analysis (EMA). The second part of the theoretical frameworks is dedicated to showcasing the state of the art in OMA, showing the principal applications where OMA is currently involved and the areas in which it appears that it will gain ground soon.

3.1 Operational Modal Analysis

"The engineering field that studies the modal properties of systems under ambient vibrations or normal operating conditions is called Operational Modal Analysis (OMA) and provides useful methods for modal analysis of many areas of structural engineering" (BRINCKER; VENTURA, 2015). As the name implies, OMA uses operational data exclusively (which means that the traditional techniques like the Frequency Response Function (FRF) of EMA are not available) instead, according to (SIEMENS, 2020) OMA relies on the correlation and the power spectral density (PSD) functions of the signals

measured. However, before embarking on the complexities of OMA, a brief historical background is important to understand how and why OMA was developed in the first place.

> "It is fair to say that processing of data in OMA is challenging; one can even say that this is close to torturing the data". (BRINCKER; VENTURA, 2015)

3.2 Historical Background

OMA gained traction as an important tool to perform modal analysis in the mid 1990's with the publication in 1996 of a book by van Overschee and De Moor in which the Subspace Stochastic Identification (SSI) methods were presented, showcasing the effectiveness of these techniques to identify modal parameters for a natural input modal analysis (BRINCKER; ANDERSEN, 2006).

However, there is evidence of OMA being implemented in the 1930's and even OMA concepts being applied in ancient history, as far as Pythagoras, in which he discovered that a tensioned string with half the length of another tensioned string would produce a sound an octave above the longer string according to (BRINCKER; VENTURA, 2015). In the 1930's the first studies on shock and vibrations affecting civil engineering structures were conducted, to better understand the effects of earthquakes in building, and after the 1933 Long Beach earthquake in California, D.S. Carder conducted a series of tests of ambient vibrations in more than 200 buildings applying rudimentary OMA techniques, to determine the natural modes of vibrations of these building, whose results were used to design codes to identify the natural frequency of new buildings, setting the first modern history serious studies using OMA.

In the 1970's M. Trifunac demonstrated that the analysis of ambient vibrations tests (AVT - OMA) and forced vibration tests (FVT - EMA) yielded the same results for practical engineering purposes.

And finally, since the 1990's with the publication of the book "Subspace Identification for Linear Systems" by Van Overschee and De Moor OMA, and with the availability of better sensors and computers, OMA has become a very well consolidated modal analysis technique, even leading to the creation of the International Operational Modal Analysis Conference (IOMAC) in 2005.

However, knowing that OMA uses exclusively operational data does not tell the reasons of why it was developed in the first place nor why to use it instead of the

traditional Experimental Modal Analysis (EMA). In the next section, the main reasons that led to the creation of OMA are presented.

3.3 Reasons to Use OMA

OMA was developed to overcome the limitations that other modal analysis techniques such as EMA presented. Even though EMA gives good and reliable results, there times in which performing one is very difficult, from either a technical point of view such as difficulty to excite the structure, or from an operational point of view, in which performing an EMA could cause economical loses due to the structure being analyzed being retired temporarily from operation. According to Siemens A.G. 2020 there are three main benefits of performing an OMA instead of an EMA:

3.3.1 Real world operational conditions differ significantly from laboratory conditions:

One of the advantages of an OMA is that the nature of the excitation, in magnitude and direction are more accurate as they are the ones that the structure will have to withstand. However, another reason to perform an OMA instead of an EMA is, as stated by Siemens, that some structures will exhibit a high degree of non-linearity when they are tested in a laboratory environment compared to their real-world usage. One example of this non-linearity can be found in an automotive suspension system:

> The shock absorbers in the suspension have a high level of static friction when the vehicle is at rest that isn't present when the vehicle is in motion on the road. This friction not only artificially raises the stiffness of the local structure but can also exhibit non-linear behavior when the friction is overcome, and the suspension begins to articulate. Non-linear behavior can wreak havoc when attempting to accurately measure and analyze structural dynamics data on vehicles in the lab (SIEMENS, 2020).

Aside from non-linearity, there are also other types of complications when trying to perform a modal analysis caused by the nature of the excitations that are not easily replicated in a laboratory environment, such as the ones caused by environmental factors

such as aero-elastic interactions or by external factors such as the vibration caused by pedestrians crossing a bridge as referenced previously in this work.

3.3.2 Practical / Size Limitations:

Another obvious limitation when performing an OMA is the size of the structure being tested. Very large structures, such as bridges, buildings, ships, commercial airplanes, wind turbines, etc. are simply too large to be tested inside a laboratory. Aside from their size, another problem that appears when trying to perform an EMA in large structures is that "often is impossible to properly excite the structures using traditional input methods" (SIEMENS, 2020). In these cases, the best solution is to use the natural *in-situ* loads, that will be the only ones being able to properly excite the structure (wind, pedestrian traffic, traffic loading, etc.). This can be done by placing a series of accelerometers in specific points of the structures being analyzed to measure the response of the systems to these natural excitations.

3.3.3 Ongoing Health Monitoring / Damage Detection

One form of determining the health of a structure or to detect any type of internal damage invisible from the outside is by measuring the modal parameters of the structure. Changing modal parameters, such as the natural frequency of the structure, can be signs of increased wear or internal damage that can cause an impending failure of a machine or structure. As OMA is performed with the operational conditions, machinery and buildings health can be assessed without removing them from service nor interrupting operations. In recent years, this type of damage detection has also been used by engineers to assess the health of structures after exposure to potentially damaging events like earthquakes and other types of natural phenomena.

3.3.4 Cost of Analysis

Additionally from the reasons presented by (SIEMENS, 2020), another very important reason to use OMA instead of EMA is due to the cost of the analysis. As mentioned previously, it is very hard to perform an EMA on big structures, like buildings or planes

due to their size and the difficulty of recreating the excitation conditions. However, it is possible to do so to an extent, but to do it, very big and expensive equipment is necessary.

In the case of the Millennium Bridge mentioned in chapter 1, a shaker with a mass of 1000 Kg was used for the EMA performed on the bridge. Shakers with these dimensions can cost up to hundreds of thousands of dollars, and additional to the cost of the equipment itself, the structure has to be shut down from its normal operation, which in the case of commercial planes for example can lead to thousands of dollars in loses to the company for every hour that the plane is out of operation. Therefore, and as mentioned by Magalhães (2010) OMA is cheaper alternative solution, as accelerometers, even the most sophisticated ones, are several times cheaper than the equipment used in EMA, with the additional advantage of not having to shut down the structure.

3.4 OMA Main Theory

As stated by (SIEMENS, 2020), Operational Modal Analysis (OMA) is a family of techniques used to identify the dynamic characteristics of a system while it's in operation, thus its name. This has the advantage that the boundary conditions and the excitation forces being applied in the system are the real conditions expected in magnitude, duration, frequency, etc., instead of being artificially recreated through other techniques. However, OMA is an *output-only* technique, which means that some crucial considerations must be made as the input is unknown.

Traditionally, in techniques like EMA, both the input and the output of the system are measured, which allows for the creation of Frequency Response Functions (FRF) from which the modal parameters can be extracted through curve-adjustment techniques. However, as in OMA only the output is measured an assumption is needed, the input excitation needs to be considered to be in the format of Gaussian white noise, as it excites the system with the same magnitude across all the frequency band of interest. This assumption allows for the calculation of the system matrix **H** as the output matrix is assumed to be the system matrix multiplied by a white noise as shown in figure 3.1.

According to (SIEMENS, 2020), in OMA the output measurements are used to create the time-domain functions called correlation functions. They are a useful statistical tool as they allow us to find repeating patterns in apparent random signals. A correlation function is the result of the comparison between a signal with a delayed version of another signal at increasing time lags. If the comparison is done with itself, it is called an auto-correlation function (ACF) and if it is done with another signal, it is called a

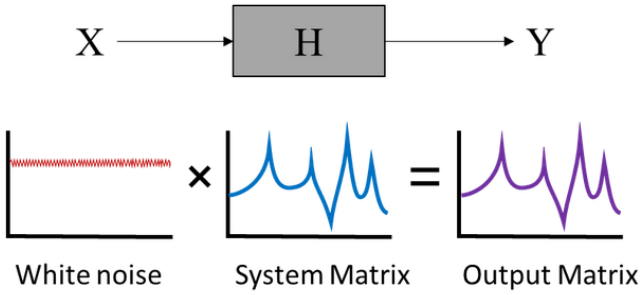

Source: (SIEMENS, 2020).

Figure 3.1: Gaussian white noise assumption needed for OMA

cross-correlation function (CCF).

Correlation functions provide a measurement of the amount of correlation between two signals giving a value varying from -1 to 1. “If the original signal contains periodic information (such as natural frequencies) then the delayed version of the signal will have a high amount of correlation with the original signal at certain periodicities (time lags)” ((SIEMENS, 2020)). However, as the delay between the two signals increases, the correlation between them decreases progressively to zero. The correlation function is able then to extract the periodicities between the two signals, which when transformed into the frequency domain allows to visualize the dominant frequencies. The ACF functions are done with each point measured, whereas the CCF are done with some selected measurement points called reference points.

Once the family of correlation functions is created, it is possible to transform them into the frequency domain using the Discrete Fourier Transform (DFT), where the ACF transforms into the Auto-Power Spectra and the CCF transforms into the Cross-Power Spectra. The complete family of these spectra are called correlograms, and they highlight the dominant frequencies across the different measured points, analogous to the FRFs in EMA. However, “[. . .] due to the fact that the correlation functions produce an unscaled value between -1 and 1, and the input forces are unmeasured, the concepts of modal participation factor or modal scaling do not exist in OMA” (((SIEMENS, 2020)). A visualization of the ACF process can be seen below in figure 3.2.

According to (COVIOLI, 2021) from the University of Rome "*La Sapienza*" the assumption of white noise as the input excitation has several advantages as modes at different frequencies can be excited with a single test run which consequently reduce test times. However, as the energy is spread over a wide spectrum, higher energy modes might not be excited appropriately which need to be taken in consideration when performing

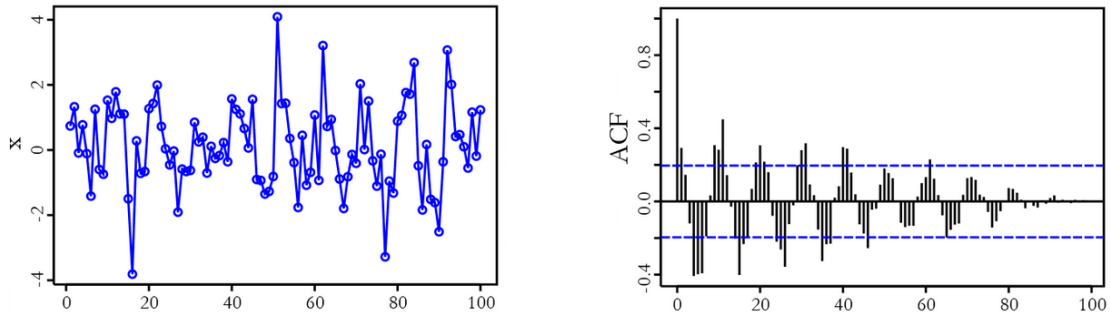

(a) Apparent random signal in the time-domain. (b) Periodicity found in the apparent r. signal.

Source: (SIEMENS, 2020).

Figure 3.2: Autocorrelation Function (ACF) Process

the analysis.

To understand how OMA uses the correlation functions and correlograms to extract the modal parameters, it is useful to review the response model in the frequency domain used in EMA as seen below in equation 3.1, expressed as a function of modal parameters:

$$H_{ij}(\omega) = \sum_{n=1}^{N} \left(\frac{\varphi_i^n \varphi_j^n}{m_n(j\omega - \lambda_n)} + \frac{\varphi_i^{n*} \varphi_j^{n*}}{m_n^*(j\omega - \lambda_n^*)} \right) \tag{3.1}$$

In which every term of the FRF $H_{ij}(\omega)$ is a function that relates the $i-th$ degree of freedom of the system response with the $j-th$ degree of freedom of the excitation, φ are the mode shapes, λ_n are the $n-th$ eigenvalues related to each $n-th$ mode and ω is the driving frequency. The superscript "*" indicates the complex pair conjugate of each function. According to (COVIOLI, 2021) from the measurement of the output response (eq. 3.2):

$$\mathbf{Y} = \begin{bmatrix} y_{1,1} & \cdots & y_{N_0,1} \\ \vdots & \ddots & \vdots \\ y_{1,N_t} & \cdots & y_{N_0,N_t} \end{bmatrix} \tag{3.2}$$

Y being the output response matrix of the system, measured at a number N_0 of points over N_t time samples.

It is possible to build the output spectral density function matrix $G_{yy}(\omega_k) \in C^{N_0 \times N_0}, k = 1, \ldots, N_t/2$ from the evaluation of the spectral density functions $G_{y_i y_j}(\omega_k)$, defined between the $i-th$ and $j-th$ output responses at the $k-th$ spectral line, as:

$$\mathbf{G}_{yy}(\omega_k) = \begin{pmatrix} G_{y_1y_1}(\omega_k) & \cdots & G_{y_1y_{N_o}}(\omega_k) \\ \vdots & \ddots & \vdots \\ G_{y_{N_o}y_1}(\omega_k) & \cdots & G_{y_{N_o}y_{N_o}}(\omega_k) \end{pmatrix} \tag{3.3}$$

((COVIOLI, 2021), p. 46)

For stationary stochastic processes, this Power Spectra Density (PSD) function matrix among the outputs, $\mathbf{G}_{yy}$ is:

$$\mathbf{G}_{yy}(\omega) = \mathbf{H}^H(\omega)\mathbf{G}_{ff}(\omega)\mathbf{H}(\omega) \tag{3.4}$$

Where the ^{H} notation is used to denote the Hermitian (conjugate transpose) of the matrix $H(\omega)$, and in which a stochastic processes is defined simply as "a family of random variables defined on a common probability space, indexed by the elements of an ordered set T, which is called the parameter set. Most often, T is taken to be an interval of time and the random variable indexed by an element $t \in T$ is said to describe the state of the process at time t" ((PAPOULIS; PILLAI, 2002),p.1)

As in OMA there is an assumption of uncorrelated and white noise inputs this causes $G_{ff}(\omega)$ to no longer be frequency dependent, equaling matrix G_{ff}. With this, it is possible then to combine equations 3.1 and 3.3 yielding an expression that decomposes the output PSD matrix into modal components, as shown in equation 3.5.

$$G_{y_iy_j}(\omega) = \sum_{n=1}^{N} \left[\frac{\varphi_i^{(n)} + \psi_j^{(n)}}{(j\omega - \lambda_n)} + \frac{\varphi_i^{(n)*} + \psi_j^{(n)*}}{(j\omega - \lambda_n^*)} + \frac{\psi_i^{(n)} + \varphi_j^{(n)}}{(-j\omega - \lambda_n)} + \frac{\psi_i^{(n)*} + \varphi_j^{(n)*}}{(-j\omega - \lambda_n^*)} \right] \tag{3.5}$$

Where $\psi_j^{(n)}$ is the output-only reference vector of the $n-th$ mode. This equation 3.5 forms the basis for the frequency domain OMA techniques and according to (COVIOLI, 2021) "it shows that if the terms related to unstable poles (the ones with positive real part) are not considered, eq. 3.5 reduces to 3.1 and the output PSD function matrix can be decomposed into modal components, as is the case of the FRF matrix."

On top of that, by taking the inverse Fourier Transform (IFT) of eq. 3.5 it is possible to obtain the output correlation function matrix $\mathbf{R}_{yy}(\tau)$, for positive and negative time lags:

$$R_{y_iy_j}(\tau) = \begin{cases} \sum_{n=1}^{N} (\varphi_i^{(n)} \psi_j^{(n)T} e^{\lambda_n \tau t_s} + \varphi_i^{(n)*} \psi_j^{(n)H} e^{\lambda_n^* \tau t_s}) for \tau \geq 0 \\ \sum_{n=1}^{N} (\psi_i^{(n)} \varphi_j^{(n)T} e^{\lambda_n |\tau| t_s} + \psi_i^{(n)*} \varphi_j^{(n)H} e^{\lambda_n^* |\tau| t_s}) for \tau < 0 \end{cases} \tag{3.6}$$

In which t_s is the sampling period. Equation 3.6 forms the basis for the time domain OMA techniques, as it shows that the output correlation function (for $\tau > 0$) can be expressed as a sum of decaying sinusoids.

Knowing the basic equations governing the OMA techniques, it is possible then to mention some of the OMA techniques available today. Section 3.4.1 shows a basic explanation of the most popular OMA techniques currently used, and in sections 3.4.2.1 and 3.4.2.2 a further explanation of the techniques used in this work are presented.

3.4.1 OMA Techniques

As seen previously in section 3.4, equations 3.5 and 3.6 are respectively the basis for the frequency-domain and the time-domain techniques to perform an OMA. Every the technique has its own advantages, disadvantages, and limitations. Therefore, it is the responsibility of the engineer to choose the best one adapted to the requirements of the test and the resources available. Some frequency and time-domain techniques will be presented here with a brief explanation of the techniques, their advantages and their respective limitations. In the next section, a more profound explanation of the three techniques used in this work will be presented.

3.4.1.1 Peak Picking (PP)

Peak picking is according to (ZAHID; CHAO; KHOO, 2020) the most undemanding OMA technique. It is a frequency domain technique in which the identification of the dynamic characteristics is done through the identification of the peaks in the power spectrum, thus the name. However, to perform it, the assumption that all the modes are well separated from one another and the damping of the system is low is needed. Nevertheless, as is the case for most real complex systems, it is almost impossible to avoid closely spaced modes and there is no guarantee that the damping of the system is low. To overcome these limitations, other frequency domain techniques were developed but the PP technique remains as a first step in most OMA performed, as it is extremely simple to perform and allows for a general idea of the localization of the modes.

3.4.1.2 Frequency Domain Decomposition (FDD)

According to (ZAHID; CHAO; KHOO, 2020), the Frequency Domain Decomposition technique (FDD) is one of the most popular OMA techniques currently used. It is an extension of the PP technique developed to overcome its modal multiplicity limitations.

It does so by using the singular value decomposition (SVD) of the PSD matrix to detect mode multiplicity. This happens because, when taking the SVD of the spectral matrix, the spectral matrix decomposes into a set of auto-spectral density functions, each one of them corresponding to a single-degree-of-freedom system which allows to identify closely spaced modes. Even so, the FDD cannot estimate damping ratios, reason why newer techniques were developed.

3.4.1.3 Enhanced Frequency Domain Decomposition (EFDD)

The Enhanced Frequency Domain Decomposition technique (EFDD) is a technique developed to overcome the limitations of the FDD technique in relation to the estimation of damping ratios. Not only that, but the EFDD can estimate mode shapes, damping ratios and even natural frequencies with better accuracy than the conventional FDD technique.

To perform an EFDD, the first step is to use the inverse discrete Fourier Transform (IDFT) to transform the PSD function into the time domain at a peak of resonance where the resonance frequency is obtained by determining the zero-crossing times. After that, the damping ratio can be obtained by using the logarithmic decrement of the corresponding normalized auto-correlation function.

EFDD is a user-friendly and fast processing technique, although exact computation of modal damping is still an open issue that tends to lead to biased damping estimates, as stated by (HASAN et al., 2018) from the University of Technology Malaysia.

3.4.1.4 Time Domain Decomposition (TDD)

The Time Domain Decomposition (TDD) as its name implies, is a time domain technique used to perform an OMA. It bases its approach using a single-degree-of-freedom (SDOF) in time domain. “Using this method, undamped mode shapes are extracted using SVD of the output correlation matrix relative to the locations of sensors” (ZAHID; CHAO; KHOO, 2020). After the extraction of the mode shapes, the rest of the modal characteristics are extracted from the SDOF signal by using the PP technique previously mentioned. However, as this method bases its approach on the SDOF system, it is difficult to extract the modal parameters from closely spaced modes.

3.4.1.5 Stochastic Subspace Identification (SSI)

The Stochastic Subspace Identification techniques (SSI) are time-domain identification techniques invented in 1991 by Van Overschee and De Moor. “SSI allows the identification of an effective state space model for a complex dynamic system subjected to stochastic excitation directly from measured data” (OVERSCHEE; MOOR, 1996a) . This method reduces problems of computational complexity which makes it faster when compared to other OMA techniques.

SSI has two main algorithms from which it bases the identification of modal parameters: data-driven SSI (SSI-DATA) and covariance-driven SSI (SSI-COV). A further explanation of these methods is offered in section 3.4.2.1.

3.4.1.6 Numerical Algorithms for Subspace System Identification (N4SID)

According to Li (2014) the N4SID method, which stands for "Numerical Algorithm for Subspace State-Space System Identification" is a powerful alternative to the classical system identification method based on iterative approaches (like the SSI-COV and SSI-DATA methods). The key step of this method is the oblique projection of subspaces generated by the block Hankel matrices formed by input/output data of system. Other geometric and mathematics tools of linear algebra like SVD are used to extract the order of the system and the observability matrix which contain the parameters of the estimated model.

Experiments have shown that N4SID algorithm can lead in some cases to ambiguous estimation due to the use of oblique projection. A further explanation of this method is presented in section 3.4.2.2

3.4.2 Techniques Used in This Work

This section encompasses a deeper explanation of the SSI and N4SID methodologies, as the software used for this work use techniques based directly or indirectly on them.

3.4.2.1 Stochastic Subspace Identification - SSI

The Stochastic Subspace Identification (SSI) techniques are modal estimation algorithms used for operational modal analysis. The breakthrough in the SSI algorithms occurred in 1996 with the publication of the book “Subspace Identification for Linear Systems” by Van Overschee and De Moor, in which the algorithms presented by them became the

de facto SSI techniques. The two main SSI algorithms are the covariance driven SSI, also known as **SSI-COV**; and the data-driven SSI, also known as **SSI-DATA**. According to (BRINCKER; ANDERSEN, 2006), the SSI-DATA algorithm is the most powerful time-domain technique used to identify the modal parameters for operational modal analysis.

However, these methods result challenging to most engineers as they use concepts covering both deterministic and stochastic algorithms, which don't tend to be present in most engineering courses. As such, some basic explanation of these field is needed.

The SSI algorithms are time-domain algorithms that base their calculus on the discrete time response **y(t)** from the system being studied.

$$y(t) = \begin{Bmatrix} y_1(t) \\ y_2(t) \\ \vdots \\ y_4(t) \end{Bmatrix} \tag{3.7}$$

Before using the discrete time domain formulations, it is necessary to first review the classical formulation for a multiple-degree-of-freedom (MDOF) of a structural system in the continuous time domain, given by:

$$\mathbf{M}\ddot{y}(t) + \mathbf{D}\dot{y}(t) + \mathbf{K}y(t) = \mathbf{f}(t) \tag{3.8}$$

Where **M, D** and **K** are the mass, damping and stiffness matrices respectively and **f**(t) is the force vector. To use this formulation with the discrete time domain responses, it is necessary to introduce the **State Space** formulation.

$$\mathbf{x_t} = \begin{bmatrix} \mathbf{y_t} \\ \dot{\mathbf{y}}_\mathbf{t} \end{bmatrix} \tag{3.9}$$

As stated by (BRINCKER; ANDERSEN, 2006), it is important not to confuse the states **x(t)** with the system input, which is still **f(t)**. Using the state space formulation (eq. 3.9), equation 3.8 simplifies to a first order equation, shown below.

$$\begin{aligned} \dot{\mathbf{x}}(\mathbf{t}) &= \mathbf{A}_c\mathbf{x}(t) + \mathbf{B}\mathbf{f}(t). \\ \mathbf{y}(t) &= \mathbf{C}\mathbf{x}(t) \end{aligned} \tag{3.10}$$

Where $\mathbf{A_c}$ is the system matrix in continuous time and **B** is the load matrix. They are given by:

$$\mathbf{A_c} = \begin{bmatrix} 0 & I \\ -\mathbf{M^{-1}K} & -\mathbf{M^{-1}D} \end{bmatrix} \quad \mathbf{B} = \begin{bmatrix} 0 \\ \mathbf{M^{-1}} \end{bmatrix} \tag{3.11}$$

The advantage of this formulation, is that it yields a direct general solution in the form:

$$\mathbf{x(t)} = \exp(\mathbf{A_c t})\mathbf{x}(0) + \int_0^t \exp(\mathbf{A_c}(t-\tau))\mathbf{B f}(\tau) d\tau \tag{3.12}$$

Where the first part of the solution is the homogeneous solution and the second part is the particular solution. However, as the time response used in OMA is discrete, it is necessary to transform this equation from the continuous time domain to the discrete time domain. To do so, all variables are sampled in the following way: $\mathbf{y}_k = \mathbf{y}(k\Delta t)$, where Δk is the sampling period and k is the measurement number. With this sampling, the new discrete homogeneous equation becomes:

$$\begin{aligned} \mathbf{x_k} = \exp(\mathbf{A_c} k\Delta t)\mathbf{x_0} = \mathbf{A}_d^k \mathbf{x}_0 \\ \mathbf{A}_d = \exp(\mathbf{A}_c \Delta t) \\ \mathbf{y}_k = \mathbf{C}\mathbf{A}_d^k \mathbf{x}_0 \end{aligned} \tag{3.13}$$

It is important to note that the system matrix in continuous time and in discrete time is not the same.

Block Hankel Matrix

In the discrete-time domain, the system response matrix is given by:

$$\mathbf{Y} = \begin{bmatrix} \mathbf{y}_1 & \mathbf{y}_2 & \dots & \mathbf{y}_N \end{bmatrix} \tag{3.14}$$

Where **N** is the number of measuring points.

According to (BRINCKER; ANDERSEN, 2006) an easy way to understand the Block Hankel Matrix is by considering the simpler case of performing the product between two matrices that are modifications of the data matrix given in eq. 3.13.

Letting $\mathbf{Y_{1:N-k}}$ be the data matrix, where the last k data point was removed and $\mathbf{Y_{k:N}}$ the data matrix where the first k data point was removed, then:

$$\hat{\mathbf{R}}_k = \frac{1}{N-k} \mathbf{Y}_{(1:N-k)} \mathbf{Y^T}_{(k:N)} \tag{3.15}$$

"$\hat{\mathbf{R}}_k$ is an unbiased estimate of the correlation matrix at time lag k. This follows directly from the definition of the correlation estimate" (BENDAT; PIERSOL,1986). As stated by (BRINCKER; ANDERSEN, 2006), the Block Hankel matrix defined in SSI is simply a gathering of a family of matrices that are created by shifting the data matrix.

$$\mathbf{Y}_h = \begin{bmatrix} \mathbf{Y}_{(1:N-2s)} \\ \mathbf{Y}_{(2:N-2s+1)} \\ \vdots \\ \mathbf{Y}_{(2s:N)} \end{bmatrix} = \begin{bmatrix} \mathbf{Y}_{(hp} \\ \mathbf{Y}_{(hf)} \end{bmatrix} \tag{3.16}$$

Where $\mathbf{Y}_h$ is the Block Data Matrix. The upper part $\mathbf{Y}_{hp}$ is called the *past* and the lower half $\mathbf{Y}_{hf}$ is called the *future*. For this matrix in particular, the total data shift is of $2s$ and is denoted "the number of block rows" ("of the upper or lower part of the Block Hankel Matrix" (BRINCKER; ANDERSEN, 2006)). This way, the total number of rows that $\mathbf{Y_h}$ will have is given by $2sM$, and the number of columns is given by $N-2s$.

Projection Matrix "O"

According to (BRINCKER; ANDERSEN, 2006), the projection matrix $\mathbf{O}$ is the most mysterious operation required in the SSI algorithms. This projection matrix is introduced as a geometrical tool by (OVERSCHEE; MOOR, 1996b). However, to deal with stochastic response the projection is defined as a conditional mean. In SSI specifically, the projection of the future unto the past defines the matrix in the following way:

$$\mathbf{O} = E(\mathbf{Y}_{hf}|\mathbf{Y}_{hp}) \tag{3.17}$$

With this conditional mean, Gaussian processes (stochastic processes) can be described completely by its covariances, in accordance to (MELSA; SAGE, 1973). However, since the shifted data matrices also defines covariances, it's not uncommon for the projection to be calculated directly as:

$$\mathbf{O} = \mathbf{Y}_{hf}\mathbf{Y}_{hp}^T(\mathbf{Y}_{hp}\mathbf{Y}_{hp}^T)^{-1}\mathbf{Y}_{hp} \tag{3.18}$$

The first four matrices in equation 3.18 ($\mathbf{Y}_{hf}\mathbf{Y}_{hp}^T(\mathbf{Y}_{hp}\mathbf{Y}_{hp}^T)^{-1}$) serve to introduce the covariances between channels at different time lags, whereas the the last matrix $\mathbf{Y}_{hp}$ defines the conditions.

"A conditional mean like given by equation 3.16 simply consist of free decays of the system given by different initial conditions specified by $\mathbf{Y_p}$. The matrix is $sM \times sM$ and any column in the matrix $\mathbf{O}$ is a stacked free decay of the system to a (so far unknown) set of initial conditions" (BRINCKER; ANDERSEN,2006). With the use of equation 3.13, any column of the projection matrix O can be expressed as:

$$\mathbf{o}_{col} = \Gamma_s \mathbf{x}_0 \quad \Gamma_s = \begin{bmatrix} \mathbf{C} \\ \mathbf{CA}_d \\ \mathbf{CA}_d^2 \\ \vdots \\ \mathbf{CA}_d^{s-1} \end{bmatrix} \tag{3.19}$$

Where Γ_s is the observability matrix. With the matrix Γ_s it is possible to find the initial conditions directly from 3.19.

Kalman States

According to (BRINCKER; ANDERSEN, 2006), the Kalman states are simply the initial conditions for all the columns of the observability matrix O. This yields:

$$\mathbf{O} = \Gamma_s \mathbf{X}_0 \tag{3.20}$$

Where the matrix x_0 contains all the Kalman states at time lag zero. In the same fashion as before, if the matrix Γ_s is known, it is possible to find all the Kalman states directly from equation 3.20. However, as matrix Γ_s is unknown up to this point, a different approach is needed to estimate the states. This can be done by performing the Singular Value Decomposition (SVD) on the observability matrix O, as seen below in equation 3.21.

$$\mathbf{O} = \mathbf{USV}^T \tag{3.21}$$

This way, it is possible to estimate the matrix Γ_s and the Kalman state matrix states x_0 using the following equations:

$$\hat{\Gamma} = \mathbf{US}^{1/2} \quad \hat{\mathbf{X}}_\mathbf{0} = S^{1/2}\mathbf{V}^T \tag{3.22}$$

It is important to note that this procedure to estimate the values of matrices $\hat{\Gamma}$ and $\hat{\mathbf{x_0}}$ is not unique. Different OMA techniques will use different approaches to calculate these matrices.

System Matrices

The discrete system matrix A_d can be found using the estimated matrix Γ by removing one block from the top and the bottom of the matrix, yielding:

$$\hat{\Gamma}_{(2:S)}\hat{\mathbf{A}}_d = \hat{\Gamma}_{(1:S-1)} \tag{3.23}$$

This way, "the system matrix can be found by regression. The observation matrix C can be found simply by taking the first block of the observability matrix Γ as shown below:

$$\hat{\mathbf{C}} = \hat{\Gamma}_{(1:1)} \tag{3.24}$$

Modal Analysis and Practical Issues

Finally, with the previous explanation is possible to explain how the SSI algorithms calculate the modal parameters. The first step is to perform an eigenvalue decomposition of the system matrix $\hat{\mathbf{A}}_\mathbf{d}$:

$$\hat{\mathbf{A}}_d = \Psi[\mu_i]\Psi^{-1} \tag{3.25}$$

Where $[\mu_i]$ and Ψ are the poles and eigenvectors of the discrete system matrix respectively. The continuous poles λ_i can be found from the discrete poles μ_i as follows:

$$\mu_i = \exp \lambda_i \tag{3.26}$$

With this, it is finally possible to find the modal parameters of the system with the well known formulas:

$$\lambda_i = \frac{\ln \mu_i}{\Delta T} \quad \omega_i = |\lambda_i| \quad f_i = \frac{\omega_i}{2\pi} \quad \zeta_i = \frac{Re(\lambda_i)}{|\lambda_i|} \tag{3.27}$$

Where ω_i are the natural frequencies in rad/s; f_i are the natural frequencies in Hz and ζ_i are the damping ratios.

Finally, the mode shapes can be obtained from

$$\Phi = \mathbf{C}\Psi \tag{3.28}$$

> [...] from a modal point of view – if we are able to make up our mind about the size of the Block Hankel matrix. As we have seen earlier, the number s defines the size of the Block Hankel matrix, and thus also the size of the projection matrix O. However, the number sM defines the number of eigenvalues in our model, thus s defines the model order. Normally we would like to vary the model order to establish a stabilization diagram. This can of course be done by establishing a series of Block Hankel matrices of different size, but it is somewhat easier, instead of varying the size of the Block Hankel matrix, to vary the number of singular values used in eq. 3.22. Thus in practice the size

of the Block Hankel matrix defines the maximum model order, and the actual model order is varied by varying the number of singular values taken into account when performing the singular value decomposition of the projection matrix. The maximum number of eigenvalues sM must be adjusted to a reasonable level to incorporate the needed range of models. (BRINCKER; ANDERSEN,2006).

SSI-DATA vs SSI-COV

Despite the fact that both the SSI-DATA and SSI-COV are methods governed by the SSI algorithms, there are some crucial differences between them that need to be taken into consideration when performing an OMA.

According to (ZAHID; CHAO; KHOO, 2020), one worth noting aspect about SSI-COV is that it is computationally faster than the SSI-DATA method because it uses the fast Fourier Transform (FFT) to compute the covariances while the SSI-DATA uses the QR factorization method, which is slower and consequently demands more computational power. The QR Factorization method is a decomposition of a matrix **A** into a product **QR** of an orthonormal matrix **Q** and an upper triangular matrix **R**.

Both the SSI-DATA and the SSI-COV methods can estimate the system modes and forced oscillations, but the SSI-COV is better at estimating damping ratios.

Both SSI methods have a high parameter estimation accuracy and are very computationally efficient, which makes them faster and more accurate than other OMA methods as mentioned by (REYNDERS et al., 2015). For these reasons, the SSI methods have become the standard OMA methods for most applications.

3.4.2.2 Numerical Algorithm for Subspace State-Space Identification - N4SID

The Numerical Subspace State Space System Identification, commonly known as the N4SID method, is according to (LJUNG, 1999) a technique used to identify linear dynamic systems from input-output data. It is part of a broader class of subspace identification methods used widely in areas like control engineering and signal processing.

According to (OVERSCHEE; MOOR, 1996b), these algorithms were created to overcome some of the main issues that traditional system identification algorithms experience. For instance, traditional identification algorithms require a previous knowledge of the order and observability indices, are iterative and need non-linear optimization, which requires additional computational power. On top of that, traditional algorithms will yield different results for zero and non-zero initial states.

However, the complete theory behind the N4SID method is very complex, involving knowledge from the deterministic and stochastic areas and a complete understanding of it is beyond the scope of this work. Therefore, only a quick overview of the most important parts of the method will be shown here.

The first step of the N4SID method is transforming the system being studied into a state-space model, which is described by:

- **State equation**: $x(k+1) = Ax(k) + Bu(k) + w(k)$
- **Output equation**: $y(k) = Cx(k) + Du(k) + v(k)$

where $x(k)$ is the state vector, $u(k)$ is the input vector, $y(k)$ is the output vector, and $w(k)$ and $v(k)$ are process and measurement noise, respectively.

Block Hankel Matrix

With the state-space system, the next step is the construction of the Block Hankel Matrices, which were explained in section 3.4.2.1 and thus will not be explained here again. These construction of this matrices is needed as they help in capturing the dynamics of the system over multiple time steps.

Singular Value Decomposition

The next step is the identification of values in the the Block Hankel matrices that could correspond to modes of the system. To do this, subspace methods, which include the N4SID, use a variety of numerical linear algebra techniques. One of the most powerful and commonly used techniques is the Singular Value Decomposition (SVD), where the singular values calculated will correspond the system's modes.

Subspace Estimation

With the SVD calculated, the next step is to estimate the subspace that contains information about the system states. To do so, the technique used in section 3.4.2.1 involving the projection of the future outputs into the past input-output space is done.

State-Space Model Extraction

Finally, it is possible to extract the the system matrices *A, B, C* and *D* from the subspace estimated. This process usually involves solving linear least-squares problems. One of the most common ways of solving this problem is through the use of QR decomposition, which is simply a decomposition of a matrix into two simpler matrices, being an orthogonal matrix Q and an upper triangular matrix R.

N4SID Advantages

The N4SID method is a very reliable method that posses some very useful advantages. According to (OVERSCHEE; MOOR, 1994) some of this advantages include:

The N4SID is a non-iterative method, which means that it yields a direct solution.

Numerically robust algorithm, able to withstand very big data sets without consuming too much computational power.

The N4SID method is effective even for measurements with high levels of noise.

3.4.3 OMA Techniques Overview

Table 3.1 showcases the methods presented in this work, including the pros and cons of each one of them.

Table 3.1: OMA Methods presented this section.

Method	Type	Pros	Cons
PP	Frequency Domain	Simplest, easiest, and computationally most undemanding method	Inaccurate if a system has closely spaced modes which is the case in most real structures.
FDD	Frequency Domain	Can identify natural frequencies and closely spaced mode shapes accurately.	Cannot estimate damping ratios.
EFDD	Frequency Domain	User-friendly and fast processing method. Can identify damping ratios along with mode shapes and natural frequencies with higher accuracy than FDD.	Exact computation of modal damping is still an issue which may often lead to biased estimates.
TDD	Time Domain	Computationally efficient method. Reduces operator interaction greatly during modal analysis process.	Difficulty to extract modal parameters from closely spaced models.

Source: (ZAHID; CHAO; KHOO, 2020), (OVERSCHEE; MOOR, 1994)

Table 3.1: OMA Methods presented this section.

SSI	Time Domain	High parameter estimation accuracy and high computational efficiency when compared to other OMA methods.	Mathematically complex method.
N4SID	Time Domain	The algorithms are non-iterative, with no non-linear optimization part involved. This is why they do not suffer from the typical disadvantages of iterative algorithms.	Can lead in some cases to ambiguous estimation due to the use of oblique projection.

Source: (ZAHID; CHAO; KHOO, 2020), (OVERSCHEE; MOOR, 1994)

3.4.4 OMA Limitations

OMA has a variety of advantages over EMA, such as the fact that the excitations and boundary conditions are the actual operational conditions for the structure, as well as the reduction of the cost and a possibility of automation of the process. However, as stated by (ZAHID; CHAO; KHOO, 2020) the lack of knowledge about the input forces does affect the modal parameters extracted, and as a result of this lack of knowledge creates some undesired limitations of OMA. The main limitations presented by OMA algorithms are:

- Mode shapes obtained from OMA cannot be normalized accurately as the input is unknown, which subsequently affects the accuracy of the mathematical models.
- As the mode shapes are unscaled, it is not possible to determine the structure's sensitivity due to particular (harmonic) forces.
- As one of the requirements for OMA methods is that the input needs to be assumed to be Gaussian white noise, the methods work nicely for civil engineering structures such as buildings and bridges, but other types of structures such as machines that have other types of excitations (like harmonic excitations from engines) can lead OMA methods to failure. However, in recent years new techniques have been developed to overcome this limitation, with the creation of new techniques such as OMAX.

Additionally, (MAGALHãES, 2010) also states than some additional disadvantages of OMA are:

- Due to the unknown input, the signal to noise ratio is lower than in other EMA.
- As the ambient vibration tends to be weaker than forced vibration, the accelerometers used need to be extremely sensible.
- The ambient vibration may fail to properly excite higher frequency modes properly.

3.5 EMA vs OMA

Table 3.2 shows the main differences between the EMA and OMA methods. Although both methods differ in many ways, both aim for the same goal, obtaining the modal parameters from any system of interest.

Table 3.2: EMA vs OMA.

	EMA	**OMA**
Measured Input?	Yes	No
Measured Format?	Frequency Response Function (FRF)	Auto and Cross-Correlation functions. Auto and Cross-Power Spectra.
Results	- Natural frequencies (ω_n) - Damping ratios (ζ) - Mode shapes (φ)	- Natural frequencies (ω_n) - Damping ratios (ζ) - Mode shapes* (φ)

*Mode shapes are unscaled and there is not a modal participation factor.

Source: (SIEMENS, 2020).

Although EMA and OMA are different techniques, both aim to obtain the same information, the modal parameters of a system. According to (SIEMENS, 2020) both are known as “parametric” methods, as the measured data is used to build mathematical models of the structure’s dynamic characteristics, which is then used to extract the modal parameters in a way known as curve-fitting.

Both EMA and OMA use a family of frequency-domain functions calculated from the measurement, the difference being that in EMA the measurements are from both the

input and output of the system, whereas in OMA only the output measurements are known, and the input measurement is considered to be Gaussian white noise. These functions are called Frequency Response Functions (FRFs) in EMA, and auto-power and cross-power spectra functions in OMA. Independently from the method, the end goal of modal analysis is the construction of the system matrix H, that relates the outputs of the system to the input. Figure 3.3 shows a summarized view of both processes.

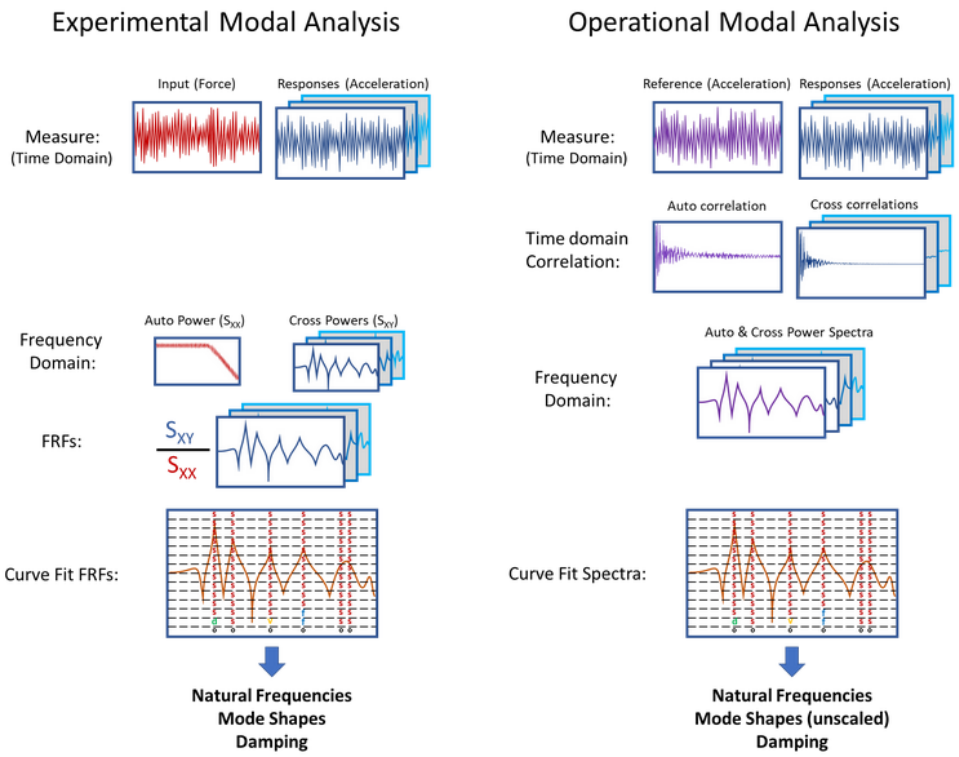

Source: (SIEMENS, 2024)

Figure 3.3: EMA vs OMA Summary.

3.6 Modal Assurance Criterion (MAC) Matrix

To evaluate the results obtained in a modal analysis it is possible to perform a quality assessment technique known as Modal Assurance Criterion (MAC) analysis. According to (SIEMENS, 2019):

MAC analysis is used to determine the similarity of two mode shapes:

- *If the mode shapes are identical (i.e., all points move the same) the MAC will have a value of one or 100%. The right side of figure 3.4 shows an Auto-MAC where this*

criterion is fulfilled.

- *If the mode shapes are very different, the MAC value will be close to zero, as seen in the left side of figure 3.4.*

In other words, a MAC compares two sets of mode shapes between each other to determine the similarity between the two of them, it does so by normalizing the vectors in a matrix known as the MAC matrix. The equation that describes the MAC matrix can be seen below:

$$MAC(\{\varphi_r\},\{\varphi_s\}) = \frac{\left|\{\varphi_r\}^{*t}\{\varphi_s\}\right|^2}{\left(\{\varphi_r^{*t}\varphi_r\}\right)\left(\{\varphi_s^{*t}\varphi_s\}\right)} \tag{3.29}$$

Where φ is a set of mode shapes obtained for a determined structure.

The comparison can be made between two different sets of modes ($MAC(\{\varphi_r\},\{\varphi_s\})$), in which case it is called **Cross-MAC**, or done with the same set of modes ($MAC(\{\varphi_r\},\{\varphi_r\})$), in which case is called **Auto-MAC**. In any of the two cases, the ideal case is given by figure 3.4 where a clean diagonal column is shown in the MAC analysis without the appearance of any other column in the graph. The presence of other columns may indicate problems with the results obtained, like coupled modes, residues in the programs being used or bad collection of data.

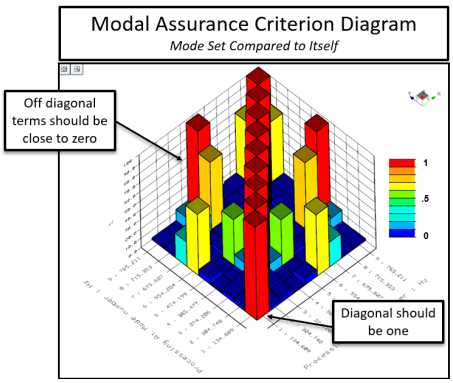

(a) MAC matrix showing a problem with the mode shapes obtained.

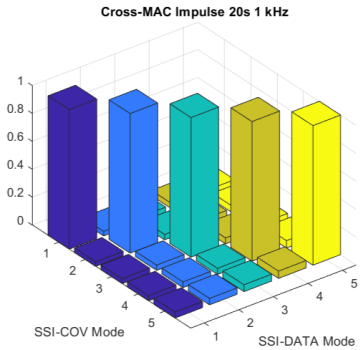

(b) The ideal MAC matrix has the shape of an identity matrix.

Source: (SIEMENS, 2019), Author (2024)

Figure 3.4: MAC matrices comparison.

CHAPTER 4

METHODOLOGY

The methodology for this work was divided into two main parts: the first part consisted in the validation of the OMA techniques being used to guarantee the fidelity of their results as it was the first time OMA was being implemented at the Faculty of Gama, to ensure that the methodology followed yielded reliable modal parameters. For the validation, it was decided that the system to be studied would be a model of a steel cantilever beam (SCB), from which a beam element model (BEM) and a real structure were created. The validation was divided into four steps, described in section 4.1, with the objective of finding the modal parameters of the beam using four different methods.

The second part of the work consisted of the analysis of different structures through OMA techniques to obtain the modal parameters of each one of them. The data obtained was then compared to simplified models of the system being studied, from which analytical or simulated modal analysis were performed to have parameters for a comparison.

4.1 OMA Validation

For the OMA validation, a model of a steel cantilever beam (SCB) was used as the system to be studied, due to the simplicity of its geometry, the consolidated theory behind its dynamic behavior and to facilitate the construction of the SCB in real life for the OMA tests. The SCB model used can be seen in figure 4.1, where its length and cross section are shown.

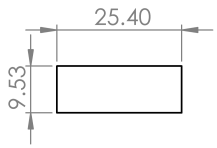

(a) Cross Section

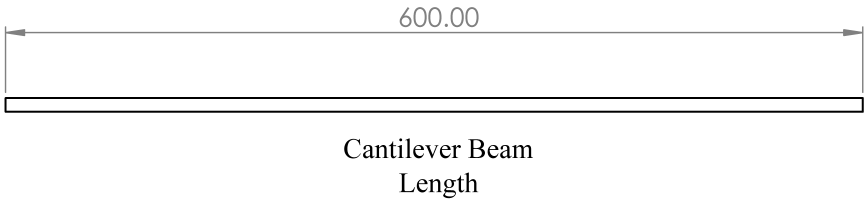

(b) Length

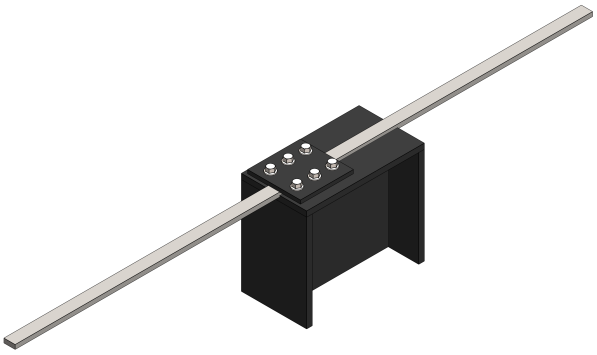

(c) SCB isometric view

Figure 4.1: Steel Cantilever Model (SCB) used for the OMA validation.

The complete parameters used for the beam can be seen below in table 4.1.

Table 4.1: SCB parameters considering the material of the beam as being steel AISI 1020.

Young Modulus [E]	186 GPa
Density [ρ]	7870 Kg
Length [l]	0.600 m
Height [h]	0.00953 m
Width [b]	0.0254 m
Inertia [I_x]	1.832E-09 m^4

With the model chosen, the validation of the OMA process was divided into four parts, where the first sixth bending modes of the SCB were obtained:

1. Theoretical analysis

2. Simulated modal analysis

3. Simulated OMA

4. OMA tests performed on the SCB

The complete process followed can be seen below in figure 4.2.

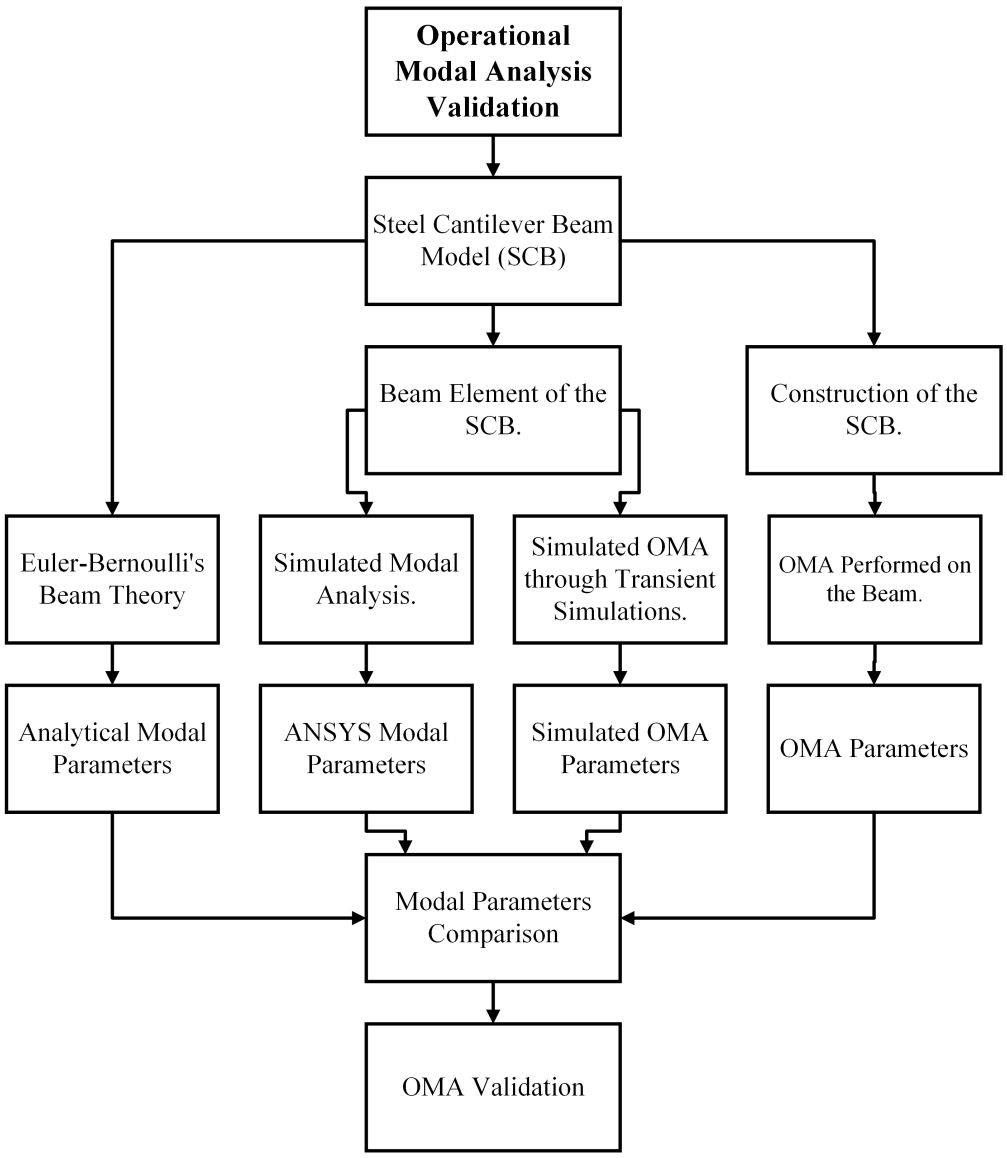

Figure 4.2: OMA Validation Process

4.1.1 Theoretical Analysis

For the theoretical analysis of the SCB it was decided that the Euler-Bernoulli equations would be used, as they offered a simple approach to calculate the bending modes in free vibration for the beam.

Natural Frequency:

According to (INMAN, 2014) the natural frequency of bending modes using the Euler-Bernoulli equations for a cantilever beam are given by:

$$\omega_n = \beta_n \sqrt{\frac{EI}{\rho A L^4}} [rad/s] \quad f_n = \frac{\omega_n}{2\pi} [Hz] \tag{4.1}$$

Where:

- β_n is the wavenumber or characteristic value: $\beta_1 = 1.8751$, $\beta_2 = 4.6941$, $\beta_3 = 7.8548$, $\beta_4 = 10.9955$, $\beta_5 = 14.1372$. For $n > 5$ $\beta_n = (2n-1)\pi/2$, where n is the number of bending mode.
- E is the Young Modulus in $[Pa]$.
- I_x is the moment of inertia given in $[m^4]$.
- ρ is the density of the beam $[kg/m^3]$.
- A is the Area of the cross section $[m^4]$.
- L is the length of the beam $[m]$.

Mode Shape:

The mode shapes in the Euler-Bernoulli beam theory are given by the following equation:

$$\varphi_n = cosh\beta_n x - cos\beta_n x - \sigma_n(sinh\beta_n x - sin\beta_n x) \tag{4.2}$$

Where σ_n is given by: $\sigma_1 = 0.7341$, $\sigma_2 = 1.0185$, $\sigma_3 = 0.9992$, $\sigma_4 = 1$ and for $\sigma_{n>4} = 1$.

With these equations it was possible to calculate the first six bending modes of the SCB model using the parameters shown in table 4.1. The mode shapes were created using the software MATLAB® Vtoolbox and are presented in chapter 5.1.1.

4.1.2 ANSYS® Modal Analysis

The simulated modal analysis was performed using the software ANSYS® Workbench using a beam element model (BEM) of the SCB. The BEM was divided into six parts and seven nodes, as seen in figure 4.3. The position of nodes recreate points were an accelerometer would be placed in a real-life test. With the BEM created, the last step

before performing the modal analysis was to add the fixed boundary condition in one of the tips of the beam to recreate the cantilever condition. After that, the modal analysis was performed and first six natural frequencies and mode shapes were created. The results are shown in chapter 5.1.2.

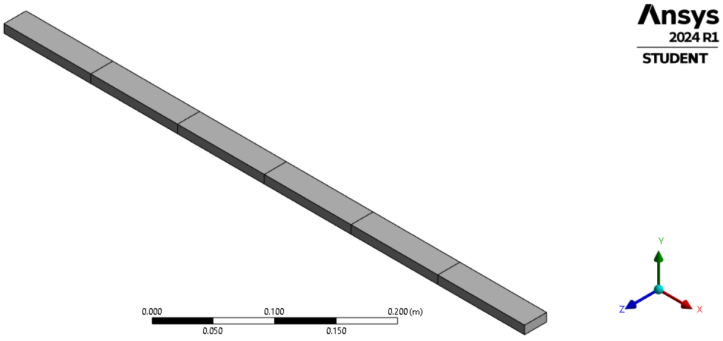

Figure 4.3: Beam Element Model (BEM) of the SCB

4.1.3 OMA with ANSYS® Transient Simulations

Using the BEM model previously created, transient simulations were performed to generate data to simulate an OMA. To do so, two forces were applied to the free tip of the beam:

1. Impulse 100 N in the +Y direction.
2. White noise with a mean value ($\mu = 0N$) and a standard deviation ($\sigma = 3N$), to simulate the vibration in the y-axis direction that would be produced by a strong wind.

With forces defined, the next step was to determine the damping ratio that the system would have. It was decided arbitrarily that the system would have a $\zeta = 0.01 = 1\%$

Finally, the last step before performing the simulations was to define the sampling frequency (f_s). To study the effect that f_s would have on the modes obtained, four simulations with four different sampling frequencies were performed: $f_s = 1024$, 2048, 4096 & $8192Hz$

With all the parameters set, the transient simulations on the beam were performed for a total time-length of 10 seconds. However, to perform the OMA from these results it was necessary to extract the acceleration data from each node. For this, the command *directional acceleration* was used in each one of the nodes shown in figure 4.1 to measure the Y-acceleration suffered in each node.

After having extracted the nodal acceleration, the next step was to construct the discrete time-domain response matrix **Y**, as seen in figure 4.4 for each one of the four simulations.

ANSYS TRANSIENT Impulse 1024 Hz - Response Matrix						
Time [s]	Node 1 [mm/s²]	Node 2 [mm/s²]	Node 3 [mm/s²]	Node 4 [mm/s²]	Node 5 [mm/s²]	Node 6 [mm/s²]
0.00000000	0.00000000	0.00000000	0.00000000	0.00000000	0.00000000	0.00000000
0.00097656	-2.91260000	-13.71500000	-28.35300000	-11.12600000	125.46000000	452.43000000
0.00195313	-23.14800000	-56.28000000	-25.10100000	118.40000000	231.78000000	-5.24160000
0.00292969	-18.33300000	26.72300000	161.16000000	178.61000000	-81.91100000	-226.19000000
0.00390625	109.64000000	255.91000000	184.04000000	-74.99600000	-105.63000000	-21.95800000
0.00488281	99.59200000	106.97000000	-20.54300000	5.41570000	4.95100000	-127.10000000
0.00585938	-164.52000000	-240.87000000	-17.59000000	83.86600000	-16.09900000	-53.15200000
0.00683594	-51.84600000	-95.68000000	-166.88000000	-133.83000000	57.33300000	132.30000000
0.00781250	114.89000000	19.27000000	-195.99000000	-192.79000000	-34.16400000	356.29000000
0.00878906	-137.18000000	-115.17000000	8.54370000	-52.68000000	-13.79400000	10.60100000
0.00976563	-11.31000000	-64.29300000	-21.01000000	163.45000000	0.44725000	-337.69000000

Figure 4.4: Example of a response matrix created on Microsoft® Excel from the acceleration data obtained in the ANSYS® transient simulations. Each column represents a node where of the SCB where the Y+ acceleration was measured.

With the response-matrix created it was possible then to perform the OMA using the software MATLAB® Output-Only Modal Analysis Toolbox and Siemens® Simcenter Testlab 2306.

MATLAB® OoMA Toolbox

The MATLAB® OoMA Toolbox allowed to perform an OMA with the data from the response matrix **Y** using three different OMA techniques: N4SID, SSI-COV and SSI-DATA. The three techniques were implemented to see if the modal parameters obtained were consistent independently from the method used.

In the OoMA toolbox there is a series of functions to assess the modal parameters from beam-like structures. To do so, a script containing the desired methods to use and the results desired is needed. For this work, the time-signals plot, PSD, mode shapes, stabilization diagrams and MAC matrices were extracted for the first six modes of the SCB using this software. An example of this script, including the considerations that need to be made can be found in the appendix of this work.

Siemens® Simcenter Testlab 2306

The process to perform an OMA on the software Siemens® Simcenter Testlab 2306 began with recreating the geometry of the SCB in the software, assigning a name for the body and nodes created, as they are required for the software to correlate the results obtained with the geometry created. This can be seen below in figure 4.5.

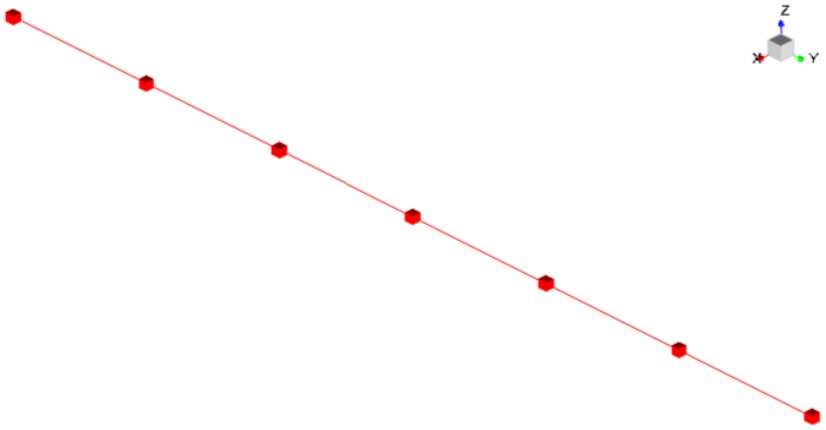

Figure 4.5: Geometry of the SCB created on Siemens® Simcenter Testlab 2306.

The process of performing an OMA on Siemens® Simcenter Testlab 2306 was very similar to the one performed on the OoMA Toolbox. However, the main difference between the two software was that in Simcenter Testlab, reference points were also selected for the calculation of the cross-correlation and cross-power functions. After which, the band frequency of interest was selected and the poles for the system resolution were selected from the stabilization diagram. After it, the last step was to extract the modal parameters and MAC matrices of the first six bending modes of the SCB from the software for their posterior analysis. A complete guide of how to perform an OMA on Siemens® Simcenter Testlab 2306 can be seen in the appendix of this work.

4.1.4 OMA on the Steel Cantilever Beam

To validate the OMA process, a real model of the SCB was built, after which the first step in performing the OMA on the steel cantilever beam built was to define the measurement points that would be used in the test. In the same fashion as with the simulations previously performed it was decided that the beam would be divided into six parts and seven nodes, as seen in figure 4.6 below.

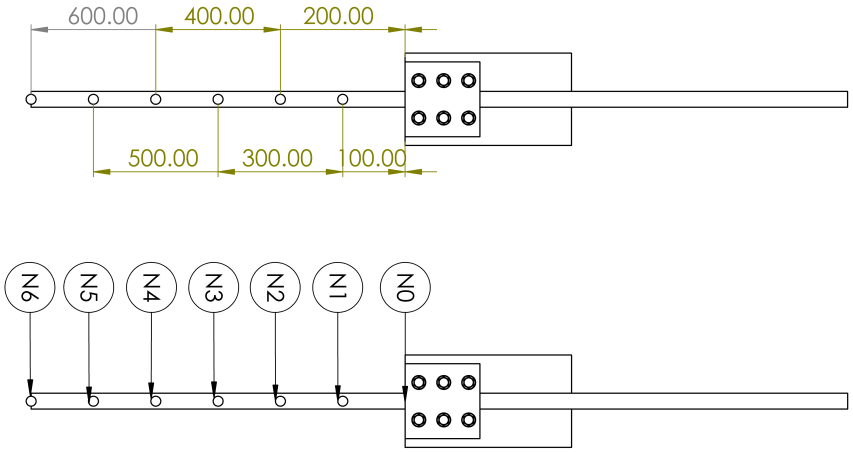

Figure 4.6: SCB measurement points and dimensions.

With the measurement points defined, the next step was to define the data acquisition equipment that would be used. For this test, the equipment used was:

PCB Piezoelectroncis® Accelerometer, ICP® - Model 35A21 as the acceleration measurement equipment, seen in figure 4.7a.

ACOEM® dB4 and dBTrig Four Channel Analyser as the data acquisition and processing equipment, seen in figure 4.7b.

(a) Accelerometer PCB® 35A21

(b) dB4 and dBTrigger

Figure 4.7: OMA Acquisition Equipment

With the equipment that would be used for the OMA test gathered, the next step in the test was to fix the beam in place to guarantee the cantilever condition and the correct length of the cantilevered beam for the test, which in this case was chosen to be of 600 mm. On top of that, marks were made on the beam surface in the measuring points to guarantee that the accelerometer would be placed in the correct position.

To fix the accelerometer to the beam, a special adhesive was used made out of *petro wax* to guarantee a good fixation to the beam surface, which was also polished previously to the test to ensure its surface would be smooth to facilitate the adherence of the accelerometer.

For practical reasons, the force was applied using a modal hammer to excite the beam with an impact directly next to node N6. For the test to be considered an OMA, only the output data was recorded during the test. The accelerometer was calibrated for a sampling frequency of 1024 Hz in the first test and was increased to 2048 Hz for the subsequent tests.

For this test, as there was only one accelerometer available, the test was performed in multiple runs, exciting the beam next to node N6 with an impact of a modal hammer and moving the accelerometer in between runs, from nodes N1 to N6. This is not ideal case as the forces being applied in the beam couldn't be recreated with a 100% accuracy, and as there was not a reference accelerometer a posterior data processing was necessary to improve the results of the mode shapes obtained.

After completing the six runs, the output data was processed and exported to perform the OMA on the software MATLAB® OoMA Toolbox and Siemens® Simcenter Testlab 2306 with the only differences being the exclusion of the N4SID method in the OoMA Toolbox and the addition of the Operational PolyMAX plugin for the Simcenter Testlab 2306 software. After that, the same steps followed in the previous section of the validation were performed and the modal parameters were extracted for their posterior analysis. Figure 4.8 shows some steps of the OMA test.

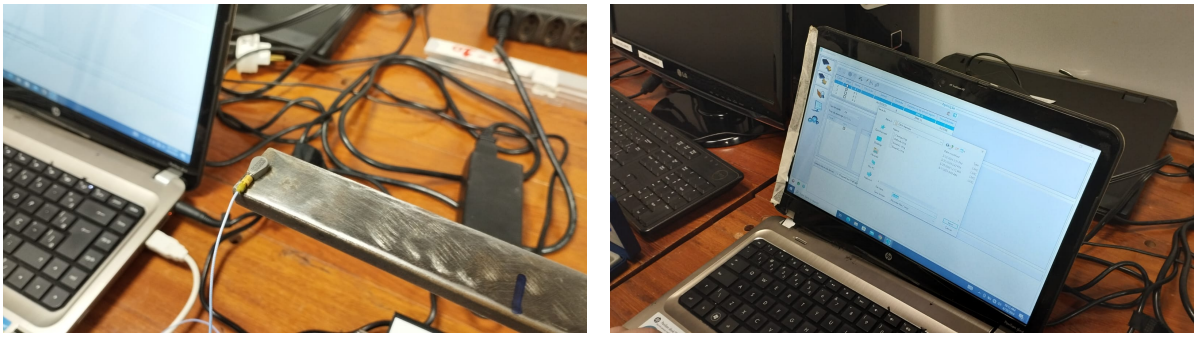

(a) Accelerometer positioned on node N6 (b) Data acquisition

Figure 4.8: OMA Test Performed on the SCB

4.2 OMA on Different Structures

With the validation of the OMA process followed in section 4.1, the second part of the work was to apply the OMA techniques into different structures to assess their modal parameters. It was decided that the process would be performed on four different structures:

1. Aluminum cantilever beam - **ACB**.
2. Steel free-free beam - **SFFB**.
3. Barbie aerodesign structure from the 'Mamutes do Cerrado' competition team - **BARBIE**.
4. Hyarra drone structure from the 'EDRA' competition team - **HYARRA**.

The process followed for this second part of the work can be seen below in figure 4.9.

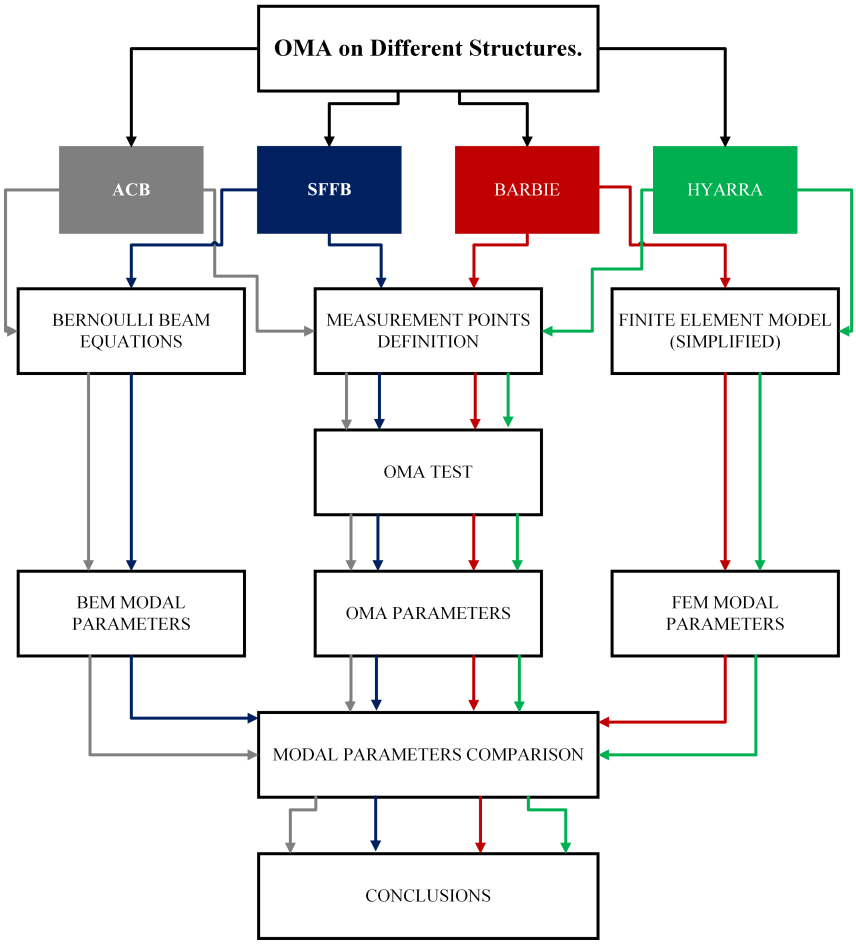

Figure 4.9: Process followed to perform the OMA on different structures.

4.2.1 Case Study - Aluminum Cantilever Beam (ACB)

The first structure chosen to be analyzed after the SCB was an aluminum cantilever beam (ACB). This was done to observe if the material of the structure affected the OMA results in any way. The model for the ACB can be seen in figure 4.10 below. Where the an isometric view model of the ACB (fig. 4.10b) and the dimensions are shown.

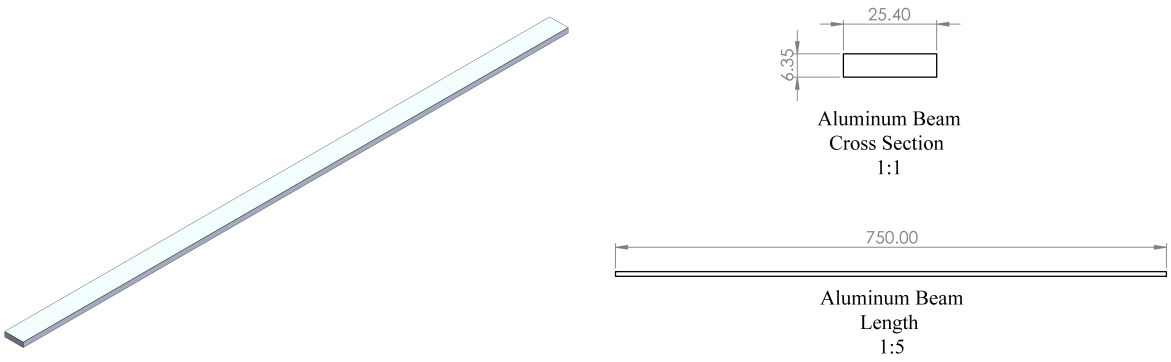

(a) ACB model. (b) ACB dimensions.

Figure 4.10: Aluminum Cantilever Beam (ACB)

Analytical Modes of the ACB

To have results for a comparison, the analytical modal parameters of the ACB were obtained through the use of the Euler-Bernoulli equations, presented in equations 4.1 and 4.2. The parameters of the ACB can be seen below in table 4.2.

Table 4.2: ACB parameters used.

Aluminum Cantilevered Beam Parameters	
Young Modulus [E]	70 GPa
Density [ρ]	2700 Kg
Length [L]	0.600 m
Height [h]	0.00635 m
Width [b]	0.0254 m
Inertia [I_x]	5.41968E-10 m^4

With these parameters it was possible to obtain the first six natural frequencies and mode shapes for the ACB.

OMA Test

The procedure followed for the OMA test, including the definition of the measurement points was the exact same one as with the SCB tests, therefore it won't be explained again here.

4.2.2 Case Study - Steel Free-Free Beam (SFFB)

The second structure analyzed via OMA tests was the steel beam used for the SCB test, but now in a free-free boundary condition. This structure was used to observe if the boundary condition had an effect on the modal parameters obtained with OMA. The model of the Steel Free-Free Beam (SFBB) can be seen below in figure 4.11a. Figure 4.11b shows the measurement points defined for this system as well as the dimensions of the beam.

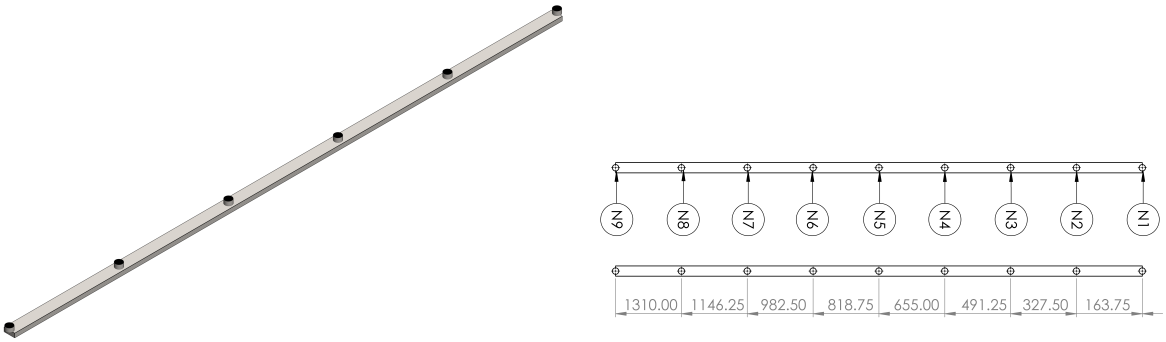

(a) Steel Free-Free Beam (SFBB) Model (b) SFFB Measuring Points

Figure 4.11: Steel Free-Free Beam

The only parameter that changed to those presented in table 4.1 was the length of the beam, which now is of $L = 1.310m$.

Analytical Modal Parameters

Before performing the OMA test, the analytical modes for the beam were calculated using the Bernoulli Equations to have parameters for a comparison. The natural frequencies were obtained from eq. 4.1 in which the only parameter changed was β_n for the correct values for the free-free condition.

The mode shapes were obtained through the use of the following equation:

$$\varphi = \cosh \beta_n x + \cos \beta_n x - \sigma_n(\sinh \beta_n x + \sin \beta_n x) \tag{4.3}$$

In the same fashion as with the SCB the final step of the analytical analysis of the SFFB was to plot the mode shapes using the MATLAB® Vtoolbox.

OMA Test

For the OMA test, the SFFB was secured in place by fastening nylon cables on two points of the beam, supported on a steel frame to recreate the free-free condition. The test was performed on 9 total runs, measuring the response of the beam in each node to an excitation caused by an impact on the beam. The procedure followed after the collection of the data was the same as with the SCB.

4.2.3 Case Study - Mamutes' Barbie Aerodesign (BARBIE)

The third structure analyzed via OMA tests was the Mamutes' Aerodesign "Barbie". A model of this aerodesign can be seen below in figure 4.12a. The aerodesing consisted of five principal sections: fuselage, left wing, right wing, tail-boom and tail. It was decided that for the OMA, the plane would be divided following these main sections, from which the measurement points were determined as seen in figure 4.12c.

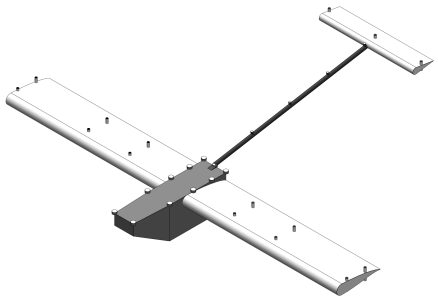

(a) Barbie Model

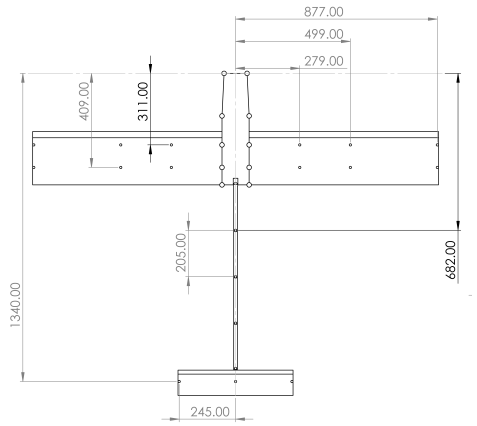

(b) Barbie Dimensions Points

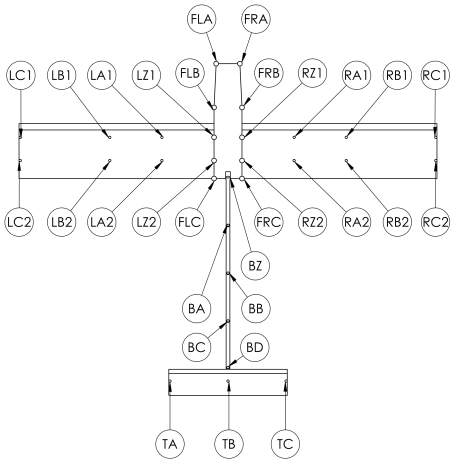

(c) Barbie Measurement Points

Figure 4.12: Mamutes' Barbie AeroDesign

To perform the test, it was decided that the plane would be tested in a free-free position to recreate the vibration during flight. This was possible by securing the fuselage of the plane to a steel frame using nylon cables. However, to avoid the plane from moving erratically due to it being suspended in the air, it was decided that the propeller would be removed from the motor of the plane. These steps can be seen below in figure 4.13.

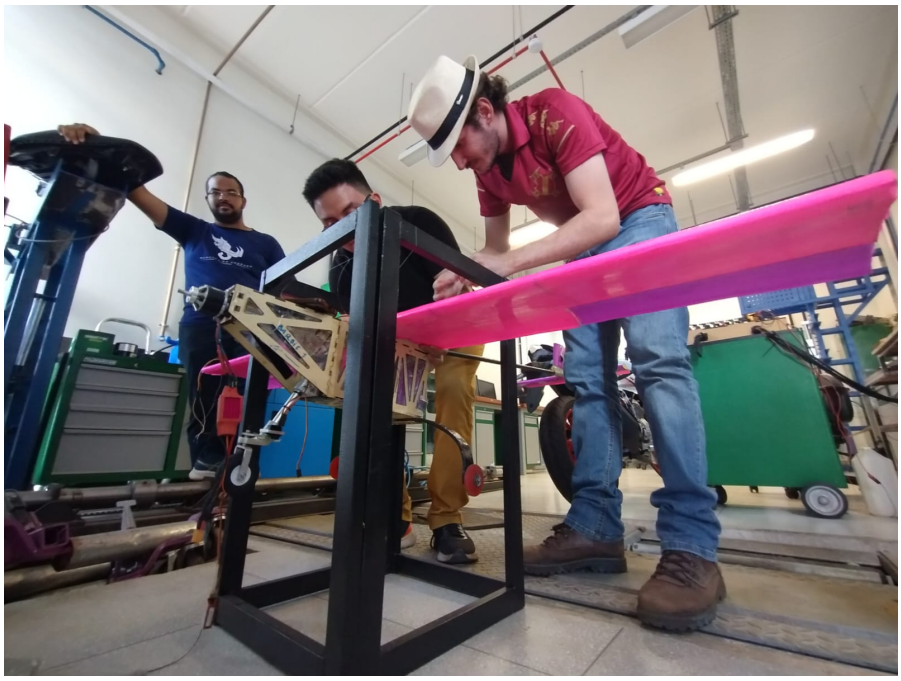

Figure 4.13: Barbie suspended in the air by nylon cables. To avoid frontal movement of the plane, the propeller was removed from the plane's motor.

After that, the motor was turned on to create vibration through the body of the plane and the measurements were recorded. These measurements were performed after 5 seconds of turning on the motor, to avoid transient effects, and the motor was kept running for an additional of 8 seconds. The measurements recorded were done with a total of 15 seconds to have enough data available during the post-processing. This procedure was repeated in every node for a total of 19 measurements. The procedure afterwards followed the same as with the SCB, ACB and SFFB.

Performing the OMA on the Barbie Aerodesign turned out to be a very complex procedure due to the number of measuring points, surface in which the accelerometer were placed and dimensions of the structure. Additionally, as only one accelerometer was available additional difficulties were found when processing the data, as there were no accelerometers in points of reference.

4.2.4 Case Study - EDRA's Hyarra Drone (HYARRA)

The final structure analyzed via OMA tests was the EDRA's Hyarra Drone structure. A model of the drone can be seen below in figure 4.14a. The dimensions and measurement points decided for this structure can also be seen in figure 4.14b and 4.14c respectively.

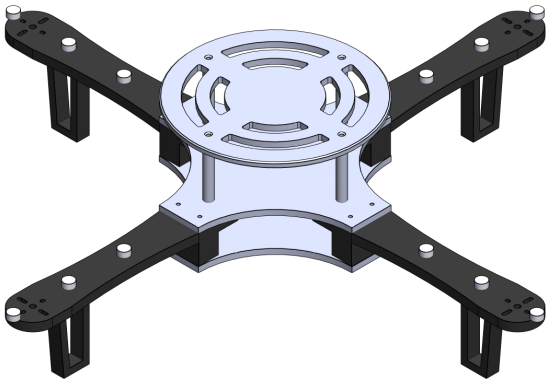

(a) Hyarra Structure

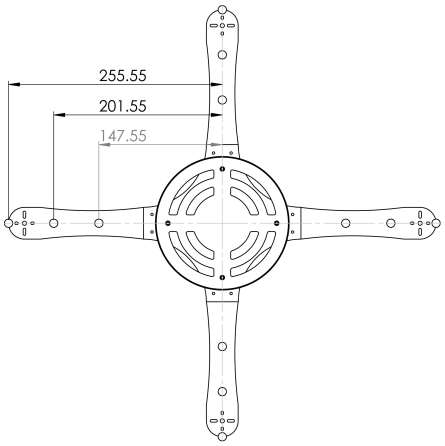

(b) Dimensions of the drone where the measurement points were localized.

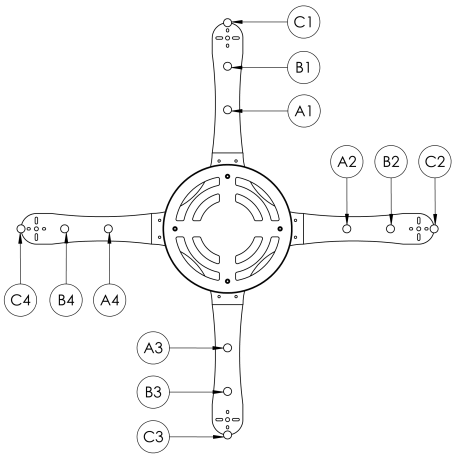

(c) Measurement points used.

Figure 4.14: EDRA's Structure

To perform the test, the drone main frame was secured to a steel structure to prevent the drone from flying and potentially causing any type of damage of the testing equipment or endanger people in the testing site. Only one propeller was used during the test despite using the four motors, originally, two propellers would be used for the test, however for technical problems with the electronic speed control (ESC) of one of the motors only one

of the propellers was used.

For the test, a different acquisition procedure was followed, in which the measured input consisted in the first five seconds of operation of the drone motors, but this time including the transient input of the motor start. The rest of the procedure was the same one followed for previous OMA tests and thus will not be discussed again. Figure 4.15 shows some of the steps followed during the test.

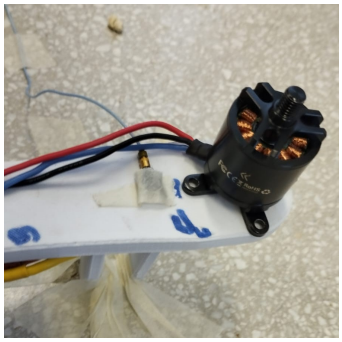

(a) Accelerometer placement on the drone arms.

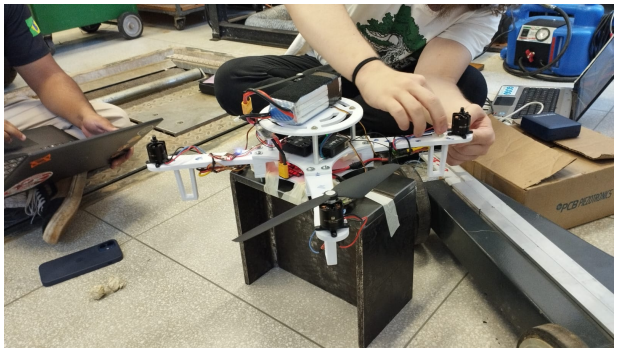

(b) Fixation of the drone.

(c) EDRA's Hyarra Drone.

Figure 4.15: OMA testing of the EDRA's Hyarra Drone.

CHAPTER 5

RESULTS

This chapter encompass all the results obtained during this work. As mentioned previously in chapter 4, the work was divided into two main parts, the first one consisting in the validation of the OMA process being implemented using a steel cantilever beam (SCB) model as the basis for the analysis; and the second part consisted in the application of the OMA techniques previously validated into more complex structures comparing the modal parameters obtained in the OMA tests with analytical or FEM modal parameters from the complex structures.

5.1 OMA Validation

The OMA validation process was divided into four parts:

1. Analytical modal parameters.
2. Simulated modal analysis.
3. Simulated OMA.
4. OMA tests on the SCB.

5.1.1 Analytical Modes

The first six analytical bending modes in the XY-plane for the SCB model were obtained through the use of the Euler-Bernoulli equations. The natural frequencies obtained are

shown in table 5.1 and their corresponding mode shapes can be seen in figure 5.1.

Natural Frequency (ω_n)

The XY-Plane bending natural frequencies obtained using the Euler-Bernoulli equations (eq. 4.1) are presented below in table 5.1.

Table 5.1: First six XY-bending modes from the SCB obtained with the Euler-Bernoulli equations.

Analytical Cantilever Beam Bending Modes Euler-Bernoulli Equations		
Mode	ω_n **[rad/s]**	f_n **[Hz]**
1	130.6230	20.7893
2	818.6003	130.2843
3	2292.1046	364.7998
4	4491.6103	714.8620
5	7424.9536	1181.7181
6	11091.5952	1765.2822

Mode Shapes (φ)

The mode mode shapes obtained analytically from the Euler-Bernoulli equations presented (eq. 4.2) were plotted with the assistance of MATLAB® *Vibration Toolbox*. The resulting mode shapes can be seen below in figure 5.1.

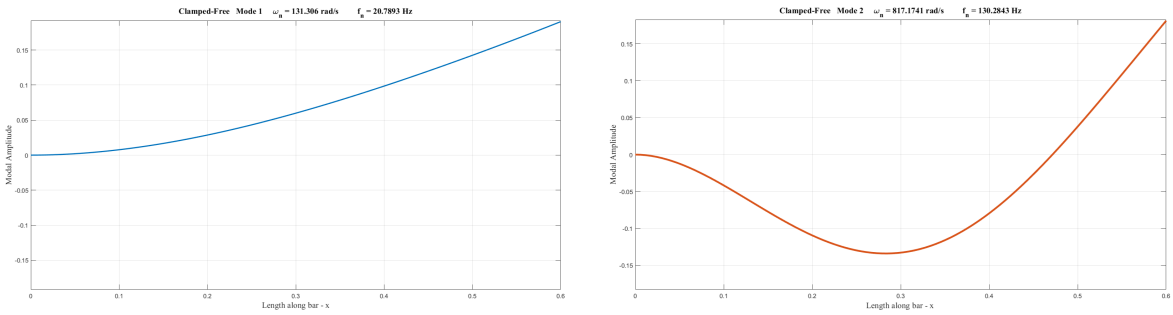

(a) Bending Mode 1 - 20.7893 Hz (b) Bending Mode 2 - 130.2843 Hz

Figure 5.1: Analytical Mode Shapes

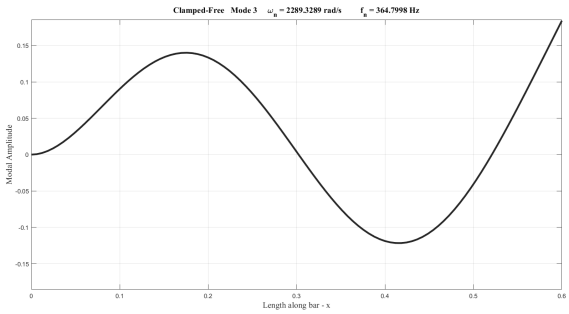

(c) Bending Mode 3 - 364.7998 Hz

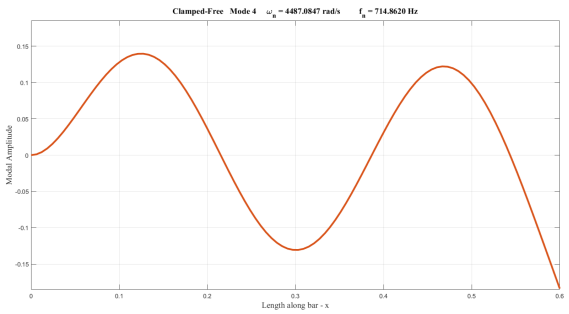

(d) Bending Mode 4 - 714.8620 Hz

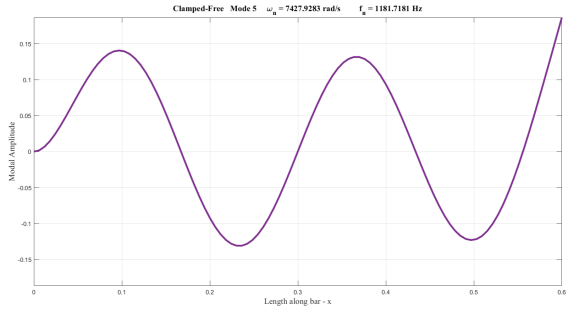

(e) Bending Mode 5 - 1181.7181 Hz

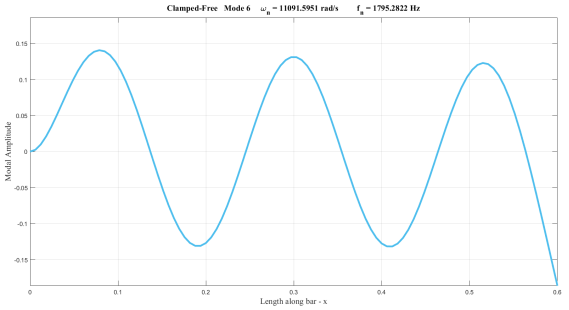

(f) Bending Mode 6 - 1765.2822 Hz

Figure 5.1: Analytical Mode Shapes

5.1.2 Simulated Modal Analysis

The modal parameters obtained from the modal simulation performed in the software *ANSYS® Mechanical* using a BEM of the SCB are presented in this section.

Natural Frequencies (ω_n)

The first six XY-plane bending mode natural frequencies are presented in table 5.2 below.

Table 5.2: First six bending mode natural frequencies obtained from the modal simulation performed in *ANSYS® Mechanical*

Steel Cantilever Beam Bending Modes ANSYS® Mechanical		
Mode	ω_n **[rad/s]**	f_n **[Hz]**
1	135.5974	21.5810
2	849.4238	135.1900
3	2385.5370	379.6700
4	4731.7412	753.0800
5	8052.5303	1281.6000
6	12840.9458	2043.7000

Mode Shapes

The corresponding mode shapes obtained in *ANSYS® Mechanical* can be seen in figure 5.2 below.

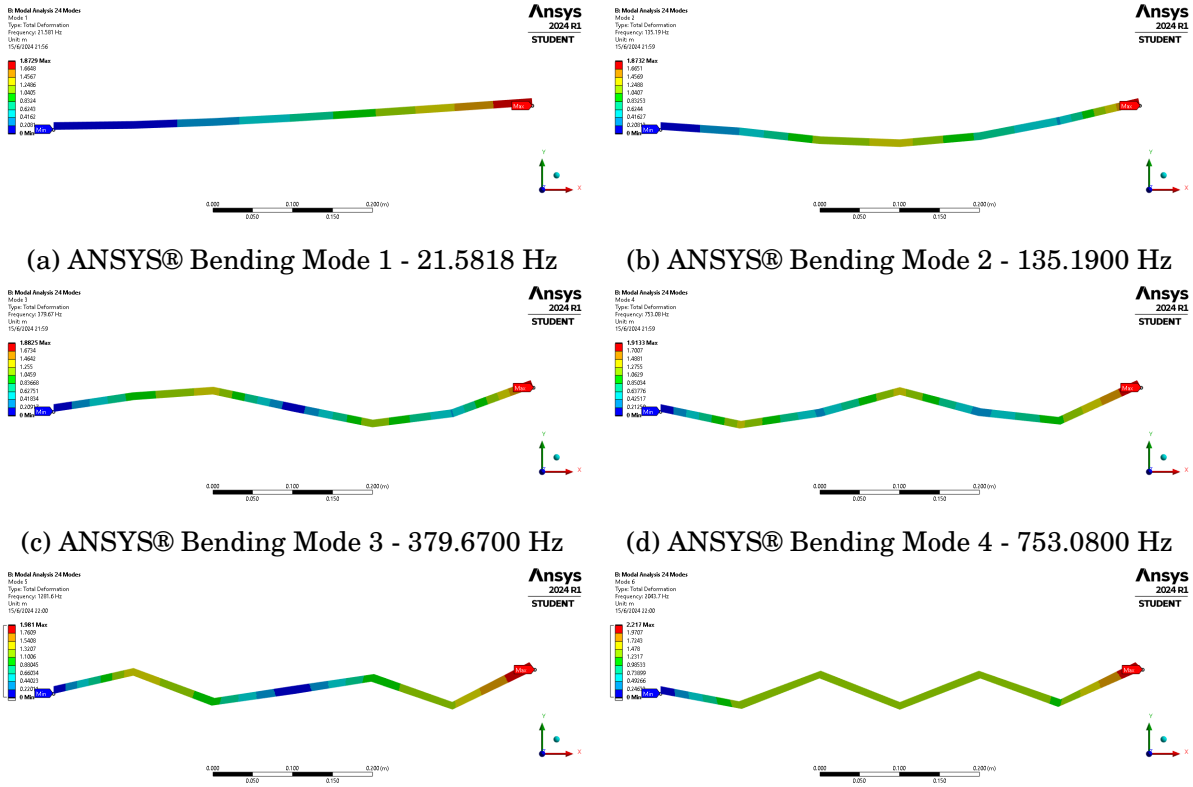

(a) ANSYS® Bending Mode 1 - 21.5818 Hz

(b) ANSYS® Bending Mode 2 - 135.1900 Hz

(c) ANSYS® Bending Mode 3 - 379.6700 Hz

(d) ANSYS® Bending Mode 4 - 753.0800 Hz

(e) ANSYS® Bending Mode 5 - 1281.6000 Hz

(f) ANSYS® Bending Mode 6 - 2043.7000 Hz

Figure 5.2: ANSYS® Bending Mode Shapes.

Observing the natural frequencies values obtained in table 5.2, it is possible to see that there is a slight difference in the values obtained with respect to the analytical modal parameters (tab. 5.1) that increases progressively. This can be better seen below in table 5.3.

These differences in values could be explained due to the material used in *ANSYS Mechanical* to perform the modal simulation. For the analytical modes, the material used was the steel AISI 1020, as it is one of the most common types of steel available. However *ANSYS Mechanical* doesn't have this specific type of steel, instead the *Structural Steel* option was used, as it has similar properties to the AISI 1020 steel. These differences could cause an effect that is small in lower frequency modes, but makes itself more apparent as the frequency increases, thus explaining this progressive difference between analytical and simulated natural frequencies.

Table 5.3: Natural frequency differences between analytical and simulated results.

Analytical vs ANSYS Modes			
Mode	**Analytical f_n [Hz]**	**ANSYS f_n**	**E. [to Analytical]**
1	20.7893	21.5810	3.8082%
2	130.2843	135.1900	3.7654%
3	364.7998	379.6700	4.0763%
4	714.8620	753.0800	5.3462%
5	1181.7181	1281.6000	8.4523%
6	1765.2822	2043.7000	15.7719

5.1.3 ANSYS® TRANSIENT SIMULATIONS

The results from the OMAs performed using the results from transient simulations are shown in this section. The transient simulations performed on *ANSYS Mechanical* used two different forces: **1.** Impulse 100 N in the +Y direction, and **2.** white noise with $\sigma = 3N$ and an mean value of 0 N, both forces applied at the free-tip of the beam.

As mentioned in chapter 4, the simulations were performed doubling the value of the sampling frequency, from $f_s = 1024Hz$ up to $f_s = 8192Hz$ to observe the effects that this parameter would produce in the modal parameters obtained with the OMAs. Thus, a total of 8 simulations were performed (4 using the impulse force and 4 with white noise force) whose results can be seen in the following sections.

5.1.3.1 MATLAB OoMA Toolbox Results

This section encompasses all the results obtained from the transient simulations performed in ANSYS Mechanical using the software MATLAB OoMA Toolbox.

MATLAB® OoMA Toolbox - Impulse Transient Simulations Modal Parameters

Table 5.4 present the OMA modal parameters (natural frequencies ω_n and damping ratios ζ) obtained with the software MATLAB OoMA Toolbox for the four impulse transient simulations.

Table 5.4: Modal parameters for the Impulse Transient Simulations obtained with the MATLAB® OoMA Toolbox.

ANSYS Transient - MATLAB OoMA Toolbox Results						
Impulse 1024 Hz box						
	N4SID M.O. 6		SSI-COV M.O. 6		SSI-DATA M.O. 6	
Mode	f_n [Hz]	ζ [%]	f_n [Hz]	ζ [%]	f_n [Hz]	ζ [%]
1	21.5503	1.0669	21.5502	1.0680	21.5504	1.0240
2	128.1375	1.0904	128.1475	1.0890	128.1424	1.0850
3	280.7796	0.9029	280.7648	0.9040	281.0169	0.9480
4	-	-	-	-	-	-
5	-	-	-	-	-	-
6	-	-	-	-	-	-
Impulse 2048 Hz						
	N4SID M.O. 18		SSI-COV M.O. 10		SSI-DATA M.O. 10	
Mode	f_n [Hz]	ζ [%]	f_n [Hz]	ζ [%]	f_n [Hz]	ζ [%]
1	21.5731	1.0158	21.5641	1.3020	21.5748	1.0477
2	133.2936	1.0732	133.3001	1.0830	133.3017	1.0712
3	343.7878	1.0647	343.8060	1.0660	343.8270	1.0619
4	558.8521	0.9106	558.8780	0.9100	558.9164	0.9061
5	717.2266	0.7300	717.1997	0.7100	719.1498	0.7722
6	-	-	-	-	-	-
Impulse 4096 Hz						
	N4SID M.O. 14		SSI-COV M.O. 14		SSI-DATA M.O. 18	
Mode	f_n [Hz]	ζ [%]	f_n [Hz]	ζ [%]	f_n [Hz]	ζ [%]
1	21.5791	1.0083	21.5322	3.499	21.5322	3.4986
2	134.7025	1.0444	134.7175	1.090	134.7175	1.0895
3	369.4421	1.0852	369.4709	1.096	369.4709	1.0957
4	682.8953	1.0657	682.9522	1.070	682.9522	1.0675
5	1012.7636	0.9599	1012.8677	0.9600	1012.8677	0.9566
6	1307.5918	0.8064	1307.6999	0.8000	1307.6999	0.7993
Impulse 8192 Hz						
	N4SID M.O. 18		SSI-COV M.O. 19		SSI-DATA M.O. 18	
Mode	f_n [Hz]	ζ [%]	f_n [Hz]	ζ [%]	f_n [Hz]	ζ [%]
1	21.5805	1.0042	21.5808	1.0036	21.5805	1.0041
2	135.0636	1.0241	135.0636	1.0241	135.0636	1.0241
3	377.0127	1.0579	377.0127	1.0579	377.0127	1.0579
4	733.1144	1.0850	733.1146	1.0850	733.1146	1.0850
5	1191.1278	1.0795	1191.1278	1.0795	1191.1278	1.0795
6	1733.3578	1.0166	1733.3579	1.0166	1733.3579	1.0166

Natural Frequency (f_n) error in relation to analytical results.

By analyzing the results shown in table 5.4 it was possible to see that the sampling

frequency used during the simulations had a significant impact on the modal parameters obtained, as it affected how many modes were possible to be found and the precision of the modes in relation to the analytical values. However if this effect was produced due to an aliasing effect created during the transient simulations or if its a flaw in the OMA methods is unknown at this point. Table 5.5 better illustrates the error between the modal parameters obtained in relation to the analytical natural frequencies calculated.

Table 5.5: Analytical vs Impulse Transient Simulations MATLAB OoMA Toolbox Modal Parameters

Analytical vs Impulse Simulations MATLAB OoMA Toolbox							
IMPULSE 1024 Hz							
M	**A.**	**N4SID**		**SSI-COV**		**SSI-DATA**	
	f_n **[Hz]**	f_n **[Hz]**	**E. [to An.]**	f_n **[Hz]**	**E. [to An.]**	f_n **[Hz]**	**E. [to An.]**
1	20.7893	21.55	-3.66%	21.55	-3.66%	21.55	-3.66%
2	130.2843	128.14	1.65%	128.15	1.64%	128.14	1.64%
3	364.7998	280.78	23.03%	280.76	23.04%	281.02	22.97%
IMPULSE 2048 Hz							
M	**A.**	**N4SID**		**SSI-COV**		**SSI-DATA**	
	f_n **[Hz]**	f_n **[Hz]**	**E. [to An.]**	f_n **[Hz]**	**E. [to An.]**	f_n **[Hz]**	**E. [to An.]**
1	20.7893	21.57	-3.77%	21.56	-3.73%	21.57	-3.78%
2	130.2843	133.29	-2.31%	133.30	-2.31%	133.30	-2.32%
3	364.7998	343.79	5.76%	343.81	5.75%	343.83	5.75%
4	714.8620	558.85	21.82%	558.88	21.82%	558.92	21.81%
5	1181.7181	717.23	39.31%	717.20	39.31%	719.15	39.14%
IMPULSE 4096 Hz							
M	**A.**	**N4SID**		**SSI-COV**		**SSI-DATA**	
	f_n **[Hz]**	f_n **[Hz]**	**E. [to An.]**	f_n **[Hz]**	**E. [to An.]**	f_n **[Hz]**	**E. [to An.]**
1	20.7893	21.58	-3.80%	21.53	-3.57%	21.58	-3.83%
2	130.2843	134.70	-3.39%	134.72	-3.40%	134.71	-3.40%
3	364.7998	369.44	-1.27%	369.47	-1.28%	369.44	-1.27%
4	714.8620	682.90	4.47%	682.95	4.46%	682.88	4.47%
5	1181.7181	1012.76	14.30%	1012.87	14.29%	1012.96	14.28%
6	1765.2822	1307.59	25.93%	1307.70	25.92%	1308.03	25.90%

Table 5.5: Analytical vs Impulse Transient Simulations MATLAB OoMA Toolbox Modal Parameters

IMPULSE 8192 Hz							
M	**A.**	**N4SID**		**SSI-COV**		**SSI-DATA**	
	f_n **[Hz]**	f_n **[Hz]**	**E. [to An.]**	f_n **[Hz]**	**E. [to An.]**	f_n **[Hz]**	**E. [to An.]**
1	20.7893	21.58	-3.81%	21.58	-3.81%	21.58	-3.81%
2	130.2843	135.06	-3.67%	135.06	-3.67%	135.06	-3.67%
3	364.7998	377.01	-3.35%	377.01	-3.35%	377.01	-3.35%
4	714.8620	733.11	-2.55%	733.11	-2.55%	733.11	-2.55%
5	1181.7181	1191.13	-0.80%	1191.13	-0.80%	1191.13	-0.80%
6	1765.2822	1733.36	1.81%	1733.36	1.81%	1733.36	1.81%

The suspected aliasing effect is more visible comparing the results obtained from a single OMA method. Table 5.6 shows the natural frequencies and error relative to analytical values obtained with the SSI-DATA method for all four simulations. Modes 2 and 5 were chosen to show how the error percentage improved as the sampling frequency was increased.

Table 5.6: The aliasing effect can be seen in the values for the natural frequencies obtained.

Analytical vs Impulse Transient Simulations SSI-DATA Aliasing Effects due to Sampling Frequency (f_s)								
M	**IMP 1024 Hz**		**IMP 2048 Hz**		**IMP 4096 Hz**		**IMP 8192 Hz**	
	f_n **[Hz]**	**E. [to An.]**	f_n **[Hz]**	**E. [to An.]**	f_n **[Hz]**	**E. [to An.]**	f_n **[Hz]**	**E. [to An.]**
1	21.55	-3.66%	21.57	-3.78%	21.58	-3.83%	21.58	-3.81%
2	128.14	1.64%	133.30	-2.32%	134.71	-3.40%	135.06	-3.67%
3	281.02	22.97%	343.83	5.75%	369.44	-1.27%	377.01	-3.35%
4	-	-	558.92	21.81%	682.88	4.47%	733.11	-2.55%
5	-	-	719.15	39.14%	1012.96	14.28%	1191.13	-0.80%
6	-	-	-	-	1308.03	25.90%	1733.36	1.81%

The results shown seen in tables 5.5 and 5.6 showed that the measurements obtained from the transient simulations presented an aliasing effect. This can be more clearly seen in figure 5.3 where the PSD functions of the sixth node for all impulse simulations were plotted. The most probable cause for this aliasing is that it was created for an unknown reason inside ANSYS Mechanical itself. This aliasing effect was decreased by increasing the sampling frequency, which allowed for all methods to converge to stable values.

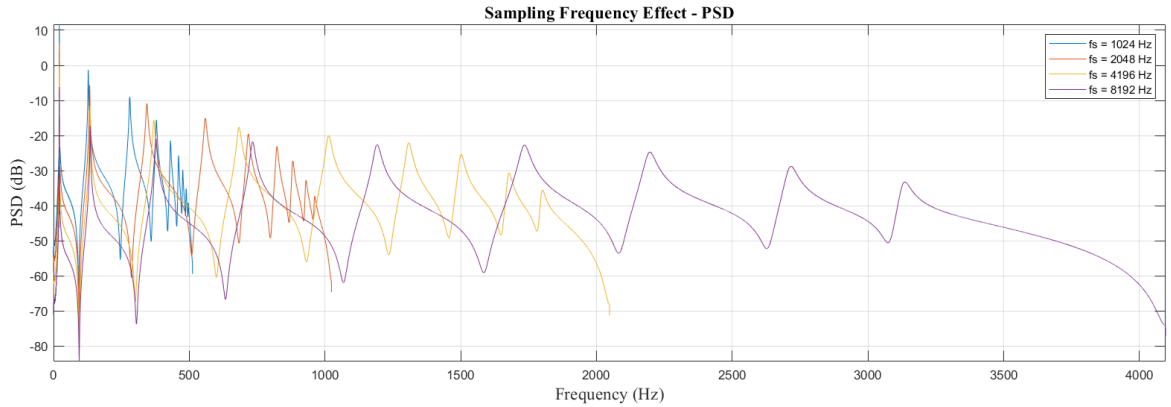

Figure 5.3: Aliasing effect in PSD for the Impulse Simulations.

Finally, it is worth noting that in table 5.4 it is possible to see that the values for the damping ratios (ζ) in all simulations and for all methods were very good as they all were very close to the $\zeta = 1\%$ set in the configurations for the simulation.

MATLAB® OoMA Toolbox - Impulse Transient Simulations Mode Shapes

As all mode shapes between the methods available in the OoMA Toolbox presented extremely similar shapes, only the mode shapes from the SSI-DATA method will be presented here for the OoMA Toolbox. The complete set of mode shapes can be found in the appendix from this work.

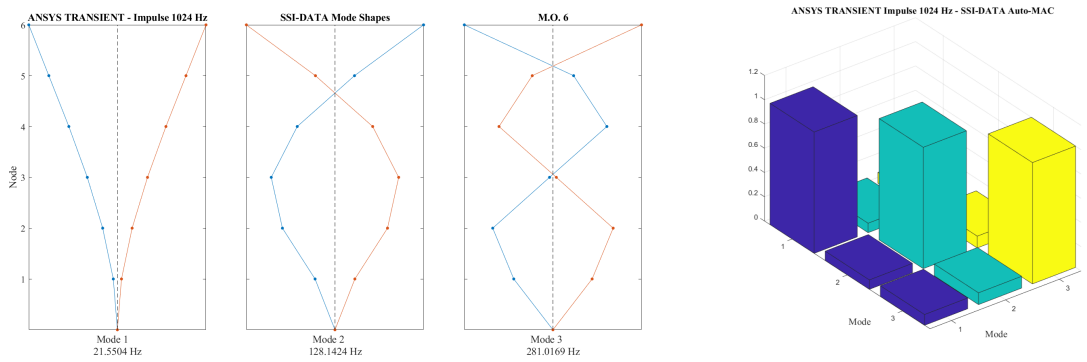

(a) Impulse Transient Simulation - 1024 Hz SSI-DATA Mode Shapes and Auto-MAC

Figure 5.4: Impulse Transient Simulations Mode Shapes - MATLAB OoMA Toolbox

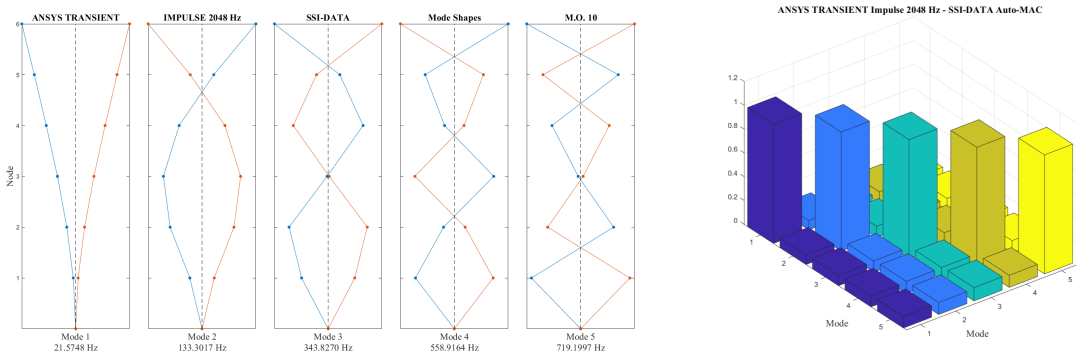

(b) Impulse Transient Simulation - 2048 Hz SSI-DATA Mode Shapes and Auto-MAC

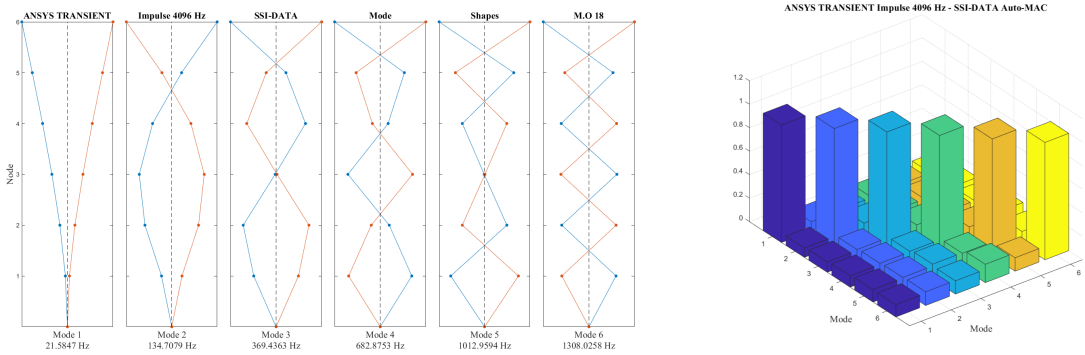

(c) Impulse Transient Simulation - 4096 Hz SSI-DATA Mode Shapes and Auto-MAC

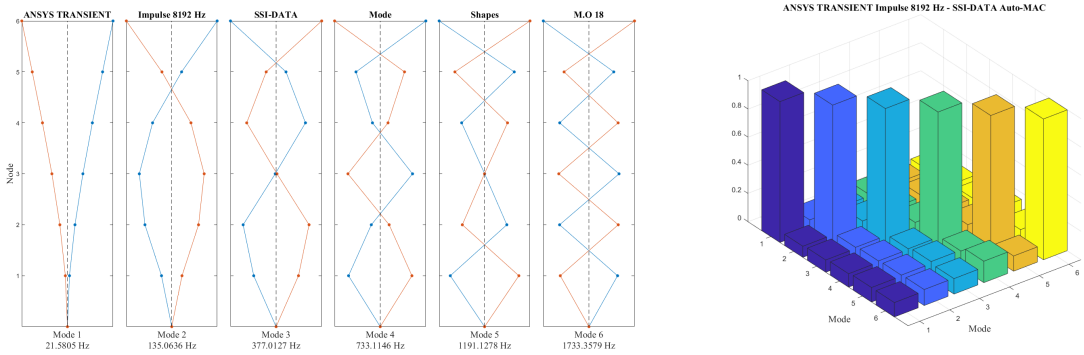

(d) Impulse Transient Simulation - 8192 Hz SSI-DATA Mode Shapes and Auto-MAC

Figure 5.4: Impulse Transient Simulations Mode Shapes - MATLAB OoMA Toolbox

MATLAB® OoMA Toolbox - White Noise Transient Simulations Modal Parameters.

The second force applied in the SCB model was a white noise force with a standard deviation of 3N and an average of 0N. The force was chosen to be very weak to partially simulate the effect that a strong wind would have on the SCB. As with the impulse simulation, a total of four simulations were performed with the white noise force, increasing

the sampling frequency. The modal parameters obtained from this simulations using the software MATLAB OoMA Toolbox can be seen in table 5.7. It is possible to see that the results for the damping ratios for all methods were fairly good as all were close to the expected $\zeta = 1\%$ that was chosen in the simulation parameters.

However, by analyzing the values of the natural frequencies and comparing them to the analytical results, it is possible to see that the same aliasing effect present in the impulse simulations is also present across all white noise simulations (tab. 5.8), indicating an intrinsically problem with the measurements obtained from ANSYS Mechanical.

Table 5.7: Modal parameters for the White Noise Transient Simulation obtained with MATLAB® OoMA Toolbox.

ANSYS Transient - MATLAB OoMA Toolbox Results						
White Noise 1024 Hz box						
	N4SID M.O. 20		SSI-COV M.O. 6		SSI-DATA M.O. 6	
Mode	f_n [Hz]	ζ [%]	f_n [Hz]	ζ [%]	f_n [Hz]	ζ [%]
1	21.5713	1.1278	21.5602	1.498	21.6346	1.0350%
2	128.0684	1.0841	127.7851	1.011	128.0508	0.9929%
3	280.4988	0.8359	280.7880	0.869	280.6383	0.7596%
4	-	-	-	-	-	-
5	-	-	-	-	-	-
6	-	-	-	-	-	-
White Noise 2048 Hz box						
	N4SID M.O. 19		SSI-COV M.O. 12		SSI-DATA M.O. 12	
Mode	f_n [Hz]	ζ [%]	f_n [Hz]	ζ [%]	f_n [Hz]	ζ [%]
1	21.5778	1.0807	21.6086	1.3960%	21.7100	1.8500
2	133.2892	1.0458	133.3753	1.0458%	133.5337	1.0248
3	343.9856	1.1447	344.2786	1.1669%	344.4732	1.0525
4	558.8754	0.8622	558.4837	0.8080%	559.1297	0.7376
5	717.3088	0.7191	716.9409	0.7008%	717.4144	0.6204
6	-	-	-	-	-	-
White Noise 4096 Hz box						
	N4SID M.O. 20		SSI-COV M.O. 14		SSI-DATA M.O. 18	
Mode	f_n [Hz]	ζ [%]	f_n [Hz]	ζ [%]	f_n [Hz]	ζ [%]
1	21.7661	0.5852	21.6016	3.2057	21.6781	5.7285
2	134.6969	1.1458	134.6391	1.2816	135.0739	1.2580
3	369.3733	1.2220	369.4187	1.1889	369.8718	1.1845
4	682.8821	1.1390	683.1326	1.1806	683.7325	1.0747
5	1012.6790	0.9123	1012.9655	0.9427	1013.5700	0.8389
6	1307.3945	0.7757	1307.4006	0.7999	1308.2541	0.7038

Table 5.7: Modal parameters for the White Noise Transient Simulation obtained with MATLAB® OoMA Toolbox.

White Noise 8192 Hz box						
	N4SID M.O. 24		SSI-COV M.O. 25		SSI-DATA M.O. 25	
Mode	f_n [Hz]	ζ [%]	f_n [Hz]	ζ [%]	f_n [Hz]	ζ [%]
1	22.0741	1.0042	21.3690	0.3746	21.4475	0.9793
2	134.9978	1.0241	134.9901	1.0771	135.0036	1.0702
3	376.6308	1.0579	376.6757	1.1473	376.6290	1.1247
4	732.8250	1.0850	732.4011	1.1114	732.6609	1.1369
5	1191.7548	1.0795	1192.8160	0.7120	1173.8219	0.5179
6	1733.0536	1.0166	1717.8138	1.0524	1725.6081	1.1574%

An interesting difference between the impulse and transient simulations results, performed in the OoMA Toolbox is the model order of resolution necessary to solve the system. In the white noise simulation, as there is much more noise present in the signals, the model orders necessary are much higher when compared to those used in the impulse simulations. Table 5.8 shows the error relative to the analytical natural frequencies.

Table 5.8: Analytical vs White Noise Transient Simulations in MATLAB OoMA Toolbox Modal Parameters

Analytical vs White Noise Transient Simulations SIEMENS Simcenter Testlab 2306							
WHITE NOISE 1024 Hz							
M	**Analytical** f_n **[Hz]**	**N4SID**		**SSI-COV**		**SSI-DATA**	
		f_n **[Hz]**	**E. [to An.]**	f_n **[Hz]**	**E. [to An.]**	f_n **[Hz]**	**E. [to An.]**
1	20.7893	21.57	-3.76%	21.56	-3.71%	21.63	-4.07%
2	130.2843	128.07	1.70%	127.79	1.92%	128.05	1.71%
3	364.7998	280.50	23.11%	280.79	23.03%	280.64	23.07%
WHITE NOISE 2048 Hz							
M	**Analytical** f_n **[Hz]**	**N4SID**		**SSI-COV**		**SSI-DATA**	
		f_n **[Hz]**	**E. [to An.]**	f_n **[Hz]**	**E. [to An.]**	f_n **[Hz]**	**E. [to An.]**
1	20.7893	21.58	-3.79%	21.61	-3.94%	21.71	-4.43%
2	130.2843	133.29	-2.31%	133.38	-2.37%	133.53	-2.49%
3	364.7998	343.99	5.71%	344.28	5.63%	344.47	5.57%
4	714.8620	558.88	21.82%	558.48	21.88%	559.13	21.78%
5	1181.7181	717.31	39.30%	716.94	39.33%	717.41	39.29%

Table 5.8: Analytical vs White Noise Transient Simulations in MATLAB OoMA Toolbox Modal Parameters

WHITE NOISE 4096 Hz							
M	**Analytical** f_n **[Hz]**	**N4SID** f_n **[Hz]**	**N4SID E. [to An.]**	**SSI-COV** f_n **[Hz]**	**SSI-COV E. [to An.]**	**SSI-DATA** f_n **[Hz]**	**SSI-DATA E. [to An.]**
1	20.7893	21.77	-4.70%	21.60	-3.91%	21.68	-4.28%
2	130.2843	134.70	-3.39%	134.64	-3.34%	135.07	-3.68%
3	364.7998	369.37	-1.25%	369.42	-1.27%	369.87	-1.39%
4	714.8620	682.88	4.47%	683.13	4.44%	683.73	4.35%
5	1181.7181	1012.68	14.30%	1012.97	14.28%	1013.57	14.23%
6	1765.2822	1307.39	25.94%	1307.40	25.94%	1308.25	25.89%
WHITE NOISE 8192 Hz							
M	**Analytical** f_n **[Hz]**	**N4SID** f_n **[Hz]**	**N4SID E. [to An.]**	**SSI-COV** f_n **[Hz]**	**SSI-COV E. [to An.]**	**SSI-DATA** f_n **[Hz]**	**SSI-DATA E. [to An.]**
1	20.7893	22.07	-6.18%	21.37	-2.79%	21.45	-3.17%
2	130.2843	135.00	-3.62%	134.99	-3.61%	135.00	-3.62%
3	364.7998	376.63	-3.24%	376.68	-3.26%	376.63	-3.24%
4	714.8620	732.83	-2.51%	732.40	-2.45%	732.66	-2.49%
5	1181.7181	1191.75	-0.85%	1192.82	-0.94%	1173.82	0.67%
6	1765.2822	1733.05	1.83%	1717.81	2.69%	1725.61	2.25%

As with the impulse simulations, table 5.9 shows the effect of the sampling frequency in the modal parameters obtained, showing once again that by increasing the sampling frequency is possible to obtain more accurate results.

Table 5.9: The aliasing effect in the modal parameters from the white noise simulations can be seen in the natural frequency values obtained.

Analytical vs White Noise Transient Simulations **SSI-DATA Aliasing Effects due to Sampling Frequency (f_s)**								
M	**WN 1024 Hz** f_n **[Hz]**	**WN 1024 Hz E. [to An.]**	**WN 2048 Hz** f_n **[Hz]**	**WN 2048 Hz E. [to An.]**	**WN 4096 Hz** f_n **[Hz]**	**WN 4096 Hz E. [to An.]**	**WN 8192 Hz** f_n **[Hz]**	**WN 8192 Hz E. [to An.]**
1	21.63	-4.07%	21.71	-4.43%	21.68	-4.28%	21.45	-3.17%
2	128.05	1.71%	133.53	-2.49%	135.07	-3.68%	135.00	-3.62%
3	280.64	23.07%	344.47	5.57%	369.87	-1.39%	376.63	-3.24%
4	-	-	559.13	21.78%	683.73	4.35%	732.66	-2.49%
5	-	-	717.41	39.29%	1013.57	14.23%	1173.82	0.67%
6	-	-	-	-	1308.25	25.89%	1725.61	2.25%

The effect can also be seen by plotting the PSD function of the sixth node for all the simulations, seen in figure 5.5.

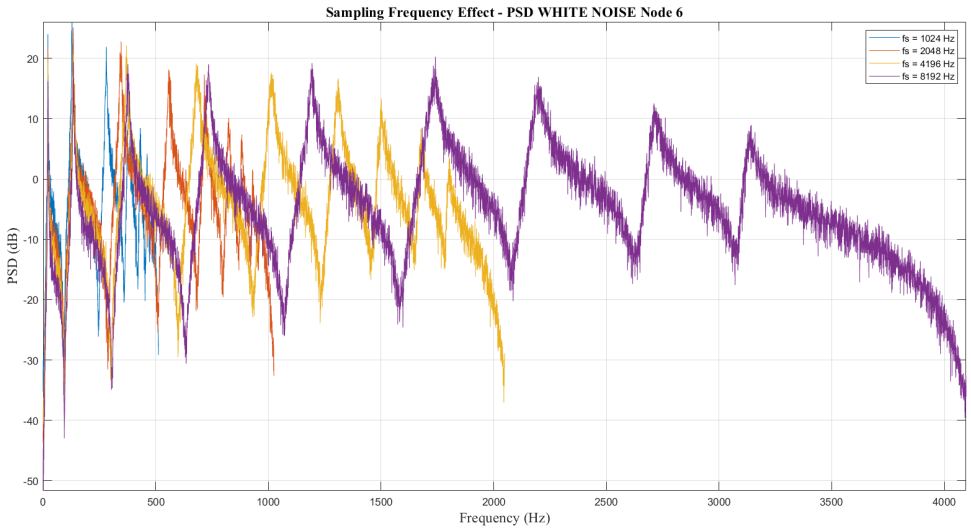

Figure 5.5: Alasing effect in the PSD for the White Noise Simulations.

MATLAB® OoMA Toolbox - White Noise Transient Simulations Mode Shapes

As all mode shapes between the methods available in the OoMA Toolbox presented extremely similar shapes, only the mode shapes from the SSI-DATA method will be presented here for the OoMA Toolbox. The complete set of mode shapes can be found in the appendix from this work.

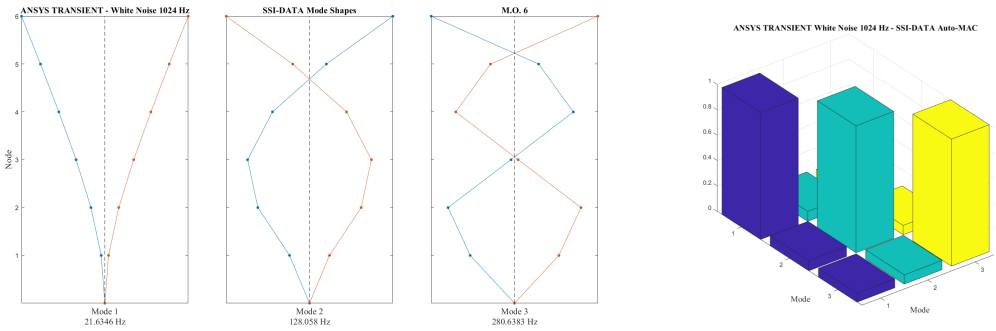

(a) White Noise Transient Simulation - 1024 Hz SSI-DATA Mode Shapes and Auto-MAC

Figure 5.6: White Noise Transient Simulations Mode Shapes - MATLAB OoMA Toolbox.

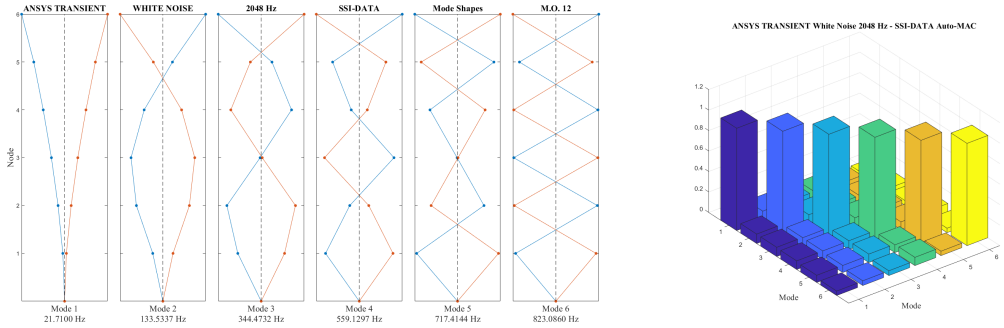

(b) White Noise Transient Simulation - 2048 Hz SSI-DATA Mode Shapes and Auto-MAC

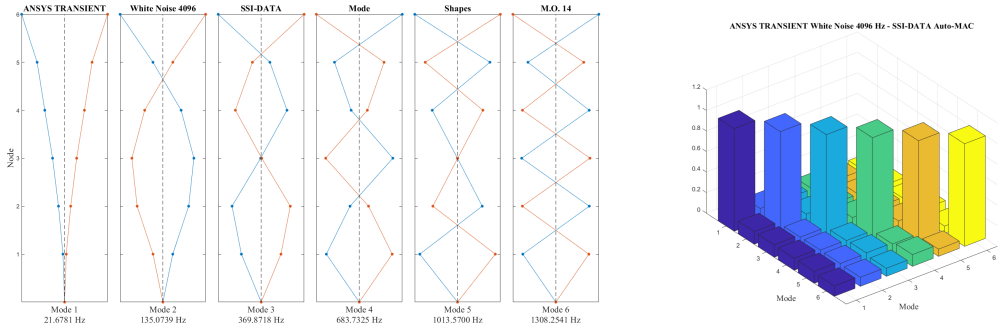

(c) White Noise Transient Simulation - 4096 Hz SSI-DATA Mode Shapes and Auto-MAC

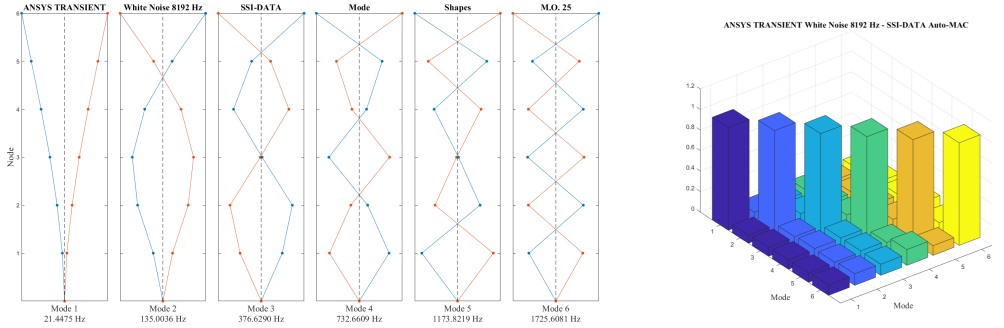

(d) White Noise Transient Simulation - 8192 Hz SSI-DATA Mode Shapes and Auto-MAC

Figure 5.6: White Noise Transient Simulations Mode Shapes - MATLAB OoMA Toolbox.

5.1.3.2 SIEMENS Simcenter Testlab 2306 Results

The OMA results obtained with the software SIEMENS Simcenter Testlab 2306, done from the data obtained from transient simulations can be seen below in table 5.10. Once again, it was possible to obtain very good results for the values of the damping ratios (ζ), whereas in the same fashion as with the OoMA Toolbox, the aliasing effect in the values of the natural frequencies obtained persisted despite using a different software, which strongly suggests that the problem is in the data itself rather than in the OMA methods.

Table 5.10: Modal Parameters obtained from the Transient Simulations with SIEMENS Simcenter Testlab 2306

Transient Simulations - SIEMENS Simcenter Testlab 2306 Results							
M.	**A.** f_n [Hz]	**Impulse 1024 Hz** f_n [Hz]	E. [to A.]	ζ	**White Noise 1024 Hz** f_n [Hz]	E. [to A.]	ζ
1	20.79	21.55	-3.65%	1.03%	21.58	-3.80%	1.52%
2	130.28	128.14	1.65%	1.09%	128.05	1.71%	1.10%
3	364.80	280.78	23.03%	0.91%	280.50	23.11%	0.83%
	A.	**Impulse 2048 Hz**			**White Noise 2048 Hz**		
1	20.79	21.57	-3.77%	1.01%	21.58	-3.81%	1.04%
2	130.28	133.29	-2.30%	1.07%	133.37	-2.37%	1.06%
3	364.80	343.77	5.76%	1.06%	344.42	5.59%	1.18%
4	714.86	588.83	17.63%	0.91%	558.21	21.91%	0.80%
5	1181.72	717.21	39.31%	0.73%	716.82	39.34%	0.72%
	A.	**Impulse 4096 Hz**			**White Noise 4096 Hz**		
1	20.79	21.46	-3.24%	0.85%	21.64	-4.07%	0.92%
2	130.28	134.70	-3.39%	1.04%	134.43	-3.18%	1.38%
3	364.80	369.42	-1.27%	1.09%	369.50	-1.29%	1.25%
4	714.86	682.86	4.48%	1.07%	683.89	4.33%	1.05%
5	1181.72	1012.72	14.30%	0.96%	1013.62	14.22%	1.01%
6	1765.28	1307.55	25.93%	0.81%	1306.06	26.01%	0.77%
	A.	**Impulse 8192 Hz**			**White Noise 8192 Hz**		
1	20.79	21.57	-3.76%	1.14%	21.47	-3.25%	3.49%
2	130.28	135.06	-3.66%	1.02%	135.13	-3.72%	0.89%
3	364.80	376.99	-3.34%	1.06%	376.82	-3.29%	1.26%
4	714.86	733.07	-2.55%	1.09%	733.17	-2.56%	1.18%
5	1181.72	1191.06	-0.79%	1.08%	1190.13	-0.71%	0.90%
6	1765.28	1733.29	1.81%	1.02%	1734.85	1.72%	0.91%

SIEMENS Simcenter Testlab 2306 - Mode Shapes

The mode shapes obtained with the Simcenter Testlab 2306 software can be seen below in figure 5.7 and 5.8. However, to simplify the visualization, only the mode shapes obtained with the simulations sampled at $f_n = 8192Hz$ will be shown in this section. The complete set of mode shapes can be seen in the appendix from this work. It is possible to see that the mode shapes are almost identical to the analytical (fig. 5.1) and simulated (fig 5.2) mode shapes.

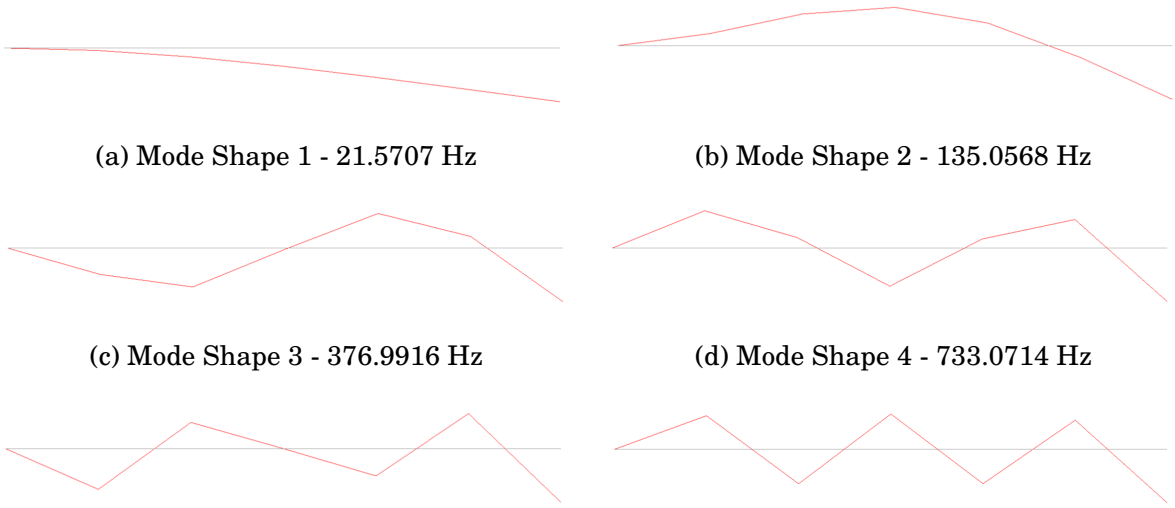

(a) Mode Shape 1 - 21.5707 Hz

(b) Mode Shape 2 - 135.0568 Hz

(c) Mode Shape 3 - 376.9916 Hz

(d) Mode Shape 4 - 733.0714 Hz

(e) Mode Shape 5 - 1191.0584 Hz

(f) Mode Shape 6 - 1733.2863 Hz

Figure 5.7: SIEMENS Simcenter Testlab - Impulse Simulation 8192 Hz - Mode Shapes.

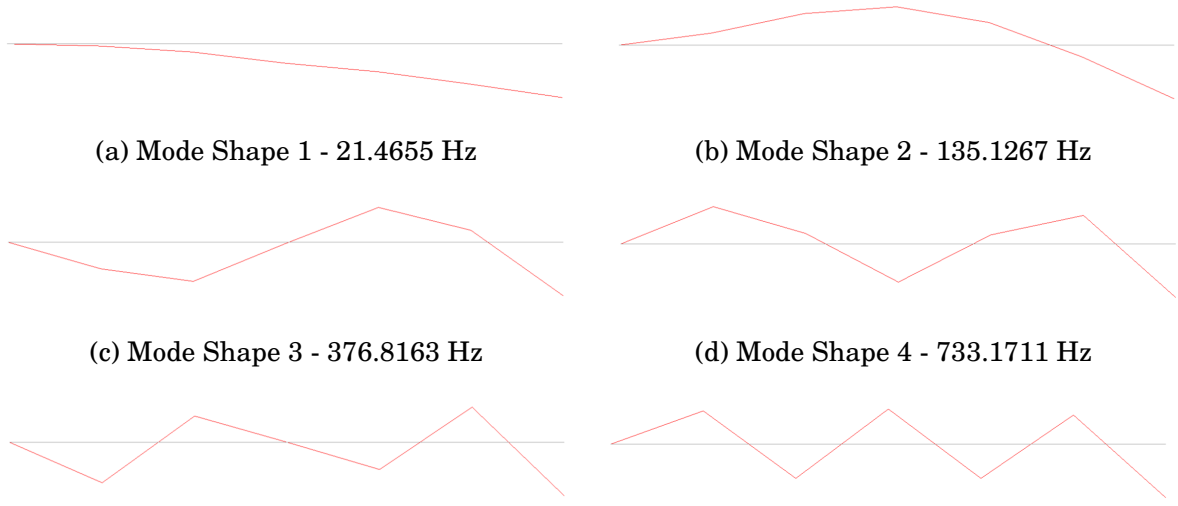

(a) Mode Shape 1 - 21.4655 Hz

(b) Mode Shape 2 - 135.1267 Hz

(c) Mode Shape 3 - 376.8163 Hz

(d) Mode Shape 4 - 733.1711 Hz

(e) Mode Shape 5 - 1190.1250 Hz

(f) Mode Shape 6 - 1734.8535 Hz

Figure 5.8: SIEMENS Simcenter Testlab - **White Noise** Simulation 8192 Hz - Mode Shapes.

5.1.4 OMA Performed on the SCB

The final step of the OMA validation process was performing an OMA on an actual steel cantilever beam (SCB), which was constructed for this work. Three different tests were

performed in the SCB to obtain the modal parameters using the software MATLAB® OoMA Toolbox and SIEMENS® Simcenter Testlab 2306.

5.1.4.1 SCB Test - May 14th, 2024

The first test was conducted on May 14th, 2024, with $f_n = 1024Hz$ and the total time-length of 02 seconds. With the measured data, the software MATLAB® OoMA Toolbox and SIEMENS® Simcenter Testlab 2306 were used to extract the modal parameters from the SCB, as shown in table 5.11 and figures 5.9 and 5.10.

Natural Frequencies and Damping Ratios

The modal parameters obtained from the OMA test performed on the SCB in May 14th, 2024 are shown below in table 5.11.

Table 5.11: Modal parameters from the OMA test performed on the SCB in 14/05/2024.

SCB Test - 14/05/2024							
MATLAB OoMA Toolbox							
M.	A.	SSI-COV M.O.22			SSI-DATA M.O.7		
	f_n [Hz]	f_n [Hz]	E. [to A.]	ζ	f_n [Hz]	E. [to A.]	ζ
1	20.79	19.21	-8.20%	1.85%	19.16	-8.48%	2.03%
2	130.28	124.16	-4.93%	1.50%	125.56	-3.76%	1.56%
3	364.80	334.62	-9.02%	-0.02%	347.44	-5.00%	0.22%
4	714.86	-	-	-	-	-	-
SIEMENS Simcenter Testlab 2306							
M.	A.	OMA			Op. PolyMAX		
	f_n [Hz]	f_n [Hz]	E. [to A.]	ζ	f_n [Hz]	E. [to A.]	ζ
1	20.79	19.25	-7.99%	1.50%	19.23	-8.11%	1.77%
2	130.28	124.15	-4.94%	1.47%	125.62	-3.71%	0.81%
3	364.80	347.76	-4.90%	0.17%	347.96	-4.84%	0.19%
4	714.86	-	-	-	-	-	-

Mode Shapes

The mode shapes obtained from the OMA test performed on the SCB in May 14th, 2024 are shown below in figures 5.9 and 5.10.

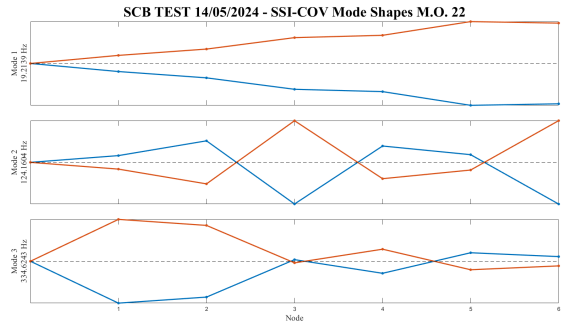

(a) SSI-COV Mode Shapes

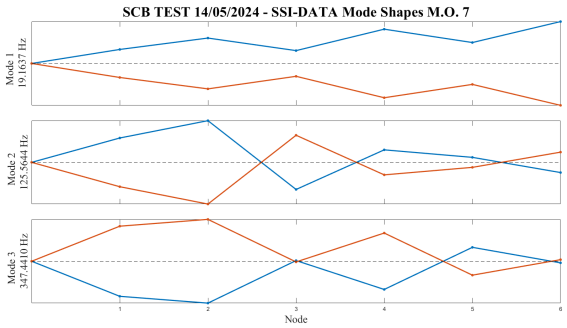

(b) SSI-DATA Mode Shapes

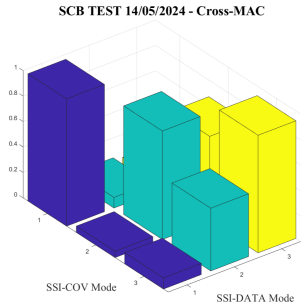

(c) OoMA Toolbox Cross-MAC

Figure 5.9: SCB Test 14/05/2024 - Mode Shapes obtained with the OoMA Toolbox.

(a) OMA MS1

(b) Op. PolyMAX MS1

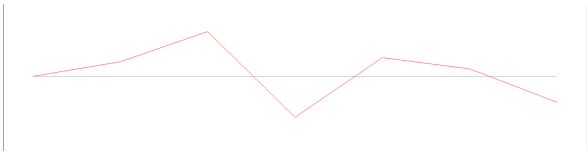

(c) OMA MS2

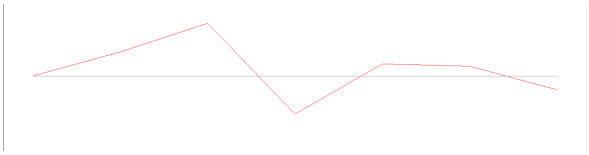

(d) Op. PolyMAX MS2

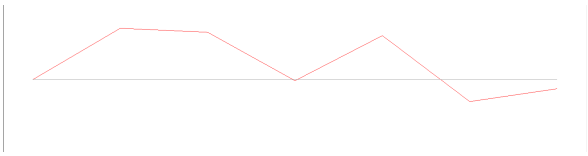

(e) OMA MS3

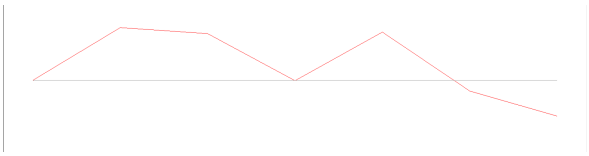

(f) Op. PolyMAX MS3

Figure 5.10: SCB Test 14/05/2024 - Mode Shapes obtained with the OoMA Toolbox.

By observing the values of the natural frequencies obtained during this test (tab. 5.11) it is possible to see that all the results were within an acceptable margin when compared

to analytical results. It is also worth mentioning that all the natural frequencies obtained showed slightly lower values than the analytical natural frequencies, suggesting that the actual natural frequencies of the SCB are lower than the values obtained analytically.

However, by looking at the mode shapes obtained (figs. 5.9, 5.10) it is possible to see that the mode shapes are considerably different from the ones expected analytically. Nonetheless, a problem found during this first OMA test was that the base of the cantilever system was not perfectly flat due to manufacturing defects, as a result the entire system slightly vibrated along with the beam, which impacted in the modal parameters obtained, particularly in the mode shapes. To guarantee more consistent results, two additional tests were performed on June 12th whose results can be seen in the following sections.

5.1.4.2 SCB Test - June 12th, 2024 - RUN 1

With corrections done in the cantilever system a second test was conducted on June 12th, 2024 with $f_n = 2048Hz$ and the total time-length of 10 seconds. For this test, as the measured data had a longer time-length, two different pre-processing criteria were applied. The total time-length of the filtered results was of 08 seconds and the results are presented in this section.

1st Filtering Process - Modal Parameters

Table 5.12: Modal parameters from the OMA test performed on the SCB in 12/06/2024 in the 1st run and 1st filtering process.

SCB Test - 12/06/2024 - Run 1 Filter 1							
MATLAB OoMA Toolbox							
M.	A.	SSI-COV M.O.24			SSI-DATA M.O.17		
	f_n [Hz]	f_n [Hz]	E. [to A.]	ζ	f_n [Hz]	E. [to A.]	ζ
1	20.79	19.18	-8.39%	0.70%	19.18	-8.38%	0.61%
2	130.28	133.46	2.38%	1.89%	134.77	3.33%	2.13%
3	364.80	351.02	-3.93%	0.14%	351.48	-3.79%	0.08%
4	714.86	682.10	-4.80%	0.12%	683.41	-4.60%	0.08%
SIEMENS Simcenter Testlab 2306							
M.	A.	OMA			Op. PolyMAX		
1	20.79	19.17	-8.45%	0.93%	19.21	-8.21%	0.57%
2	130.28	134.18	2.90%	2.09%	135.60	3.92%	2.38%
3	364.80	351.08	-3.91%	0.15%	351.00	-3.93%	0.09%
4	714.86	682.30	-4.77%	0.01%	683.92	-4.52%	0.50%

1st Filtering Process - Mode Shapes

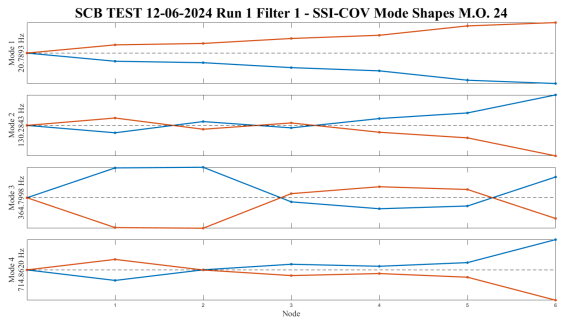

(a) SSI-COV Mode Shapes

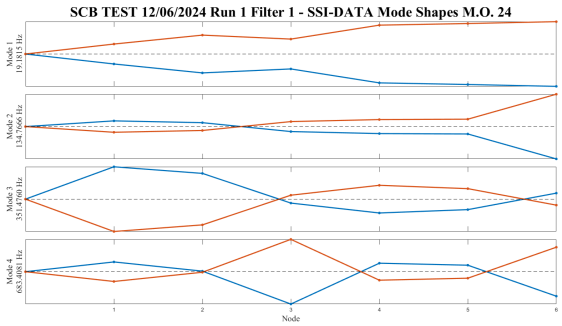

(b) SSI-DATA Mode Shapes

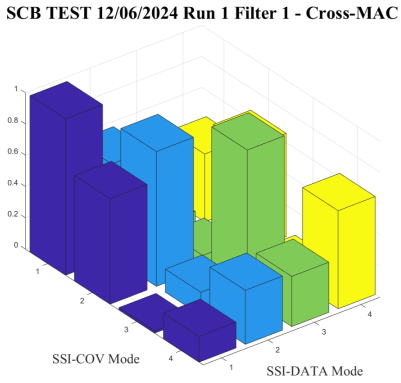

(c) OoMA Toolbox Cross-MAC

Figure 5.11: SCB Test 12/06/2024 Run 1 Filter 1 - Mode Shapes obtained with the OoMA Toolbox.

(a) OMA MS1

(b) Op. PolyMAX MS1

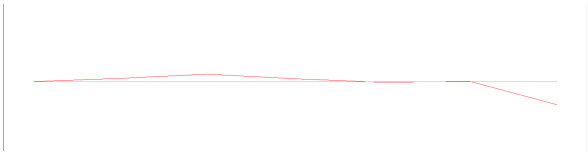

(c) OMA MS2

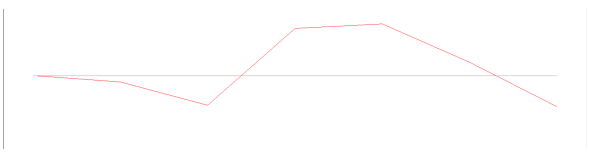

(d) Op. PolyMAX MS2

Figure 5.12: SCB Test 12/06/2024 Run 1 Filter 1 - Mode Shapes obtained with the OoMA Toolbox.

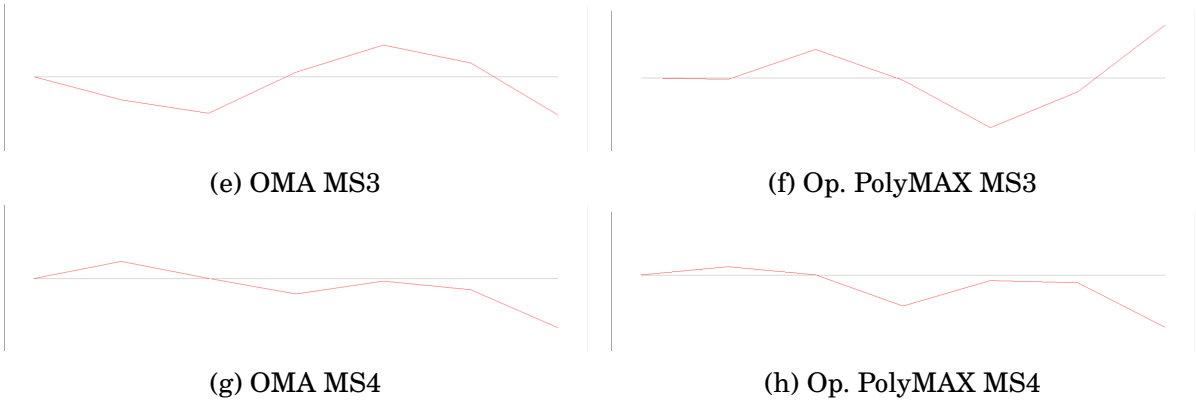

(e) OMA MS3 (f) Op. PolyMAX MS3

(g) OMA MS4 (h) Op. PolyMAX MS4

Figure 5.12: SCB Test 12/06/2024 Run 1 Filter 1 - Mode Shapes obtained with the Simcenter Testlab 2306.

An improvement in the mode shapes is clearly visible by observing figures 5.11 and 5.12, whereas the natural frequencies shown in table 5.12 shown very similar results to those obtained in the previous test.

2nd Filtering Process - Modal Parameters

The natural frequencies obtained with the 2nd filtering process can be seen below in table 5.13, where again very similar results to the previous tests were obtained.

Table 5.13: Modal parameters from the OMA test performed on the SCB in 12/06/2024 in the 1st run and 2nd filtering process.

SCB Test - 12/06/2024 - Run 1 Filter 2							
MATLAB OoMA Toolbox							
M.	A.	SSI-COV M.O.26			SSI-DATA M.O.18		
	f_n [Hz]	f_n [Hz]	E. [to A.]	ζ	f_n [Hz]	E. [to A.]	ζ
1	20.79	19.17	-8.46%	0.69%	19.20	-8.27%	0.69%
2	130.28	133.38	2.32%	1.95%	135.11	3.57%	2.14%
3	364.80	345.99	-5.44%	2.77%	351.07	-3.91%	0.27%
4	714.86	698.49	-2.34%	1.07%	681.90	-4.83%	0.26%
SIEMENS Simcenter Testlab 2306							
M.	A.	OMA			Op. PolyMAX		
	f_n [Hz]	f_n [Hz]	E. [to A.]	ζ	f_n [Hz]	E. [to A.]	ζ
1	20.79	19.20	-8.27%	0.95%	19.24	-8.07%	0.66%
2	130.28	133.19	2.18%	2.55%	136.20	4.34%	7.83%
3	364.80	350.98	-3.94%	0.13%	351.09	-3.91%	0.20%
4	714.86	681.85	-4.84%	0.12%	682.41	-4.76%	0.09%

2nd Filtering Process - Mode Shapes

The mode shapes obtained with both software can be seen below in figures 5.13 and 5.14.

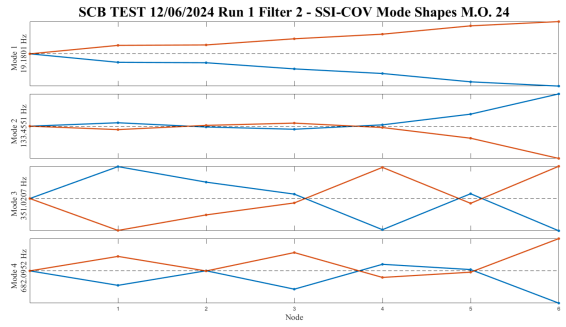

(a) SSI-COV Mode Shapes

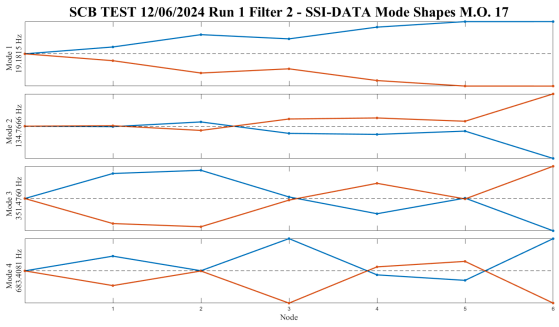

(b) SSI-DATA Mode Shapes

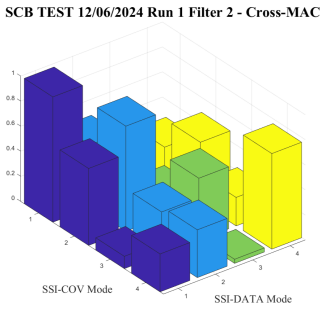

(c) OoMA Toolbox Cross-MAC

Figure 5.13: SCB Test 12/06/2024 Run 1 Filter 2 - Mode Shapes obtained with the OoMA Toolbox.

(a) OMA MS1

(b) Op. PolyMAX MS1

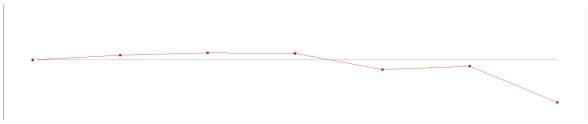

(c) OMA MS2

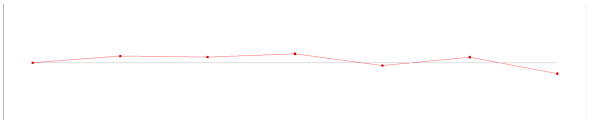

(d) Op. PolyMAX MS2

(e) OMA MS3

(f) Op. PolyMAX MS3

Figure 5.14: SCB Test 12/06/2024 Run 1 Filter 2 - Mode Shapes obtained with Simcenter Testlab 2306.

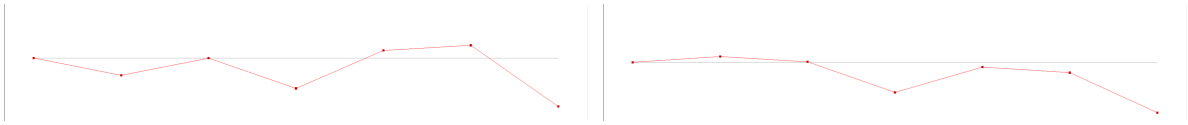

(g) OMA MS4 (h) Op. PolyMAX MS4

Figure 5.14: SCB Test 12/06/2024 Run 1 Filter 2 - Mode Shapes obtained with Simcenter Testlab 2306.

5.1.4.3 SCB Test - June 12th, 2024 - RUN 2

To further verify the modal parameters from the SCB, a third test was performed on June 12th, 2024. The test was a continuation of the previous test and will be called RUN 2 for reference. In the same fashion as the previous test, this one was also recorded at $f_s = 2048Hz$ and two filtering processes were also performed to have two data-sets with a time-length of 8 seconds.

1st Filtering Process - Modal Parameters

The modal parameters obtained for the 2nd run and 1st filtering process can be seen below in table 5.14 where once again, the natural frequencies founded showed slightly lower frequencies than those obtained analytically.

Table 5.14: Modal parameters from the OMA test performed on the SCB in 12/06/2024 in the 2nd run and 1st filtering process.

SCB Test - 12/06/2024 - Run 2 Filter 1							
MATLAB OoMA Toolbox							
M.	A.	SSI-COV M.O.20			SSI-DATA M.O.16		
	f_n [Hz]	f_n [Hz]	E. [to A.]	ζ	f_n [Hz]	E. [to A.]	ζ
1	20.79	19.17	-8.46%	0.52%	19.18	-8.42%	0.58%
2	130.28	133.89	2.69%	2.20%	134.47	3.11%	2.52%
3	364.80	363.66	-0.31%	2.12%	351.42	-3.81%	0.09%
4	714.86	658.64	-8.54%	1.15%	662.66	-7.88%	0.27%
SIEMENS Simcenter Testlab 2306							
M.	A.	OMA			Op. PolyMAX		
	f_n [Hz]	f_n [Hz]	E. [to A.]	ζ	f_n [Hz]	E. [to A.]	ζ
1	20.79	19.13	-8.65%	0.28%	19.23	-8.09%	0.59%
2	130.28	134.45	3.10%	1.84%	134.01	2.78%	2.24%
3	364.80	351.45	-3.80%	0.10%	350.99	-3.94%	0.13%
4	714.86	687.73	-3.94%	1.35%	682.21	-4.79%	0.10%

1st Filtering Process - Mode Shapes

The mode shapes obtained with the 1st filtering process can be seen below in figures 5.15 and 5.16

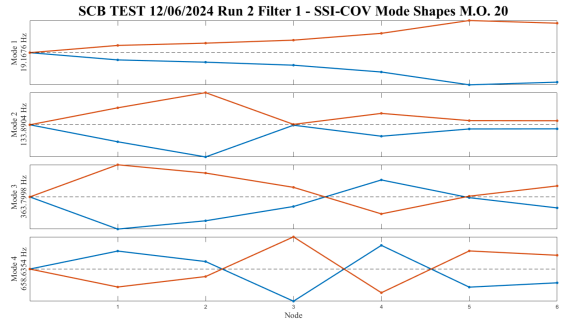

(a) SSI-COV Mode Shapes

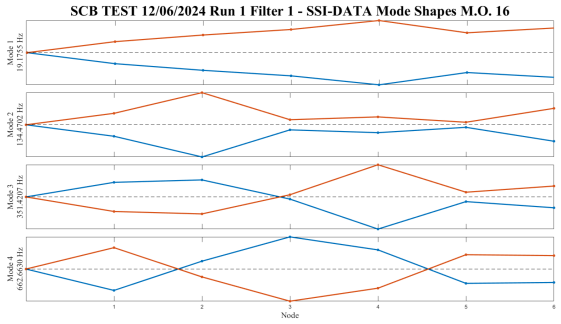

(b) SSI-DATA Mode Shapes

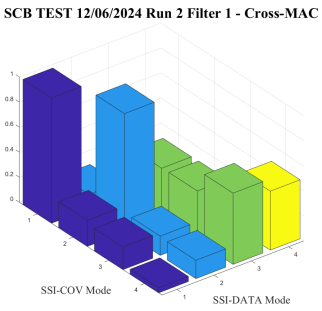

(c) OoMA Toolbox Cross-MAC

Figure 5.15: SCB Test 12/06/2024 Run 2 Filter 1 - Mode Shapes obtained with the OoMA Toolbox.

(a) OMA MS1

(b) Op. PolyMAX MS1

(c) OMA MS2

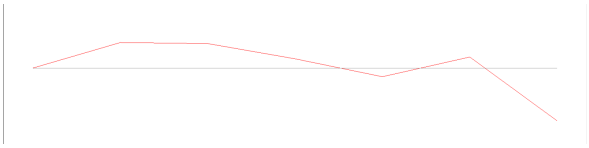

(d) Op. PolyMAX MS2

Figure 5.16: SCB Test 12/06/2024 Run 2 Filter 1 - Mode Shapes obtained with Simcenter Testlab 2306.

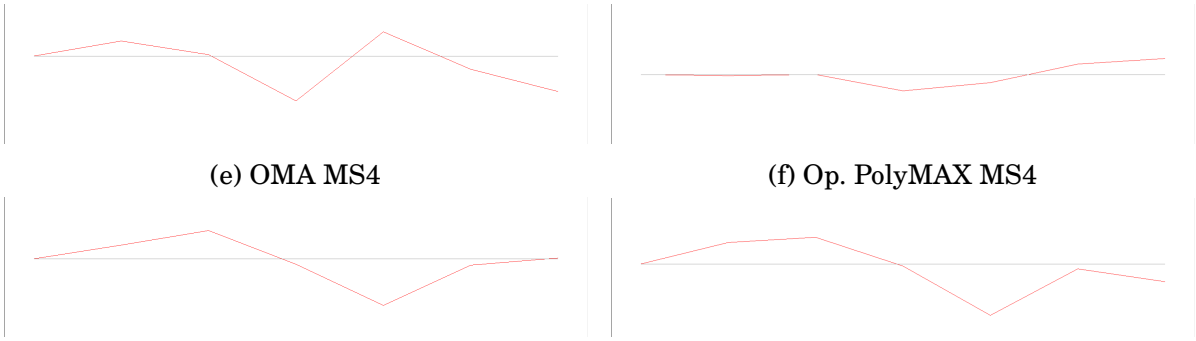

(e) OMA MS4 (f) Op. PolyMAX MS4

(g) OMA MS3 (h) Op. PolyMAX MS3

Figure 5.16: SCB Test 12/06/2024 Run 2 Filter 1 - Mode Shapes obtained with Simcenter Testlab 2306.

2nd Filtering Process - Modal Parameters

Finally, the modal parameters from the 2nd filtering process for RUN 2 can be seen below in table 5.15 where once again, natural the natural frequencies found showed lower values than the analytical values calculated.

Table 5.15: Modal parameters from the OMA test performed on the SCB in 12/06/2024 in the 2nd run and 2nd filtering process.

SCB Test - 12/06/2024 - Run 2 Filter 2							
MATLAB OoMA Toolbox							
M.	A.	SSI-COV M.O.20			SSI-DATA M.O.15		
	f_n [Hz]	f_n [Hz]	E. [to A.]	ζ	f_n [Hz]	E. [to A.]	ζ
1	20.79	19.19	-8.32%	0.62%	19.19	-8.31%	0.61%
2	130.28	133.98	2.76%	2.10%	134.64	3.23%	2.53%
3	364.80	350.02	-4.22%	1.63%	351.41	-3.81%	0.08%
4	714.86	653.92	-9.32%	2.81%	682.02	-4.82%	0.27%
SIEMENS Simcenter Testlab 2306							
M.	A.	OMA			Op. PolyMAX		
	f_n [Hz]	f_n [Hz]	E. [to A.]	ζ	f_n [Hz]	E. [to A.]	ζ
1	20.79	19.08	-8.98%	0.41%	19.24	-8.03%	0.56%
2	130.28	135.35	3.75%	2.46%	136.37	4.47%	2.15%
3	364.80	350.83	-3.98%	0.19%	350.67	-4.03%	0.22%
4	714.86	682.34	-4.77%	0.08%	654.26	-9.26%	0.50%

2nd Filtering Process - Mode Shapes

The mode shapes obtained with the 2nd filtering process for RUN 2 can be seen below in figures 5.17 and 5.18

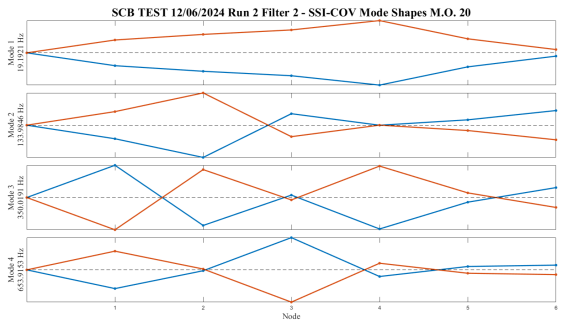

(a) SSI-COV Mode Shapes

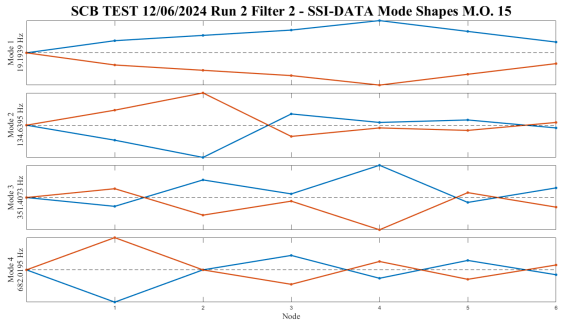

(b) SSI-DATA Mode Shapes

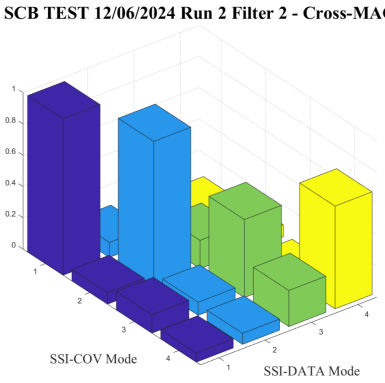

(c) OoMA Toolbox Cross-MAC

Figure 5.17: SCB Test 12/06/2024 Run 2 Filter 2 - Mode Shapes obtained with the OoMA Toolbox.

(a) OMA MS1

(b) Op. PolyMAX MS1

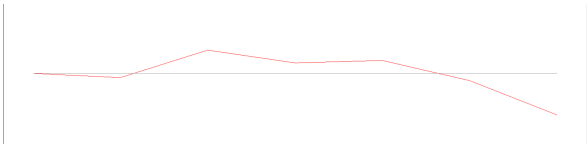

(c) OMA MS2

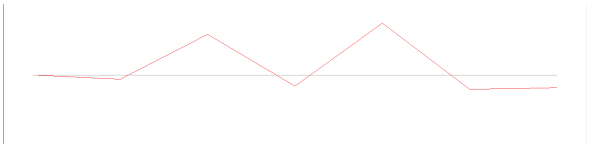

(d) Op. PolyMAX MS2

Figure 5.18: SCB Test 12/06/2024 Run 2 Filter 2 - Mode Shapes obtained with Simcenter Testlab 2306.

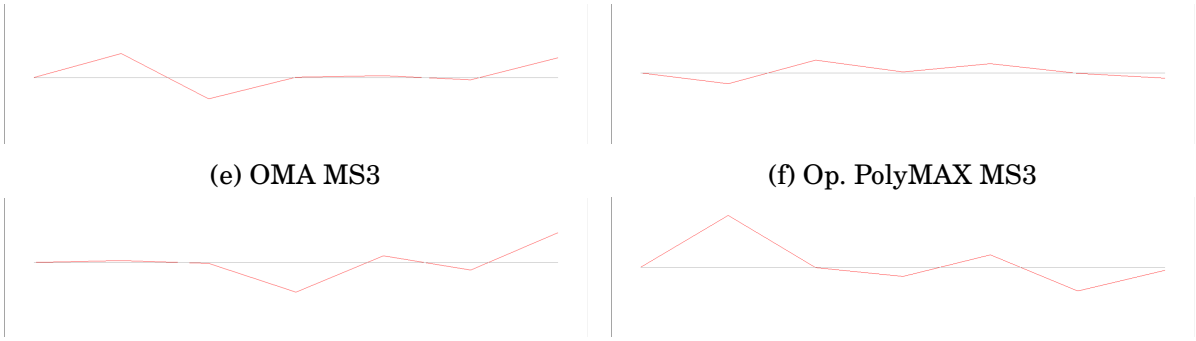

(e) OMA MS3 (f) Op. PolyMAX MS3

(g) OMA MS4 (h) Op. PolyMAX MS4

Figure 5.18: SCB Test 12/06/2024 Run 2 Filter 2 - Mode Shapes obtained with Simcenter Testlab 2306.

5.1.5 Final Remarks of the OMA Validation Process

The results obtained from the SCB OMA tests showed very consistent values for all natural frequencies and damping ratios calculated. This is especially useful as they strongly suggest that the actual modal parameters are slightly different from the ones obtained analytically, indicating one of two options:

1. That the Young modulus or the density of the steel beam being used are different from the AISI 1020 steel suspected.

2. That the cantilever system being used adds damping in the measurements, producing lower natural frequencies than the analytical ones.

To confirm any of these hypotheses, another test with different boundary conditions or a test of the cantilever system itself would be required.

Table 5.16 shows a comparison of the first six bending natural frequencies of the SCB using all all four validation methods. It is possible to see that the natural frequencies found were fairly consistent in relation with the analytical modes used as the basis for the validation process. Therefore, indicating that the OMA methods followed are adequate to obtain the natural frequencies and damping ratios of not only the SCB model used, but more complex structures as well.

However, the mode shapes obtained, although acceptable, did not always present the expected shapes when compared to the analytical mode shapes. Although there is an exceedingly high variety of reasons for this to have happened, four main reasons were identified during the tests:

1. Use of a single accelerometer

As stated by (BRINCKER; VENTURA, 2015), to perform an OMA in multiple runs

Table 5.16: OMA validation process results comparison.

OMA Validation Summary - Natural Frequencies: f_n (Hz)						
M.	**A.**	**Sim. Modal A.**	**Tran. IMP 8192 Hz Avg.**	**Tran. WN 8192 Hz Avg.**	**OMA Test 12/06 R1F1 Avg.**	**OMA Test 12/06 R2F1 Avg.**
1	20.79	21.58	21.57	21.47	19.19	19.18
2	130.28	135.19	135.06	135.13	134.50	134.20
3	364.80	379.67	376.99	376.82	351.14	354.378
4	714.86	753.08	733.07	733.17	682.93	672.81
5	1181.72	1281.60	1191.06	1190.13	-	-
6	1765.28	2043.70	1733.29	1734.85	-	-

(a test in which all the measurements are taken at separate times instead of being measured simultaneously) a minimum of two accelerometers are required to link the measurements obtained. However, as there was only one accelerometer available at the time the linking of the measured data had to be done manually. This is a problem, particularly for complex structures and high frequency modes as the manual linking can lead to spatial displacement problems in the mode shapes, which was seen in some of the mode shapes obtained.

2. Cantilever condition

Another problem that appeared during the tests was that the cantilever condition was not ideal, as the base of the beam presented irregularities not allowing a completely flat surface. As a result, the cantilever system vibrated simultaneously with the beam, which was enough to affect the measurements obtained.

3. Use of different forces.

As the test was performed in multiple runs, the force being applied in the structure varied between each run. Despite efforts were put in trying to recreate the forces the same for each run, this was not completely possible, causing some runs to have a higher magnitude of force being applied to the beam, which affected the resulting mode shape.

4. Discrepancies with the accelerometer

One final problem was found while pre-processing the data that was obtained from the accelerometer. In the measurements, it was found that the acquisition software started the measurements at slightly various times, causing a problem to link the measurements obtained. Further research regarding t the data-acquisition equipment is needed to solve this problem.

Overall, despite the difficulties experienced during the tests, the results obtained were satisfactory as they calculated with all the modal parameters expected for the SCB

withing an acceptable margin of error.

5.2 OMA Tests

With the OMA validation completed, other cases were also analyzed applying the OMA techniques to extract the modal parameters from four different structures:

1. Aluminum Cantilever Beam

2. Steel Free-Free Beam

3. Mamutes' Barbie Aerodesign

4. EDRA's Hyarra Drone

The results can be seen in the following sections.

5.2.1 Case Study: Aluminum Cantilever Beam (ACB)

The first structure analyzed after the OMA validation process was an aluminum cantilever beam (ACB), that was fixated in the same cantilever system used during the validation process. The reason for choosing this structure was to determine if the material of the structure being analyzed had any impact in the modal parameters founded with the OMA methods. The aluminum beam properties used for this structure can be seen below in table 5.17.

Table 5.17: Aluminum cantilever beam properties.

Aluminum Cantilever Beam Properties			
Parameter	**Symbol**	**Magnitude**	**Unit**
Young Modulus	E	7.00E+10	Pa
Width	b	0.0254	m
Height	h	0.00635	m
Length	l	0.6	m
Inertia	I	5.41968E-10	m^4
Density	ρ	2700	kg/m^3

Analytical Modal Parameters

In the same fashion as with the SCB, analytical modal parameters were calculated for the ACB using the Euler-Bernoulli equations, to have parameters for a comparison. The analytical natural frequencies founded for the ACB can be seen below in table 5.18.

Table 5.18: ACB - Analytical Modal Parameters

Aluminum Cantilever Beam Theoretical Analysis	
Mode	f_n [Hz]
1	14.5842
2	90.7640
3	254.2771
4	498.3830
5	825.0242

Analytical Mode Shapes

The mode shapes, obtained with the Euler-Bernoulli equations were plotted with the use of MATLAB® Vibration Toolbox. They can be seen below in figure 5.19.

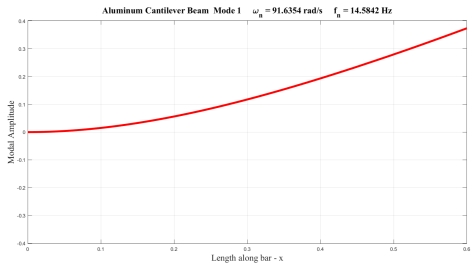

(a) Mode 1 - 14.5842 Hz

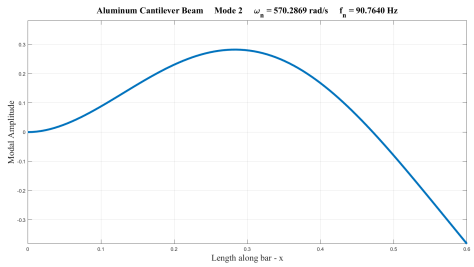

(b) Mode 2 - 90.7640 Hz

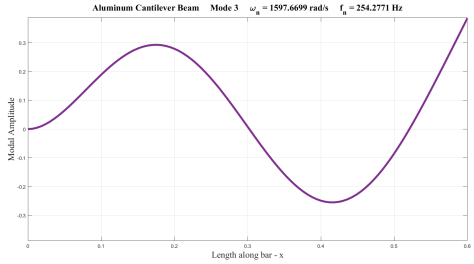

(c) Mode 3 - 254.2771 Hz

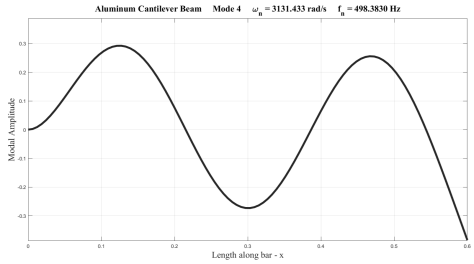

(d) Mode 4 - 498.3830 Hz

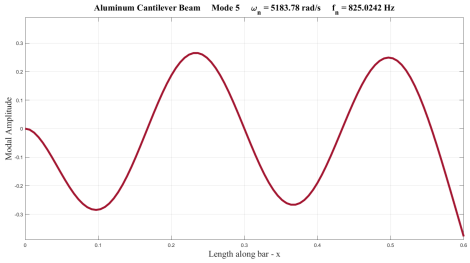

(e) Mode 5 - 825.0242 Hz

Figure 5.19: Aluminum Cantilever Beam - Analytical Mode Shapes

With analytical values for the natural frequencies and mode shapes calculated, the next step was to perform an OMA test on the ACB.

ACB - Modal Parameters

The modal parameters obtained with both software for the ACB can be seen below in table 5.19.

Table 5.19: ACB - OMA Modal Parameters

Aluminum Cantilever Beam - OMA Tests					
TEST 28/06/2024					
f_s **= 2048 Hz**				**t = 7s**	
MATLAB OoMA Toolbox					
	Analytical	SSI-COV M.O. 14		SSI-DATA M.O. 16	
Mode	f_n [Hz]	f_n [Hz]	ζ	f_n [Hz]	ζ
1	14.5842	14.9123	3.3281%	11.8184	1.8028%
2	90.7640	88.5871	0.4393%	88.4496	0.3130%
3	254.2771	248.0454	0.1575%	248.0824	0.1765%
4	498.3830	486.0621	0.1468%	485.6217	0.0781%
5	825.0242	800.5955	0.0733%	800.2801	0.1011%
SIEMENS Simcenter Testlab 2306					
	Analytical	OMA		Op. PolyMAX	
Mode	f_n [Hz]	f_n [Hz]	ζ	f_n [Hz]	ζ
1	14.5842	13.934	4.220%	13.817	1.450%
2	90.7640	88.571	0.400%	88.704	0.190%
3	254.2771	248.087	0.290%	248.226	0.200%
4	498.3830	485.571	0.110%	485.442	0.120%
5	825.0242	801.132	0.100%	798.143	0.280%

It is possible to see that all the natural frequencies obtained were very close to the analytical values, however with the only exception being the natural first natural frequency of the SSI-COV method, all the rest of frequencies calculated are consistently lower than the analytical ones. This could be due to the material being used in the analytical calculations, caused by the damage in the beam, or be an indicator that the cantilever system is dampening the vibration of the beam as suspected with the SCB results.

Mode Shapes

The mode shapes obtained with the four OMA methods used can be seen in this section.

OoMA Toolbox - Mode Shapes

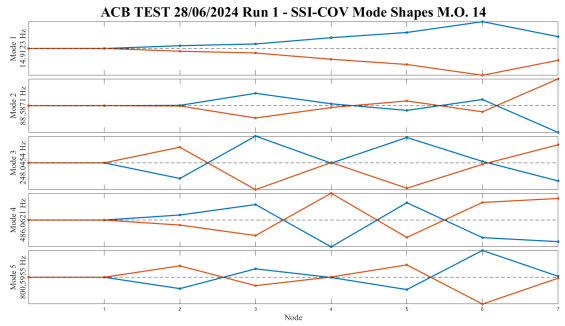

(a) SSI-COV Mode Shapes

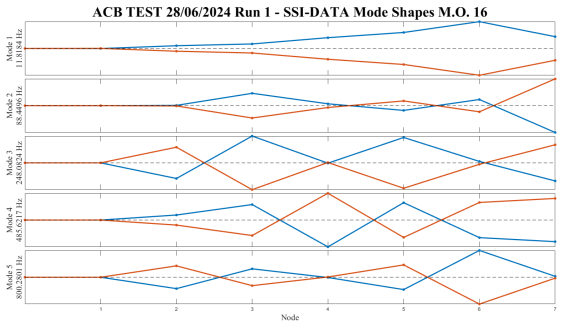

(b) SSI-DATA Mode Shapes

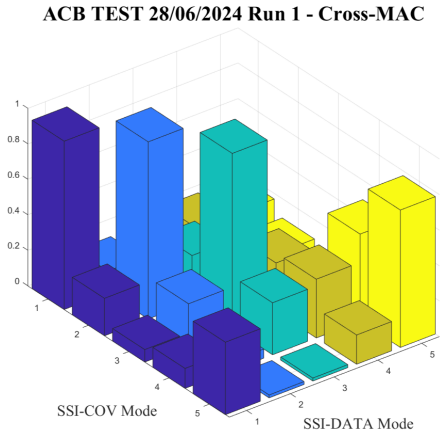

(c) Cross-MAC

Figure 5.20: Mode shapes of the ACB obtained with the OoMA Toolbox.

From the Cross-MAC matrix obtained, it is possible to see that there is a high coherence between modes 1, 2, 3 and 5 from the SSI methods, although the shape of the third mode is not the expected one when compared to the analytical shape. It is unknown if the damage on the beam is responsible for this strange mode shape, reason why a test using an undamaged beam would be needed.

Simcenter Testlab 2306 OMA Mode Shapes

(a) OMA MS1 - 13.9343 Hz

(b) Op. PolyMAX MS1 - 13.8171 Hz

Figure 5.21: Mode shapes of the ACB obtained with the Simcenter Testlab 2306 software.

(c) OMA MS2 - 88.5708 Hz

(d) Op. PolyMAX MS2 - 88.7040 Hz

(e) OMA MS3 - 248.0868 Hz

(f) Op. PolyMAX MS3 - 248.2258 Hz

(g) OMA MS4 - 485.5713 Hz

(h) Op. PolyMAX MS4 - 485.4418 Hz

(i) OMA MS5 - 801.1318 Hz

(j) Op. PolyMAX MS5 - 798.1429 Hz

Figure 5.21: Mode shapes of the ACB obtained with the Simcenter Testlab 2306 software.

Final Remarks for the ACB OMA Test

As seen by the values of the natural frequencies (tab.5.19) and mode shapes (fig. 5.20, 5.21) it is possible to conclude that the OMA test performed on the ACB yielded adequate results, proving that the material being used does not affect the OMA methods in any way.

Furthermore, as the values of the natural frequencies obtained are lower than the ones obtained analytically, following the same behavior as the OMA tests performed in the SCB, this strongly suggests that the cantilever system being used to secure the beams is dampening the vibration causing the OMA methods to find lower natural frequencies.

5.2.2 Case Study: Steel Free-Free Beam (SFFB)

The second structure analyzed with the OMA techniques was a steel beam in a 'free-free' boundary condition. This beam was chosen to observe if the boundary condition of the structure being analyzed had a negative effect on the modal parameters obtained using OMA techniques. Additionally, it is important to note that the beam being used for this

analysis is the same one used in the validation process, with the only difference now being the boundary condition and consequently the increased length.

Analytical Modal Parameters

The first five bending mode natural frequencies for the SFFB were calculated using the Euler-Bernoulli equations for free-free conditions, whose results can be seen below in table 5.20.

Table 5.20: SFFB - Analytical Modal Parameters

Steel Free-Free Beam Theoretical Analysis	
Mode	f_n **[Hz]**
1	27.7510
2	76.4967
3	149.9641
4	247.8983
5	370.3173

Analytical Mode Shapes

The analytical mode shapes were plotted using the MATLAB® Vibration toolbox and can be seen in figure 5.22 below.

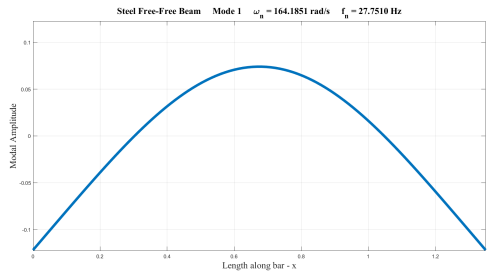

(a) Mode 1 - 27.7510 Hz

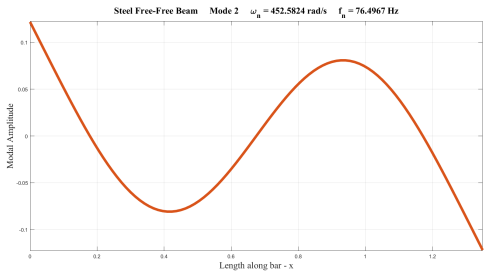

(b) Mode 2 - 76.4967 Hz

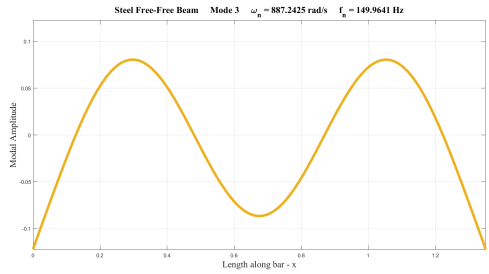

(c) Mode 3 - 149.9641 Hz

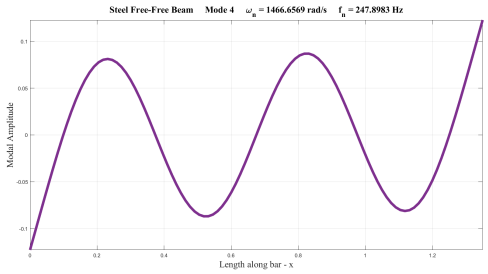

(d) Mode 4 - 247.8983 Hz

Figure 5.22: SFFB - Analytical mode shapes.

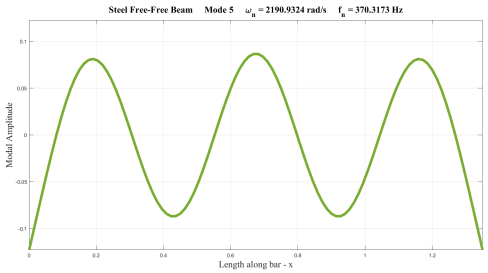

(e) Mode 5 - 370.3173 Hz

Figure 5.22: SFFB - Analytical mode shapes.

Geometry Creation

The geometry created in the Simcenter Testlab 2306 software for this test can be seen below in figure5.23

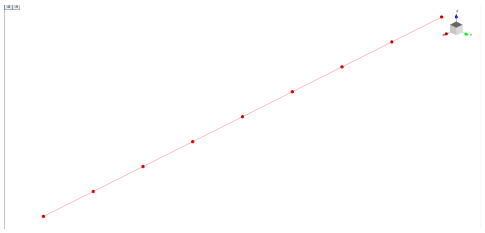

Figure 5.23: SFFB - Geometry created in Simcenter Testlab 2306

Modal Parameters

The modal parameters obtained from the OMA test performed on the SFFB can be seen below in table 5.21. Analyzing the results, it is possible to see that the values for the natural frequencies are extremely close to those calculated analytically, being slightly higher than the values expected. This is a clear indication that in the case of the OMA tests performed in the SCB, the lower values in the natural frequencies were caused by the cantilever system rather than being a problem with the material properties chosen.

Table 5.21: SFFB Test - OMA Modal Parameters

Steel Free-Free Beam - OMA Tests					
TEST 24/05/2024					
f_s = 4096 Hz				**t = 4s**	
MATLAB OoMA Toolbox					
	Analytical	SSI-COV M.O. 72		SSI-DATA M.O. 72	
Mode	f_n [Hz]	f_n [Hz]	ζ	f_n [Hz]	ζ
1	27.7510	32.364	1.359%	32.530	1.472%
2	76.4967	78.104	0.095%	78.106	0.086%
3	149.9641	152.401	0.044%	152.383	0.014%
4	247.8983	251.152	0.050%	251.155	0.047%
5	370.3173	374.305	0.034%	374.219	0.040%
SIEMENS Simcenter Testlab 2306					
	Analytical	OMA		Op. PolyMAX	
Mode	f_n [Hz]	f_n [Hz]	ζ	f_n [Hz]	ζ
1	27.7510	32.286	1.430%	-	-
2	76.4967	78.123	0.140%	78.109	0.100%
3	149.9641	152.325	0.050%	152.313	0.040%
4	247.8983	251.211	0.050%	251.167	0.050%
5	370.3173	374.428	0.020%	374.215	0.040%

Mode Shapes

The mode shapes obtained for the SFFB can be seen below in figures 5.24 and 5.25. It is possible by seeing the mode shapes that for this test, the shapes obtained are very similar to the analytical mode shapes previously obtained, especially in the case of the Operational PolyMAX mode shapes, where even the points where the nylon ropes were secured are visible.

However, for an unknown reason, in the case of the mode shapes obtained with the Operational PolyMAX method, the first mode shape was not correctly identified and thus, was not shown in these results.

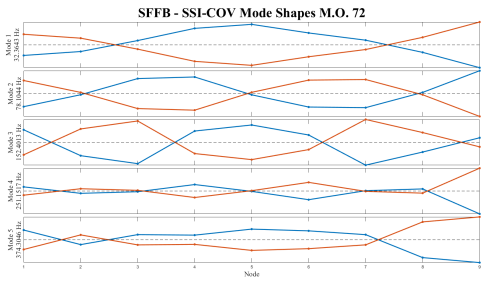

(a) SSI-COV Mode Shapes

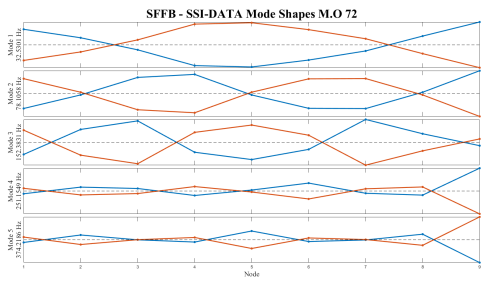

(b) SSI-DATA Mode Shapes

Figure 5.24: SFFB - Mode shapes obtained with the OoMA Toolbox.

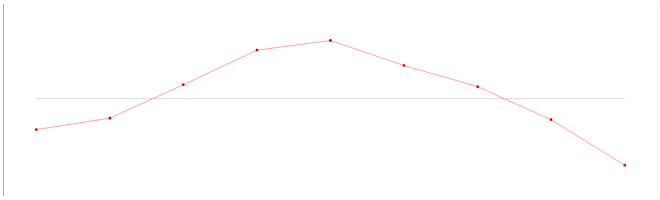

(a) OMA MS1 - 32.2857 Hz

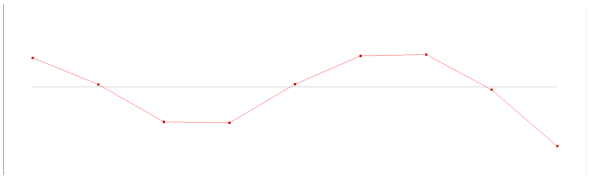

(b) OMA MS2 - 78.1225 Hz

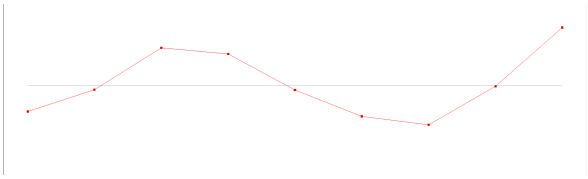

(c) Op. PolyMAX MS2 - 78.1085 Hz

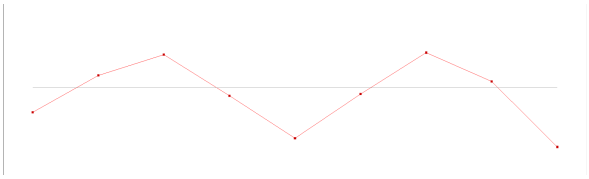

(d) OMA MS3 - 152.3250 Hz

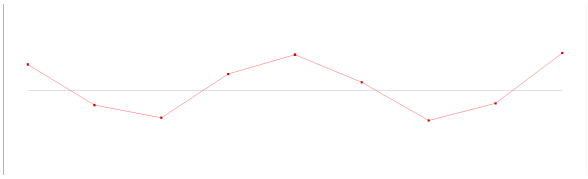

(e) Op. PolyMAX MS3 - 152.3125 Hz

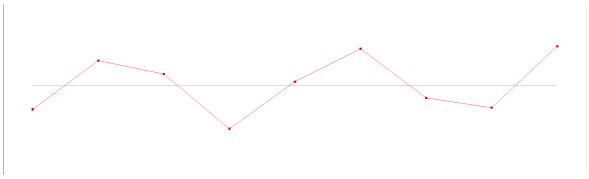

(f) OMA MS4 - 251.2106 Hz

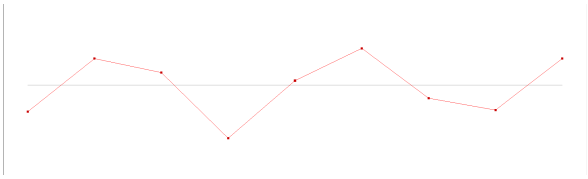

(g) Op. PolyMAX MS4 - 251.1671 Hz

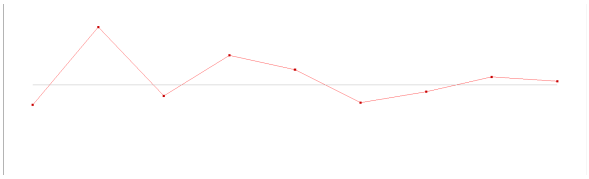

(h) OMA MS5 - 374.4282 Hz

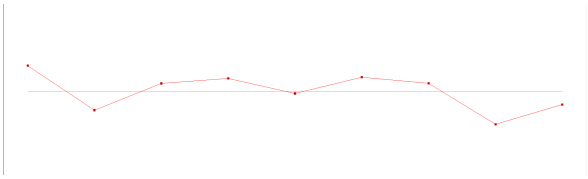

(i) Op. PolyMAX MS5 - 374.2154 Hz

Figure 5.25: SFFB Mode shapes obtained with the Simcenter Testlab 2306 software.

MAC Analysis

Finally, to validate the mode shapes obtained with all the methods (with the exception of the mode shapes obtained with the Operational PolyMAX method), MAC analysis were performed. A Cross-MAC between the SSI-COV and SSI-DATA methods for the mode shapes obtained with the OoMA Toolbox, and an Auto-MAC for the mode shapes obtained with the OMA analysis in the Simcenter Testlab 2306 software, as seen in figure 5.26

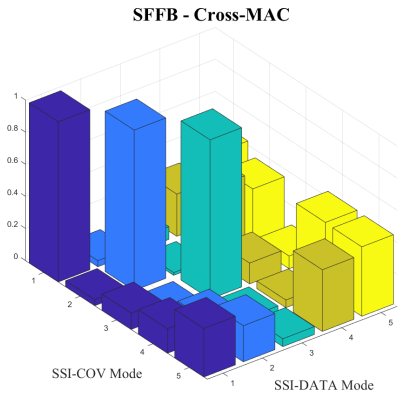

(a) Cross-MAC between the SSI-DATA and SSI-COV methods from the mode shapes obtained with the OoMA Toolbox software.

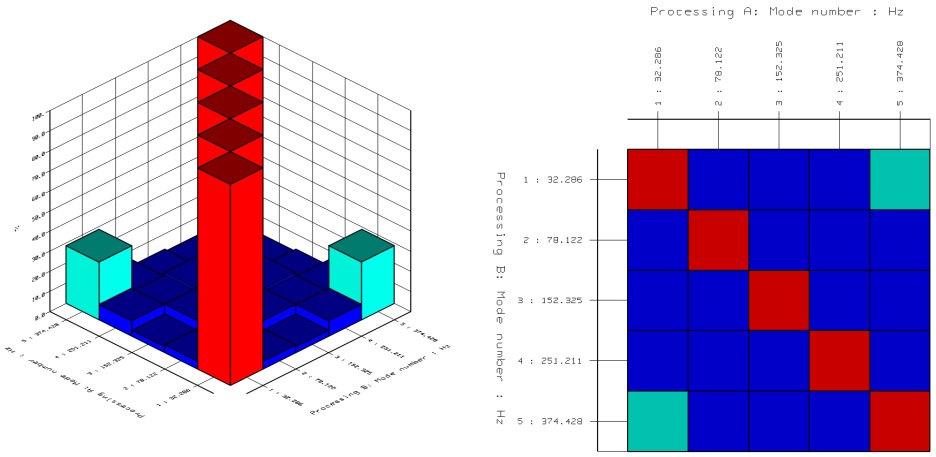

(b) Auto-MAC from the OMA mode shapes obtained with the Simcenter Testlab 2306 software

Figure 5.26: SFFB - MAC Matrices

The results obtained show excellent results for the mode shapes obtained in the Simcenter Testlab software, whereas for the ones obtained in the OoMA Toolbox the Cross-MAC shows very good results for the first three modes, however the last two modes shows low coherence between the two modes.

Final Remarks for the SFFB OMA Test

Despite the low coherence between modes 4 and 5 for the mode shapes obtained with the OoMA Toolbox software and the problem of the first mode shape obtained with the Operational PolyMAX plugin, the OMA test performed showed remarkable results, with very accurate results for all the natural frequencies.

Additionally, this test also reasserted the hypothesis that the cantilever system dampened the natural frequencies obtained for the cantilever tests.

5.2.3 Case Study: Mamutes' Barbie Aerodesign (BARBIE)

To further explore the effectiveness of the OMA techniques, a series of OMA tests were performed on the Mamutes' Aerodesign "Barbie" to identify all the modal parameters: natural frequencies (ω_n), damping ratios (ζ) and mode shapes (φ).

Simulated Modal Analysis

To have data for a comparison, data from a simulated modal analysis performed by the team on the wing was used. This is not the ideal case as it is only one part of the entire structure of the aerodesign and the complete parameters for the simulation are unknown. However, for confidentiality and practical reasons this data was accepted as the one for reference.The simulated modal analysis yielded results for the first two bending and torsional modes, as shown in table 5.22.

OMA performed on the Barbie Aerodesign

The modal parameters obtained from the OMA test performed on the Barbie aerodesign can be seen below in table 5.22. However, as in this case the structure was more complex than in the previous OMA tests, only the Simcenter Testlab 2306 software was used.

In table 5.22, it is possible to see that some of the natural frequencies obtained have a considerable error when compared to the expected value from the simulations. However, as the natural frequencies of the simulations were obtained from a single wing without, they do not consider the effect that the other components of the aircraft had on the modal parameters, due to the added mass, connections between the components, electronic equipment, etc. which contribute significantly to dampening or in some cases to even increasing of the natural frequencies.

Table 5.22: Mamutes' Barbie Aerodesign - Modal parameters

Mamutes' Barbie Aerodesign Modal Parameters								
Mode		**Simulation**	**OMA**			Op. PolyMAX		
No.	**Type**	f_n **[Hz]**	f_n **[Hz]**	**E. [OMA]**	ζ	f_n **[Hz]**	**E. [OMA]**	ζ
1	Bending	19.14	10.62	-80.29%	3.61%	10.66	-79.65%	3.91%
2	Bending	98.06	91.93	-6.66%	0.06%	91.95	-6.65%	0.09%
3	Torsion	146.56	179.92	18.54%	0.03%	179.35	18.28%	0.05%
4	Torsion	347.17	360.22	3.62%	0.21%	356.99	2.75%	0.02%

By observing mode 1 from both the OMA plugin and the Operational PolyMAX results, it is possible to see that both have a significantly lesser value than the one expected from

the simulation. A plausible reason for this can be due to damping added to the system during the construction of the aircraft, as in constructions of this type there are several factor that are not taken into consideration that can add up in the values obtained. Another plausible reason for this discrepancy can be that the simulations do not take into consideration the rest of the components of the plane as previously mentioned.

The rest of the modes founded presented considerably satisfactory results when compared to the simulated ones, indicating that the added dampening effect might be more present in lower frequencies, which is also reinforced by observing the damping ratio in mode 1 when compared to the rest of the modes.

Mode Shapes

Despite the satisfactory results obtained in the natural frequencies and damping ratios obtained, the mode shapes presented additional challenges that couldn't be solved and thus are considerably different from those expected from the simulations. The main challenges found during the test were:

Use of a single accelerometer:. As stated by (BRINCKER; VENTURA, 2015), to perform an OMA in multiple runs, a minimal of two accelerometers are needed. This is because one of the accelerometers must remained fixed in all runs while the other one is rovered across all the other measurement points. This fixed accelerometer is crucial for OMA as it is the only way to link all the measurements obtained with one another.

In previous tests, despite the lack of the fixed accelerometer the results were acceptable as the beam geometries were simple enough to compensate for this effect manually. However, in the case of Barbie, the aerodesign structure has too many measurement points and the structure is far too complex to do so manually. Therefore, only a vague representation of the mode shapes was obtained.

Fixation problems: For a good measurement, it is crucial that the accelerometer is well fixed in the measurement point. In previous tests, as the surfaces were smooth, flat and metallic, it was possible to fixate the accelerometer in place with the special *petro wax* used. However, in the case of Barbie, the surfaces were irregular, rough and from materials to which the wax had little adherence. This made the fixation difficult and the whole process costly as plenty of wax was required for every test, limiting greatly the capacity to do multiple tests.

Mode Shapes - Mamutes' Barbie Aerodesign Wing Simulation

The mode shapes obtained from the simulation performed by the Mamutes' Aerodesign can be seen below in figure 5.27.

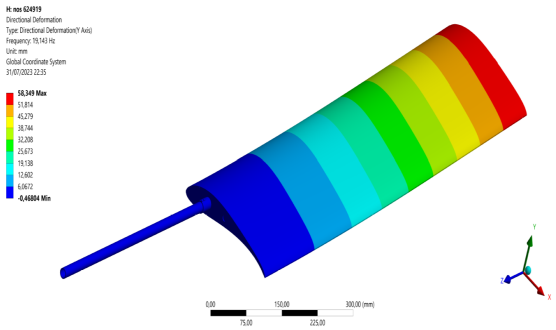

(a) Bending Mode 1 - 19.143 Hz

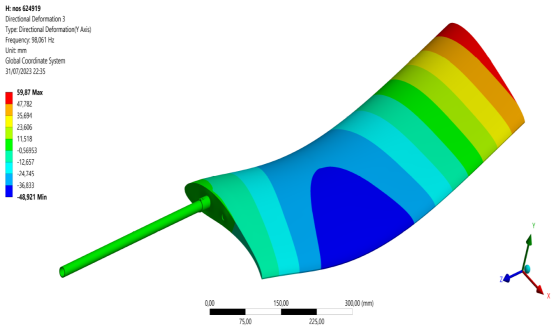

(b) Bending Mode 2 - 98.061 Hz

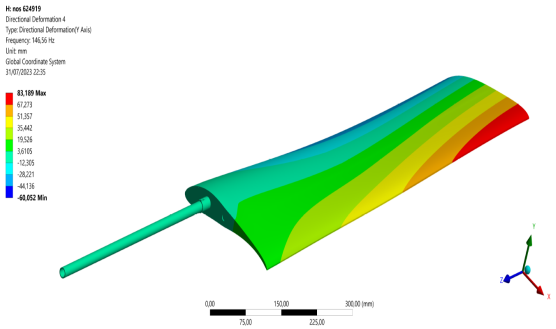

(c) Torsional Mode 1 - 146.56 Hz

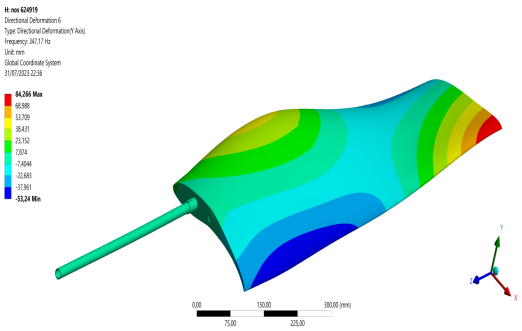

(d) Torsional Mode 2 - 347.170 Hz

Figure 5.27: Mode shapes obtained from the simulated modal analysis of the Barbie aerodesign provided by the team. Source: Mamutes do Cerrado Aerodesign

Mode Shapes of the Barbie aerodesign obtained with the Simcenter Testlab 2306 software.

The mode shapes obtained with the Simcenter Testlab 2306 software can be seen below in figure 5.28.

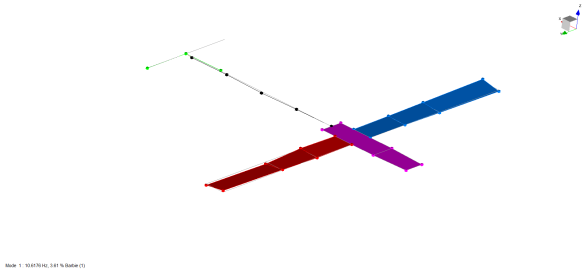

(a) OMA MS1 - 10.6176 Hz, 3.610%

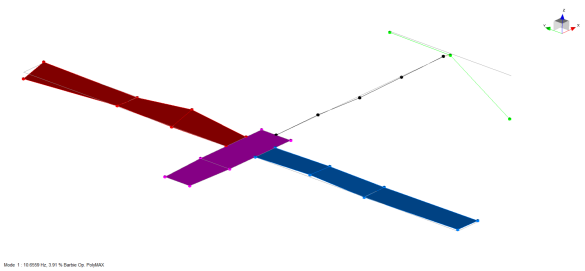

(b) Op. PolyMAX MS1 - 10.6559 Hz, 3.910%

Figure 5.28: Barbie Mode Shapes obtained with Simcenter Testlab 2306 - OMA Analysis

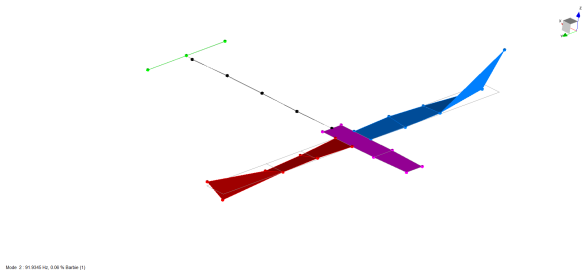

(c) OMA MS2 - 91.9345 Hz, 0.060%

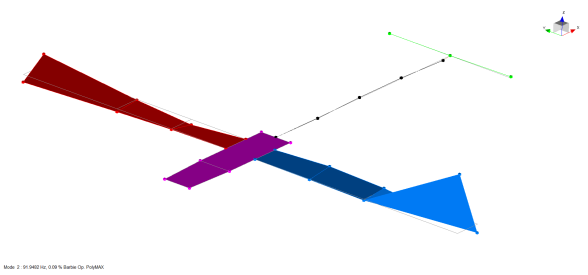

(d) OMA MS2 - 91.9482 Hz, 0.090%

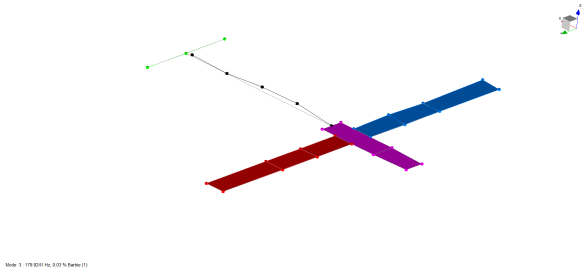

(e) OMA MS3 - 179.9241 Hz, 0.030%

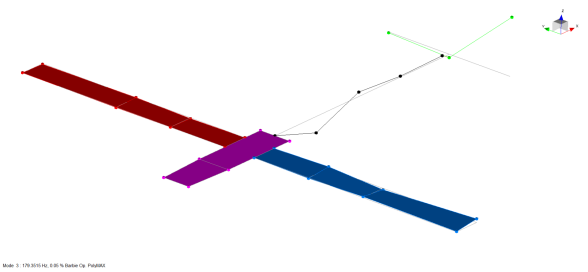

(f) Op. PolyMAX MS3 - 179.3515 Hz, 0.050%

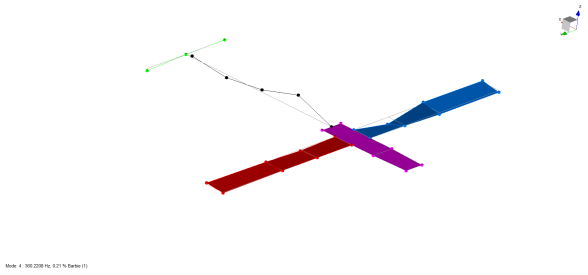

(g) OMA MS4 - 360.2208 Hz, 0.210%

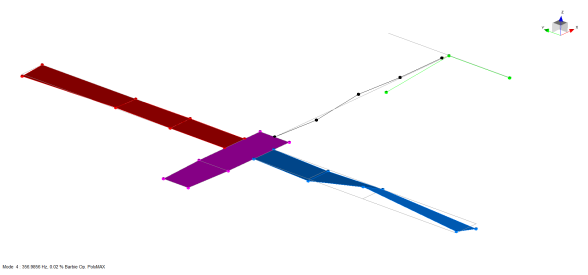

(h) Op. PolyMAX MS4 - 356.9853 Hz, 0.020%

Figure 5.28: Barbie mode shapes obtained with Simcenter Testlab 2306 software with the OMA and Operational PolyMAX add-ins.

An Auto-MAC of the mode shapes obtained (fig. 5.29) shows that the modes obtained are uncoupled for the first three modes but showed a great level of modal coupling for the fourth mode using the OMA plugin.

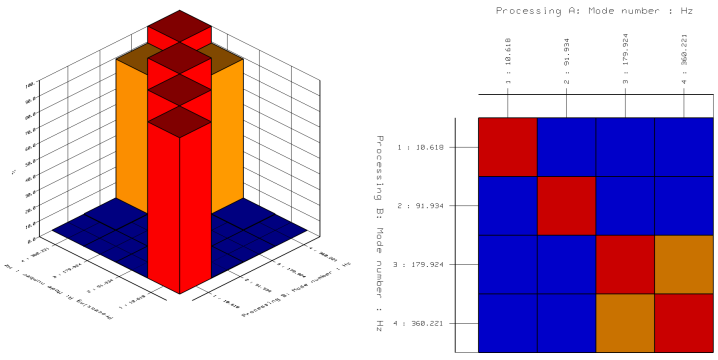

Figure 5.29: Barbie - OMA analysis Auto-MAC

However, in the case of the Operational PolyMAX plugin, the third mode showed a great level of coupling, whereas the rest showed fair results.

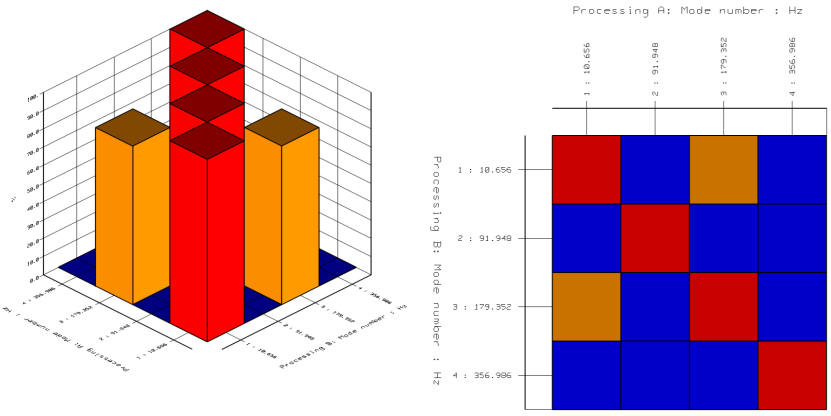

Figure 5.30: Barbie - Operational PolyMAX analysis Auto-MAC

Barbie Aerodesign Final Remarks

The Barbie aerodesign OMA test proved to be challenging during all the stages of the test, from the definition of the measurement points where the accelerometers would be placed, to the acquisition of the data itself as the surface of the aerodesign made it difficult to correctly adhere the accelerometers. To identifying the modes of the structure in the cross-spectra due to the presence of harmonic excitations. However, this challenging nature it turned out to be a very educational experience as it illustrated perfectly all the difficulties that could appear during a test with a bigger aircraft or similar aeronautic/aerospace structures, forcing even to adopt a new mode identification approach known as narrow-band identification, in which a very narrow band of the spectra is analyzed individually where a mode is suspected to be instead of the complete frequency band.

An important observation to do about the test is that the cross-power spectra obtained for the Barbie Aerodesign during the OMA test showed indications that a higher number of modes could have been obtained if the simulations performed by the team would have included a higher number of modes. This can be seen by observing the cross-power spectra (fig. 5.31) in which the upper part of the upper section shows the power magnitude in dB whereas the lower section shows the phase. By analyzing the number of peaks (which indicate possible modes of the Barbie aerodesign) it is possible to see that there are a considerable higher number of peaks than the modes founded during the test. This peaks could indicate additional modes of the structure, however, as in the simulations only the four modes presented in table 5.22 and figure 5.27 there is no

way of indicating if this is the case. Therefore, they were not considered for the analysis. A recommendation for future tests is coordination with the Mamutes' team to discuss beforehand the parameters for the modal analysis simulations that would allow for a better identification of all the modes present in the bandwidth selected for the OMA tests.

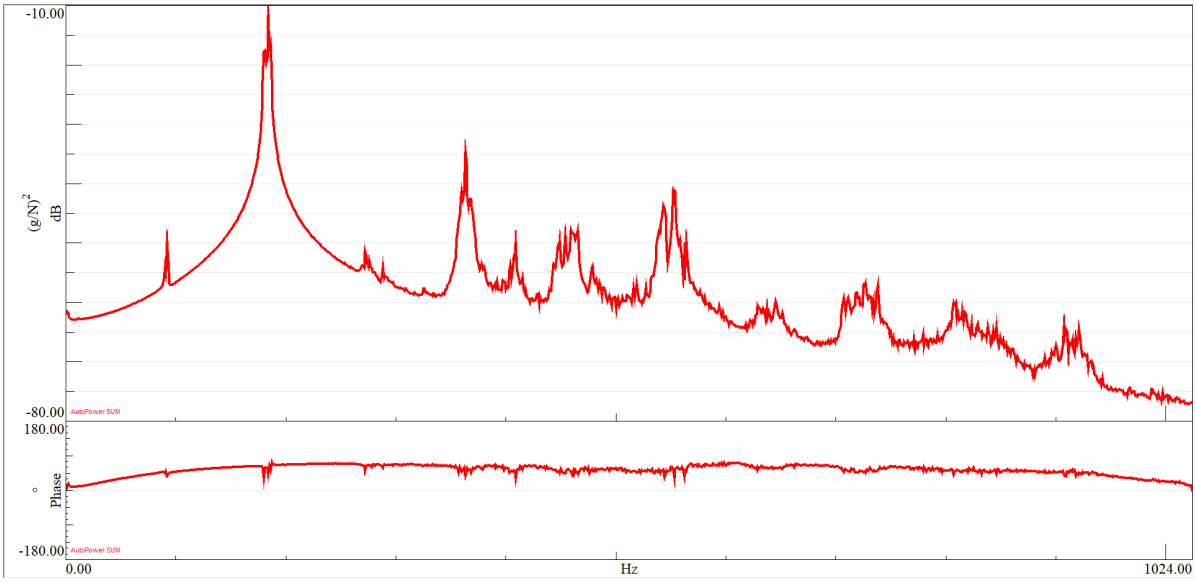

Figure 5.31: Barbie Cross-Power Spectra

5.2.4 Case Study: Hyarra's Drone Structure (HYARRA)

The competition team EDRA's Hyarra drone structure was chosen as the final structure to be analyzed using different OMA techniques. However, before presenting the results of the analysis it is important to note that due to a technical problem, only one propeller was available during the test, which affected all the modal parameters obtained, particularly the mode shapes obtained.

Hyarra Simulated Modal Analysis

In the same fashion as with the Barbie structure, a simulated modal analysis was performed to have modal parameters to be used as a reference, which can be seen in table 5.23 and figure 5.32.

OMA test

The modal parameters obtained from the OMA test performed on the Hyarra structure can be seen below in table 5.23 where the results from the Simcenter Testlab 2306 OMA and Operational PolyMAX analysis are shown.

Table 5.23: EDRA's Hyarra Drone - Modal Parameters with Simcenter and Op. PolyMAX

EDRA's Hyarra Drone Modal Parameters								
Mode		**Simulation**	**OMA**			**Op. PolyMAX**		
No.	**Type**	f_n **[Hz]**	f_n **[Hz]**	**E. [OMA]**	ζ	f_n **[Hz]**	**E. [OMA]**	ζ
1	Bending	64.83	-	-	-	-	-	-
2	Bending	65.637	-	-	-	-	-	-
3	Bending	66.009	75.80	14.48%	0.08%	74.18	12.60%	0.02%
4	Bending	66.856	76.88	14.63%	0.12%	75.46	13.02%	0.68%
5	Bending	314.1200	-	-	-	-	-	-
6	Bending	315.55	-	-	-	-	-	-
7	Bending	319.02	302.23	-3.93%	0.16%	304.31	-3.22%	0.08%
8	Bending	320.47	302.27	-4.39%	0.13%	308.49	-2.29%	0.18%

As seen in table 5.23, some natural frequencies couldn't be found with the OMA analysis by any of the two methods used. Aside from the reasons explained with the Barbie Aerodesign that difficulted the OMA tests, a plausible reason of why these natural frequencies couldn't be identified is due to the use of the single propeller during the test. With 4 propellers, the drone would have had a similar excitation across all of its structure, however as only one of the arms of the drone had a propeller, the relative movement caused in the arm with the propeller was considerably higher than the other 3 arms, causing some problems during the identification that allowed only the identification of the modes in which the arm with the propeller were involved.

Nonetheless, the modes that could be identified showed good accuracy with respect to the expected values, having a difference of around 13% to the expected values. This difference is expected as not all the components that the drone carried were used during the simulation.

In addition to that, during the assembly of the structure, some unknown procedure done by the CeSE team caused the drone structure to bend, creating stress across the body of the drone and being a plausible explanation for the higher natural frequencies obtained.

Mode Shapes

After the test, it was observed that the number of measurement points chosen for the drone was not enough to properly capture the mode shapes of the drone. As a result, higher frequency mode shapes appear to be the same as lower frequency modes. In addition to that, as only a straight line was formed in the arms of the drone, only the

bending modes were identified (tab. 5.23).

Mode Shapes - EDRA's Hyarra Drone Simulation

The mode shapes obtained from the modal simulation performed on the drone structure are shown below in figure 5.32, where the number of the bending mode is correlated to the ones shown in table 5.23.

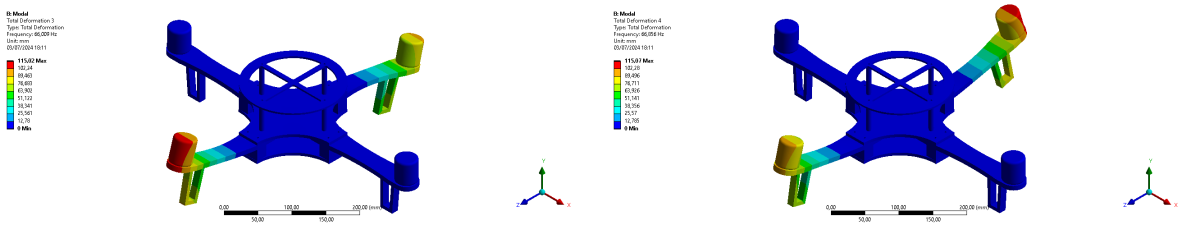

(a) Bending Mode 3 - 66.009 Hz

(b) Bending Mode 4 - 66.856 Hz

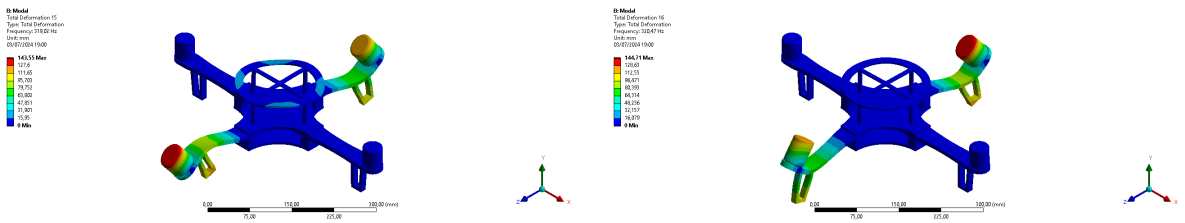

(c) Bending Mode 7 - 319.020 Hz

(d) Bending Mode 8 - 320.47 Hz

Figure 5.32: Mode shapes from the simulated modal analysis of the EDRA's Hyarra drone structure provided by the team. Source: Equipe de Robótica Aérea - EDRA

Mode Shapes - Simcenter Testlab

The mode shapes obtained with Simcenter Testlab 2306 can be seen below in figure 5.34.

(a) OMA MS3 - 75.8046 Hz, 0.08%

(b) Op. PolyMAX MS3 - 74.1765 Hz, 0.02%

Figure 5.33: Hyarra mode shapes obtained with Simcenter Testlab 2306 software.

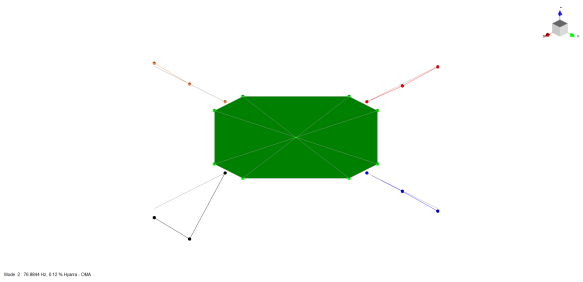

(a) OMA MS4 - 76.8844 Hz, 0.12%

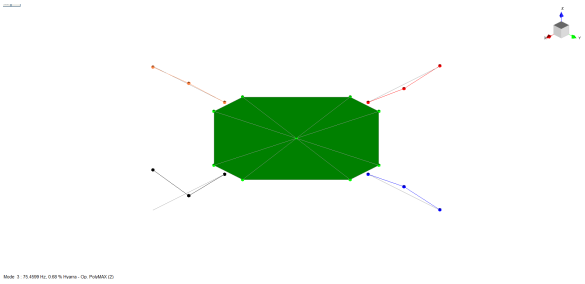

(b) Op. PolyMAX MS4 - 75.4599 Hz, 0.68%

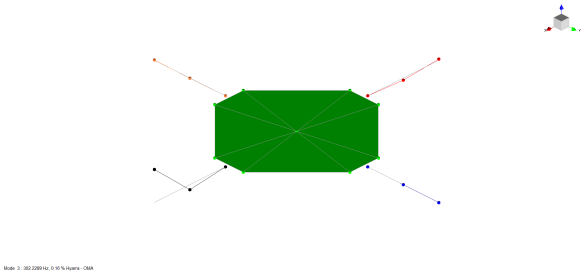

(c) OMA MS7 - 302.2289 Hz, 0.16%

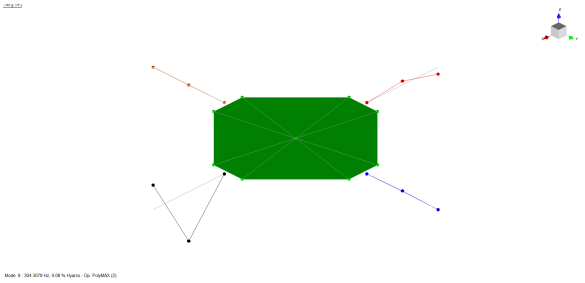

(d) Op. PolyMAX MS7 - 304.3079 Hz, 0.08%

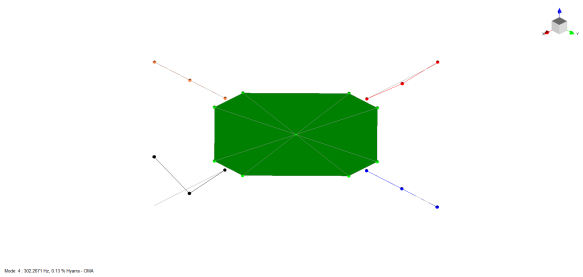

(e) OMA MS8 - 302.2671 Hz, 0.13%

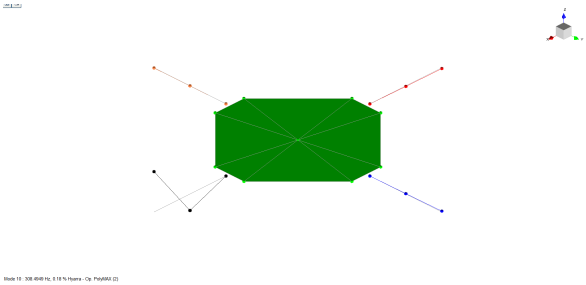

(f) Op. PolyMAX MS8 - 308.4949 Hz, 0.18%

Figure 5.34: Hyarra mode shapes obtained with Simcenter Testlab 2306 software.

EDRA's Hyarra Drone - Final Remarks

Despite the technical problems that occurred before performing the OMA test on the drone structure, the OMA test allowed for a fairly good identification of all the modal parameters of the structure. An interesting observation founded during the test was the effect that having a single propeller had on the modal parameters, as only the modes in which the arm with the propeller were involved were identified.

CHAPTER 6

CONCLUSIONS

Throughout this work it was possible to observe that Operational Modal Analysis (OMA) is an immensely powerful tool used to assess the modal parameters from different system, with the additional advantage of doing so by using the operational data from the structures themselves, allowing for more accurate excitations and boundary conditions.

The validation process for the OMA techniques implemented showed remarkable results at estimating all the modal parameters: natural frequency (ω_n), damping ratio (ζ) and mode shapes (φ).

Through the implementation of the OMA techniques during the validation process, it was possible to observe that the data generated in *ANSYS Mechanical* produced an aliasing effect on the values of the natural frequencies obtained, that didn't follow the Nyquist Sampling Theorem, suggesting the existence of an intrinsically problem with the data generated. Future simulations modifying the time-steps or using the APDL commands are suggested to see if the problem resides within the *Workbench* interface.

One aspect identified through the OMA tests performed on the SCB and in subsequent tests with the ACB and the SFFB is that, all tests performed in the cantilever system showed lower natural frequencies than those obtained analytically, strongly suggesting that cantilever system dampens the vibration of the beam producing lower natural frequencies during the analysis.

The impact that multiple accelerometers had on the results obtained, especially the mode shapes, was seen during the validation process, as the mode shapes obtained from

the simulated data that would correspond to a test in which multiple accelerometers are placed simultaneously in the nodes showed excellent results when compared to those obtained analytically and through the simulated modal analysis. On the other hand, the OMA tests performed on the SCB showed slightly different mode shapes from those expected as the link between all the measurements had to be done manually. Nonetheless, the beam structures proved to be simple enough to be able to overcome the accelerometer number limitation showing acceptable results.

All the cases, including the simulations, simulated OMA and actual OMA tests showed satisfactory results when compared to the analytical values expected, thus validating the OMA methodology followed in both the MATLAB® OoMA Toolbox and the SIEMENS® Simcenter Testlab 2306 software.

The results obtained from the SFFB and the ACB further demonstrated the accuracy of the OMA methods, showing that the techniques can be applied in different materials and boundary conditions without affecting the modal parameter obtained.

One important aspect identified during the OMA tests is that for better results, it is necessary that the fixation of the accelerometer is done adequately and that is not placed in a nodal point, for which a simulated modal analysis (to know the mode shapes) previous to the test is necessary.

In tests with multiple runs, as was the case for all the OMA tests performed showed that it is fundamental that the force between each run are recreated as similarly as possible, otherwise the mode shapes obtained will show a distortion in their shape.

The OMA results obtained from the Mamutes' Barbie aerodesign and from the EDRA's Hyarra drone showed satisfactory results for the natural frequencies and damping ratios estimated for both structures. However, the natural frequencies obtained showed results slightly different for the lower frequency modes in comparison to the expected analytical results. A possible explanation for this differences in lower modes for both structures could be a series of several factors during the manufacturing of both structures.

In the case of the Barbie aerodesign, the lower natural frequency obtained for mode 1 (10.62 Hz vs 19.14 Hz) showed that additional damping was present in the structure as suggested by the damping ratio obtained for this first mode (3.61%). This additional damping could be result of not anticipated conditions, like a lower stressed covering in the wings, the presence of actuators and cables in the wings and slightly lose connections. However, these effects showed to have affected only the first mode, as the subsequent higher frequency modes are much closer to the values expected from the simulation.

The modes of Barbie's tail could not be obtained as the simulation provided by the

team Mamutes Aerodesign only presented the modes for a single cantilever wing. Thus, additional peaks showed in the cross-power could be from the tail of the aircraft, however as there was not information available for a comparison these additional peaks were disconsidered for the final results.

In the case of the Hyarra drone, the higher natural frequencies obtained could be explained due to a bending in the structure produced during the assembly of the structure. This bending was caused by misaligning of the holes for the screws that secured the structure in place, causing some pre-stress in the structure that was not accounted during the simulation.

Despite efforts, it was seen in the mode shapes obtained for the complex structures, especially for the Barbie aerodesign, that the accelerometer number limitation has an enormous impact in the results. This limitation was overcome on the three beam-cases as the beams were simple enough to manually modify the measurements to be correctly aligned. However, as the aircraft and the drone structures proved to be far more complex, this manual process was not possible.

6.1 Future Works

With the knowledge obtained during the implementation of OMA in different structures and aiming to further improve this technique and the methodology followed here, there are four recommendations for future works.

1. Use of multiple accelerometers: Considering the problems founded during the identification of the mode shapes, especially in the case of the Barbie and Hyarra structures, the most important future work to be implemented is the use of multiple accelerometers simultaneously on the structures being studied. As seen during this work, the use of at least a second accelerometer for reference is fundamental to properly identify the mode shapes of any structure being analyzed due to the necessity of the synchronization of the measurements. Without a fixed accelerometer for reference this process is difficult as seen during the SCB tests, however for the Barbie and Hyarra structures it became practically impossible due to the substantial number of measurement points and the nature of the random excitation.

2. Complete information of the acquisition system: Another hardship founded during the tests performed was the lack of knowledge about the acquisition system used, as it would record the response of the systems at slightly different times that difficulted even more the synchronization of the measurements. Further research about the system

is required to guarantee more accurate and reliable measurements.

3. Harmonic excitations: During the Barbie and Hyarra tests, harmonic excitations were present due to the necessity of using the motors to excite the structures. As mentioned in chapter 3 these type of excitations wreak havoc during the data analysis as the excitation itself can be mistakenly identified as a mode of the structure. Fortunately, the *narrow band* approach allowed to correctly identify the modes by isolating the suspected frequency of the motor. However, it is not clear if despite this approach the modes were affected due to the presence of harmonic excitations. New tests with the SCB using harmonic excitations are suggested to verify if their presence modifies any of the modal parameters previously obtained during this work.

4. New fixation techniques: A problem founded during the tests was that the *petrowax* used to fix the accelerometer failed to correctly adhere to rough surfaces like the ones founded in the Barbie and Hyarra structures. This led to an excessive use of wax with the added problem of lack of adherence which is not only costly but can led to bad measurements or even to the accelerometer to come loose and fall damaging it. For these reasons, research to find new forms of fixation of the accelerometer is suggested.

5. Different excitation techniques: A final recommendation for future works is trying different types of excitations to test the structures when the exact operational data is not available. This can be visualized with the case of the Barbie aerodesign, where the excitation for this test was recreated artificially using the vibration of the motor. However, a test using a fan to recreate the excitation that the airflow has on the structure can be added as a test with a different excitation source or even used in combination with the motor to recreate the operational conditions. A posterior comparison of the results will help to visualize if the modal parameters being obtained through the OMA tests are accurate, as fake modes are unlikely to appear in tests with different excitation sources.

BIBLIOGRAPHY

AVITABILE, P. *Modal Testing - A Practitioner's Guide*. [S.l.]: Society for Experimental Mechanics, 2018.

BENDAT, J. S.; PIERSOL, A. G. *Random Data: Analysis and Measurement Procedures*. [S.l.]: John Wiley & Sons, 1986.

BRINCKER, R.; ANDERSEN, P. Understanding stochastic subspace identification. *IMAC-XXIV : A Conference & Exposition on Structural Dynamics*, 2006.

BRINCKER, R.; VENTURA, C. *Introduction to Operational Modal Analysis*. [S.l.]: Wiley, 2015.

COVIOLI, J. *Developments in Reverse Engineering and Testing of Airborne Structures*. Tese (Doutorado) — Università degli Studi di Roma "La Sapienza", 2021.

FRANSEN, S. et al. The operational modal analysis of solid rocket motors. *Journal of Space Engineering*, v. 42, n. 3, p. 123–138, 2024.

HASAN, B. A. et al. Enhanced frequency domain decomposition algorithm: A review of a recent development for unbiased damping ratio estimates. *Journal of Vibroengineering*, v. 20, p. 1919–1936, 08 2018.

INMAN, D. J. *Engineering Vibrations*. 5th. ed. Michigan, USA: Pearson, 2014. ISBN 9780136809531.

LI, H. et al. Subspace identification algorithm based on non-negative matrix factorization for hammerstein model. *International Journal of Automation and Computing*, v. 11, n. 1, p. 45–52, 2014.

LJUNG, L. *System Identification: Theory for the User*. [S.l.]: Prentice Hall PTR, 1999.

MAGALHãES, F. *Operational Modal Analysis for Testing and Monitoring of Bridges and Special Structures*. Tese (Doutorado) — Universidade de Porto, 2010.

MANCHESTER, U. The millenium footbridge. 2018. Disponível em: <http://epsassets.manchester.ac.uk/structural-concepts/Dynamics/resonance/resonance_pra1.php.>

MELSA, J. L.; SAGE, A. P. *An Introduction to Probability and Stochastic Processes*. [S.l.]: Prentice-Hall Inc., 1973.

OTTO, A. *OoMA Toolbox*. 2024. <https://www.mathworks.com/matlabcentral/fileexchange/68657-ooma-toolbox>. MATLAB Central File Exchange.

OVERSCHEE, P. V.; MOOR, B. D. N4sid*: Subspace algorithms for the identification of combined deterministic-stochastic systems. *Automatica*, Elsevier, v. 30, n. 1, p. 75–93, 1994.

OVERSCHEE, P. V.; MOOR, B. D. Subspace identification for linear systems. theory, implementation, applications. incl. 1 disk. In: ____. [S.l.: s.n.], 1996. xiv, p. xiv + 254. ISBN 0-7923-9717-7.

OVERSCHEE, P. van; MOOR, B. D. *Subspace Identification for Linear Systems*. [S.l.]: Kluwer Academic Publishers, 1996.

PAPOULIS, A.; PILLAI, S. U. *Probability, Random Variables, and Stochastic Processes*. 4th. ed. [S.l.]: McGraw-Hill, 2002. ISBN 978-0072817256.

REYNDERS, E. et al. Uncertainty quantification in operational modal analysis with stochastic subspace identification: Validation and applications. *Mechanical Systems and Signal Processing*, v. 66, 05 2015.

SIEMENS, A. Modal assurance criterion (mac). 2019. Disponível em: <https://community.sw.siemens.com/s/article/modal-assurance-criterion-mac>.

SIEMENS, A. Omg! what is oma? operational modal analysis. 2020. Disponível em: <https://community.sw.siemens.com/s/article/OMG-What-is-OMA-Operating-Modal-Analysis.>

SIEMENS, S. D. I. S. *OMG! What is OMA? Operating Modal Analysis*. 2024. Accessed: 2024-07-10. Disponível em: <https://community.sw.siemens.com/s/article/OMG-What-is-OMA-Operating-Modal-Analysis>.

ZAHID, F. B.; CHAO, O.; KHOO, S. A review of operational modal analysis techniques for in-service modal identification. *Journal of the Brazilian Society of Mechanical Sciences and Engineering*, v. 42, 08 2020.

ZHANG, L. et al. Application of operational modal analysis for wind-tunnel testing of an aircraft wing model with control-surface. *Journal of Aerodynamic Studies*, v. 36, n. 4, p. 215–230, 2024.

APPENDIX

APPENDIX A

APPENDIX A: STEEL CANTILEVER BEAM CREATION

For the final part of this work, a real life model of the SCB used during the simulations was constructed. As the purpose of the work as a whole is to implement the OMA as a reliable tool to calculate the modal parameters of any structure of interest a future comparison between simulated data and operational data needs to be done.

The first step for the creation of the steel cantilever beam was the creation of technical drawings of all the components needed for constructing the system. This was done with the help of the software *SolidWorks* in which all pieces required were detailed. With these technical drawings it was possible to buy the necessary pieces to assembly the system. In figure A.1 it is possible to see the technical drawing of the main plate of the system. This plate is the base of the beam and the technical drawing was necessary to manufacture the plate with the measurements desired with the only exception being the main channel on the plate.

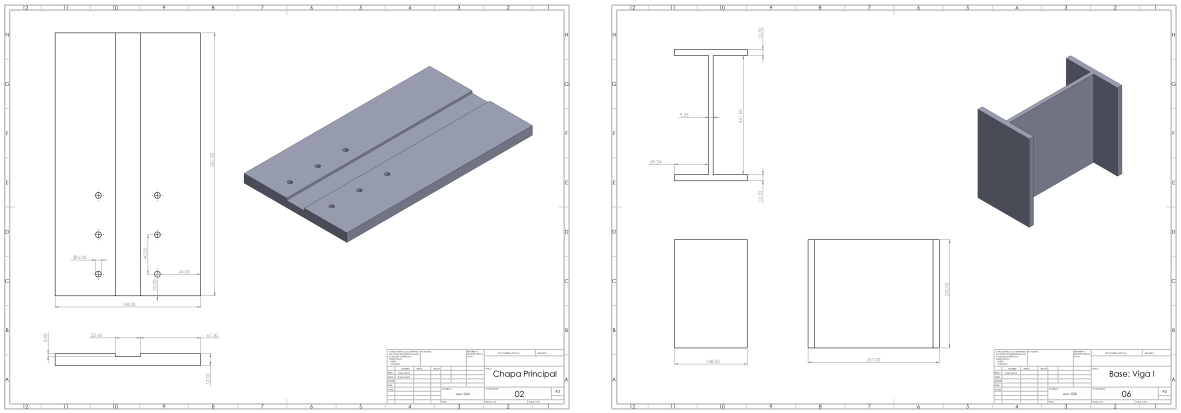

(a) SCB main plate

(b) SCB I-Beam

Figure A.1: SCB technical drawings.

After buying all the main components of the system, as seen in figure A.2 with the help of the technical drawings, the next step was the manufacturing of the system. For this, the equipments located in the workshop at the FGA campus were used. The next step in the construction of the system was the creation of the central channel in the main plate. This central channel serves to avoid any lateral movement of the beam. To create it, a steel drilling mill was used. The milling machine and the resulting channel can be seen in figure A.3.

(a) Components used in the construction of the steel cantilever beam system.

(b) CNC End mill used to create the central channel of the main plate

Figure A.2: SCB components.

(a) Milling machine used to create the central channel on the main plate.

(b) Central channel created with the milling machine.

Figure A.3: The creation of the main channel was the most complicated part of the manufacturing process as a mistake in this stage would have caused the entire main plate to be unusable.

After the creation of the central channel in the main plate, the next step in the creation of the system was welding the main plate in the I-beam used as a seismic anchor for the system seen in figure A.4a. With this done, the last step was positioning the beam in the channel and fixing the secondary plate in position as shown in figure A.4.

(a) The main plate was welded with the I-beam. The combined weight of this components serve as a seismic anchor for the system.

(b) The beam and secondary plates are fixed in their positions with six screws attached to self-locking screws.

Figure A.4: In the second part of the work both EMA and OMA will be performed on the beam to asses the accuracy of the OMA methods.

APPENDIX B

APPENDIX B: IMPULSE SIMULATION 4096 HZ CODE

As an example of how to use the OoMA Toolbox, the code used for the ***Impulse Simulation 4096 Hz*** will be shown in this section:

```
% TCC 2
% Hugo Eduardo Garcia Sosa 18/0044087
% Advisor: Dr. Sergio Henrique Carneiro
% Functions obtained thanks to the work of Andrew Otto (2024). OoMA Toolbox (https://www.mathworks.com/matlabcentral/fileexchange/68657-ooma toolbox), MATLAB Central File Exchange. Recovered March 2, 2024
clear
clc
% Parameters of the simulation:
% Force type: Impulse 100 N
fs = 4096; %Sampling frequency.
T = (1/fs); %Sampling time period.
Tf = 10; %Simulation time.
t = [0:T:Tf]; %Discrete time used in the simulation.
%Discrete Response Matrix Y:
Y =[0,-1.70970000, 4.40790000, 2.90110000, . . . ];
%Time Signals and PSD
figure(1)
[Syy,freqs] = pwelch(Y',[],[],[],fs); %Obtain estimates of the output power spectrums.
```

```
clf
subplot(2,1,1)
plot(t,Y)
title('ANSYS TRANSIENT Impulse 4096 Hz - Time Signals', 'fontname', 'times', 'FontSize', 14)
xlabel('Time (s)', 'fontname', 'times', 'FontSize', 14)
ylabel('Acceleration (mm / s÷2)', 'fontname', 'times', 'FontSize', 14)
axis tight
legend('Node 1', 'Node 2', 'Node 3', 'Node 4', 'Node 5', 'Node 6')
subplot(2,1,2)
plot(freqs,10*log10(Syy))
title('Power Spectra Density (PSD) Functions', 'fontname', 'times', 'FontSize', 14)
xlabel('Frequency (Hz)', 'fontname', 'times', 'FontSize', 14)
ylabel('PSD (dB)', 'fontname', 'times', 'FontSize', 14)
grid on
axis tight
legend('Node 1', 'Node 2', 'Node 3', 'Node 4', 'Node 5', 'Node 6')
figure(2)
plot(freqs, 10*log10(Syy))
title('Power Spectra Density Functions', 'fontname', 'times', 'FontSize', 14)
xlabel('Frequency (Hz)', 'fontname', 'times', 'FontSize', 14)
ylabel('PSD (dB)',' fontname', 'times', 'FontSize', 14)
grid on
axis tight
legend('Node 1','Node 2','Node 3','Node 4','Node 5','Node 6')
%::::::::::::::::::::::::::::::::::::::::::::::::::::::::::::::::::::::::::::::::::::::::::::
%METHOD 1: N4SID
%::::::::::::::::::::::::::::::::::::::::::::::::::::::::::::::::::::::::::::::::::::::::::::
%The first step is to create the data object for use with the built-in n4sid algorithm using iddata.
data = iddata(Y',[],T);
%Then, it is necessary to call n4sid on the data object using a model order of 14 to overspecify the identified system and then extract the A and C matrices.
sys = n4sid(data,18);
[A_n4,;C_n4, ] = ssdata(sys);
```

%After that, it is possible to obtain the modal parameters using the modalparams function from the OoMA toolbox.

[fn_n4, zeta_n4, Phi_n4] = modalparams(A_n4, C_n4, T);

%Finally, it is possible to plot the identified mode shapes. Since only one model order was used for identification, use the first index of the cell array Phi_n4.

figure(3)

plotBuildingModes(Phi_n41(:,1:6))

%::

%METHOD 2: SSI-COV

%::

%Specify the order numbers wanted and then use twice as many time lags as the model order for identification purposes.

order = 40;

s = 2*order;

%Call ssicov on the output data.

[A_cov,C_cov,G_cov,R0_cov] = ssicov(Y,order,s);

%Plot the stabilization diagram

figure(4)

err = [0.01,0.05,0.98];

[IDs_cov] = plotstab(A_cov, C_cov, Y, T, [], err);

title('ANSYS TRANSIENT Impulse 4096 Hz - SSI-COV Stabilization Diagram', 'fontname', 'times', 'FontSize', 14)

xlabel('Frequency [Hz]', 'fontname', 'times', 'FontSize', 14)

%From the stabilization diagram it is necessary to find which minimal mode order gives the best results for natural frequencies.

%Plot the mode shapes

figure(5)

[fn_cov,zeta_cov,Phi_cov] = modalparams(A_cov, C_cov, T);

plotBuildingModes(Phi_cov14(:,1:6))

%With the help of the stabilization diagram, natural frequencies, damping and mode shapes can be obtained.

%::

%METHOD 3: SSI-DATA

%::

%To begin the SSI-DATA method it is necessary to establish the maximum model order and the desired time lags. For this case, we can reuse the ones defined for the SSI-COV method. With these parameters set, the next step is to call the SSI-DATA function as follows:

[A_data,C_data,G_data,R0_data] = ssidata(Y,order,s);

%The next step is to create the stabilization diagram plot as follows:

figure(6)

[IDs_data] = plotstab(A_data, C_data, Y, T, [], err);

title('ANSYS TRANSIENT Impulse 4096 Hz - SSI-DATA Stabilization Diagram', 'fontname', 'times', 'FontSize', 14)

xlabel('Frequency [Hz]', 'fontname', 'times', 'FontSize', 14)

%Finally, it is possible to plot the mode shapes as shown below.

figure(7)

[fn_data,zeta_data,Phi_data] = modalparams(A_data, C_data, T);

plotBuildingModes(Phi_data14(:,1:6))

%::

%MAC COMPARISON

%AUTO-MACs

%::

AutoN4 = macmatrix(Phi_n41(:,1:6),Phi_n41(:,1:6));

figure(8)

bar3(AutoN4)

title('ANSYS TRANSIENT Impulse 4096 Hz - N4SID Auto-MAC', 'fontname', 'times', 'FontSize', 14)

xlabel('Mode', 'fontname', 'times', 'FontSize', 14)

ylabel('Mode', 'fontname', 'times', 'FontSize', 14)

AutoCOV = macmatrix(Phi_cov14(:,1:6),Phi_cov14(:,1:6));

figure(9)

bar3(AutoCOV)

title('ANSYS TRANSIENT Impulse 4096 Hz - SSI-COV Auto-MAC', 'fontname', 'times', 'FontSize', 14)

xlabel('Mode', 'fontname', 'times', 'FontSize', 14)

ylabel('Mode', 'fontname', 'times', 'FontSize', 14)

AutoDATA = macmatrix(Phi_data14(:,1:6), Phi_data14(:,1:6));

figure(10)

```
bar3(AutoDATA)
title('ANSYS TRANSIENT Impulse 4096 Hz - SSI-DATA Auto-MAC', 'fontname', 'times', 'FontSize', 14)
xlabel('Mode', 'fontname', 'times', 'FontSize', 14)
ylabel('Mode', 'fontname', 'times', 'FontSize', 14)
%::::::::::::::::::::::::::::::::::::::::::::::::::::::::::::::::::::::::::::::::::::::
%CROSS-MACs
%::::::::::::::::::::::::::::::::::::::::::::::::::::::::::::::::::::::::::::::::::::::
CrossMAC = macmatrix(Phi_data14(:,1:6),Phi_cov14(:,1:6));
figure(11)
bar3(CrossMAC)
title('ANSYS TRANSIENT Impulse 4096 Hz - Cross-MAC', 'fontname', 'times', 'FontSize', 14)
xlabel('SSI-DATA Mode', 'fontname', 'times', 'FontSize', 14)
ylabel('SSI-COV Mode', 'fontname', 'times', 'FontSize', 14)
```

APPENDIX C

APPENDIX C: MATLAB® OUTPUT-ONLY MODAL ANALYSIS TOOLBOX GUIDE

The MATLAB® Output-Only Modal Analysis (OoMA) Toolbox is a powerful free toolbox created by Andrew Otto for the software MATLAB® used to perform an operational modal analysis of beam-like systems using three different methods: N4SID, SSI-DATA and SSI-COV. To better illustrate the steps followed, the process to perform the OMA of the impulse transient simulation with $f_s = 4096Hz$ will be shown in this guide.

C.1 OoMA and MAC Installation

To install the OoMA Toolbox, the first step necessary is to create an account in **Mathworks** to download the toolbox and zip files needed. The OoMA Toolbox contains multiple examples of how to use the software and the functions needed to perform the OMA with the methods desired.

After the download of both archives, it is recommended to read the examples given in the ZIP file to grasp a better understanding of how the toolbox works. It is also recommended to create the *animateBuildingModes.m* and *plotBuildingModes.m* functions as instructed in *Example 1*, as they are necessary for the plot and animation of the mode shapes.

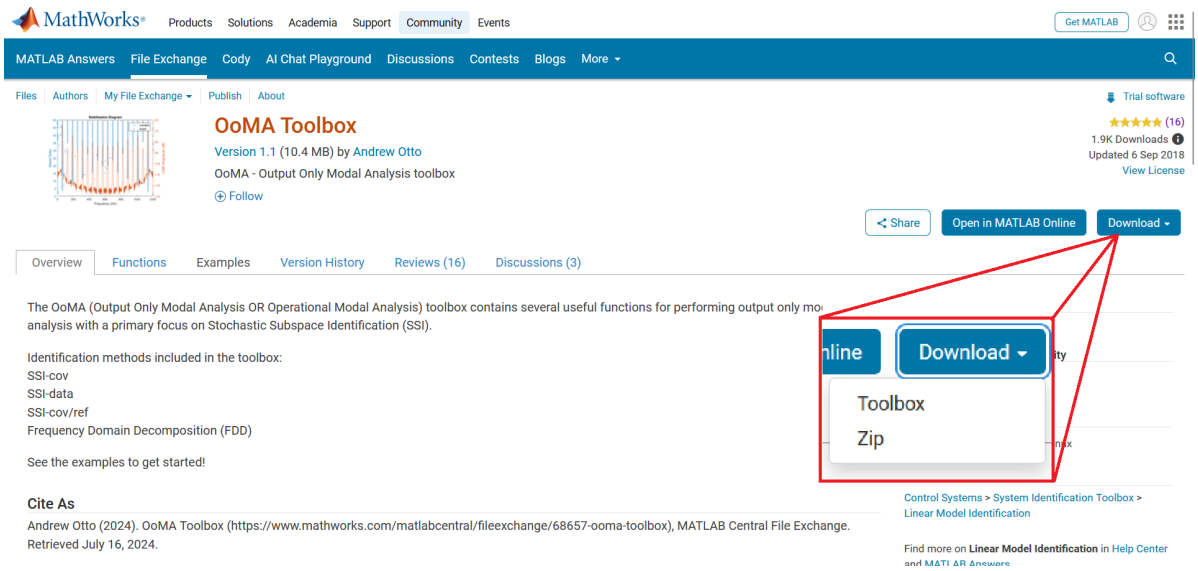

Figure C.1: OoMA Toolbox download page in the MathWorks website. It is necessary to download both the toolbox and the ZIP code available. Source: MathWorks (2024).

C.2 OoMA Script and Simulation/Experiment Parameters

With the installation completed, the first step to perform an OMA with the OoMA toolbox is to create the script that will contain all information necessary for the OMA: the parameters of the data acquisition, the methods desired and the types of MAC to be performed. In the script, the first step is to establish the parameters used during the data acquisition, which are:

Sampling Frequency f_S [Hz]: frequency at which the data was measured. For the OoMA toolbox to work properly, it is recommended that f_S is constant, as a variable f_S would require complex modification of the source code.

Sampling Time-Period $T = \frac{1}{f_s}$ [s]: time interval in seconds between each sampling measurement.

Simulation Time-Length t_f [s]: total time-length recorded of the experiment or simulation.

Discrete-time vector $t = [0 : T : T_f]$: Time vector necessary for the OMA methods to work. It is defined from $t = 0$ to the final time of recording in seconds $t = t_f$, with time-intervals given by the sampling time-period (T).

C.2.1 Transient Impulse Simulation (4096 Hz)

For the **Transient Impulse Simulation** with $f_s = 4096Hz$ performed during this work the parameters were set as:

$\mathbf{f_s}$ = **4096Hz** *%Sampling frequency used.*

T = (**1**/$\mathbf{f_s}$) *%Sampling period.*

$\mathbf{T_f}$ = **10** *%Total time of the acquisition in seconds.*

[**0** : $\mathbf{f_s}$: $\mathbf{T_f}$] *%Time vector.*

C.3 Output-Matrix Import

The next step is to import the output-matrix **Y** of the system. **Y** is the time-domain matrix formed by measuring the response in each one of the nodes of the structure being analyzed. This measurements can be given in the form of acceleration, velocity, G, etc. The dimension of the matrix will depend on the number of nodes in the structure (**N**) and the samples measured (**m**), in other words $\mathbf{Y_{(N \times M)}}$.

The matrix can be created inside the script itself or called as a function. The only requisites is that the matrix has the nodes as the rows and the measurements as the columns, otherwise the program will crash.

C.3.1 Transient Impulse Simulation (4096 Hz)

For the **Transient Impulse Simulation**, the matrix **Y** had dimensions 6 X 40,961 as the beam had 06 nodes and a total of 40,9061 samples recorded for each node. The measurements obtained corresponded to the acceleration in the y-axis direction, given in mm/s^2, however other types of measurements and other units can be used with the appropriated adaptations in the code.

For this simulation, the matrix was created inside the script itself, however for bigger matrices it is recommended to call the matrix instead, as creating it in the script consumes a significant amount of memory.

The code used to import the matrix was the following:

%Discrete Response Matrix Y:

Y = [0, -1.70970, 4.40790, 2.90110, ..., 1.32900e-05];

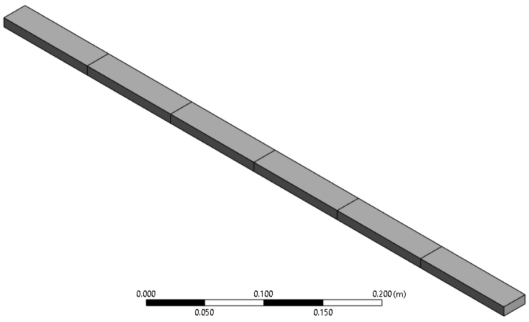

(a) SCB mesh, showing the 6 nodes considered in the transient simulations.

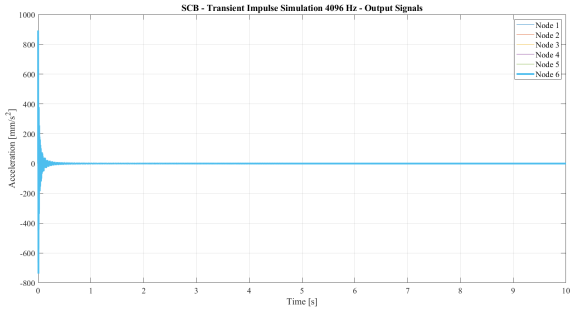

(b) Output signals obtained from the nodes of the SCB.

Figure C.2: The output matrix **Y** was created from the acceleration measurements obtained from each individual node of the SCB.

ANSYS TRANSIENT Impulse 4096 Hz - Response Matrix

Time [s]	Node 1 [mm/s²]	Node 2 [mm/s²]	Node 3 [mm/s²]	Node 4 [mm/s²]	Node 5 [mm/s²]	Node 6 [mm/s²]
0.00000000	0.00000000	0.00000000	0.00000000	0.00000000	0.00000000	0.00000000
0.00024414	-1.70970000	2.40720000	5.20500000	-25.31400000	-38.94200000	892.66000000
0.00048828	4.40790000	2.80940000	-15.98900000	-133.74000000	281.36000000	37.83700000
0.00073242	2.90110000	32.51200000	-120.63000000	-21.67600000	328.63000000	-532.13000000
0.00097656	51.19200000	-61.14200000	-215.96000000	419.09000000	-179.79000000	103.77000000
0.00122070	18.53700000	-255.62000000	197.21000000	94.15300000	-53.34500000	-196.74000000
0.00146484	-248.97000000	-109.70000000	333.13000000	-128.66000000	9.86680000	26.47100000
0.00170898	-353.98000000	277.22000000	-66.91700000	104.79000000	-94.83500000	-18.11100000
0.00195313	287.48000000	2.10800000	61.83700000	-65.16600000	38.51500000	-62.48100000
0.00219727	567.63000000	-16.38900000	-54.21500000	48.23800000	-41.52200000	-21.38900000
0.00244141	-106.66000000	445.50000000	-184.66000000	-39.45100000	41.36800000	-33.70300000

ANALYTICAL | ANSYS Modal | IMP - OoMA | fs Effect | S. IMP 1024 Hz | S. IMP 2048 Hz | S. IMP 4096 Hz | S. IMP 8192 Hz

(c) Output matrix created in Excel® from the output signals.

Figure C.2: The output matrix **Y** was created from the acceleration measurements obtained from each individual node of the SCB.

C.4 Time Signals and PSDs Plot

After the import of the output-matrix **Y**, it is necessary to confirm that the output-data is coherent. To do so, an important step consists in the visualization of the time-signals obtained and their respectives PSD functions. This step is crucial as it allows to observe if all the signals obtained have expected format and are correctly aligned, which is crucial for multiple-runs tests. Other important information that is possible to obtain by visualizing the signals and their PSDs is the level of noise present.

C.4.1 Transient Impulse Simulation (4096 Hz)

achieved with the following code:

% Time Signals and PSD Functions

figure(1) [Syy,freqs] = pwelch(Y',[],[],[],fs); % obtain estimates of the output power spectrums

clf

subplot(2,1,1) plot(t,Y)

title('ANSYS TRANSIENT Impulse 4096 Hz - Time Signals' , 'fontname', 'times', 'FontSize', 14)

xlabel('Time (s)', 'fontname', 'times', 'FontSize', 14)

ylabel('Acceleration (mm / s^2)', 'fontname', 'times', 'FontSize', 14)

axis tight

legend('Node 1', 'Node 2', 'Node 3', 'Node 4', 'Node 5', 'Node 6')

subplot(2,1,2)

plot(freqs,10*log10(Syy))

title('Power Spectra Density (PSD) Functions', 'fontname', 'times', 'FontSize', 14)

xlabel('Frequency (Hz)', 'fontname', 'times', 'FontSize', 14)

ylabel('PSD (dB)', 'fontname', 'times','FontSize', 14)

grid on

axis tight

legend('Node 1', 'Node 2', 'Node 3', 'Node 4', 'Node 5', 'Node 6')

The time signals and PSD obtained for this simulation can be seen below in figure C.3.

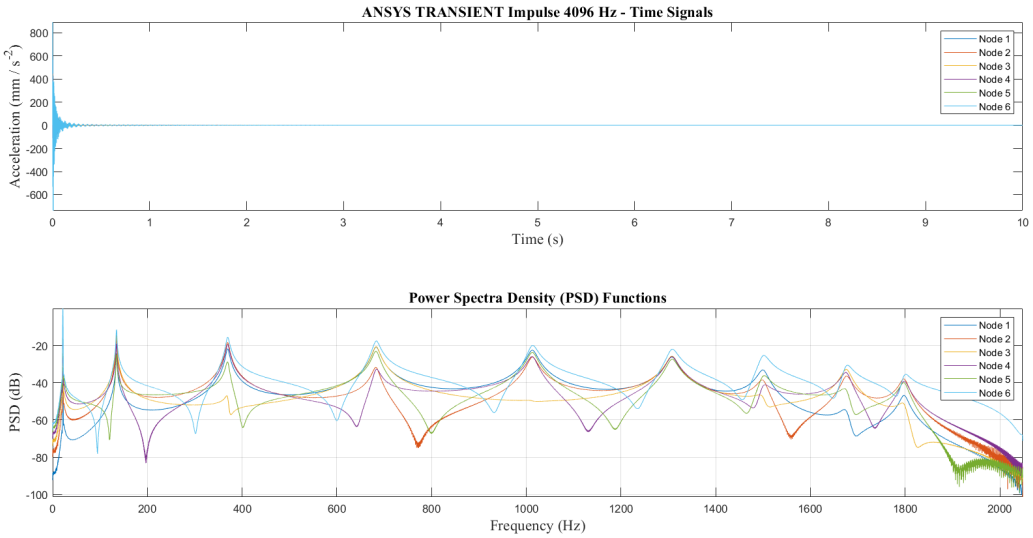

Figure C.3: Time Signals and PSD Functions from the Impulse 4096 Hz simulation.

C.5 OMA Methods

C.5.1 N4SID

After plotting the time-signals and PSD graphs, the next step is to set the OMA methods that will be implemented in the script. The first-one in the list of OMA methods available in the OoMA toolbox is the N4SID technique. The first step of the N4SID is to create the data object that will be used by the algorithm by using the built-in function *iddata*:

%Create the ID data:

data = iddata(Y',[],T);

With the creation of the data object done, the next step is to call the *n4sid* function as shown in the code below. While calling the *n4sid* function, it is necessary to establish the model order of resolution for the N4SID method. After it, the matrices A and C needed to extract the modal parameters can also be created by using the function *ssdata(sys)*.

% Call the N4SID function:

sys = n4sid(data,14);

[A_n4,;C_n4,~] = ssdata(sys);

With the A and C matrices created, the final step is the extraction of the modal parameters using the built-in function *modalparams* from the OoMA toolbox and plotting the mode shapes obtained:

```
[fn_n4,zeta_n4,Phi_n4] = [modalparams(A_n4,C_,T);

figure(2)

plotBuildingModes(Phi_n41)

title('N4SID Mode Shapes')
```

The disadvantage of the N4SID method is that it does not offer a stabilization diagram to help identify the model order necessary to obtain all the modes of interest. Therefore, it is necessary to use a try and error approach to obtain good results, which depending on the model order used can take a considerable amount time and computational resources. Figure C.4 shows the mode shapes obtained with the N4SID method for the $f_s = 4096Hz$ Impulse Simulation.

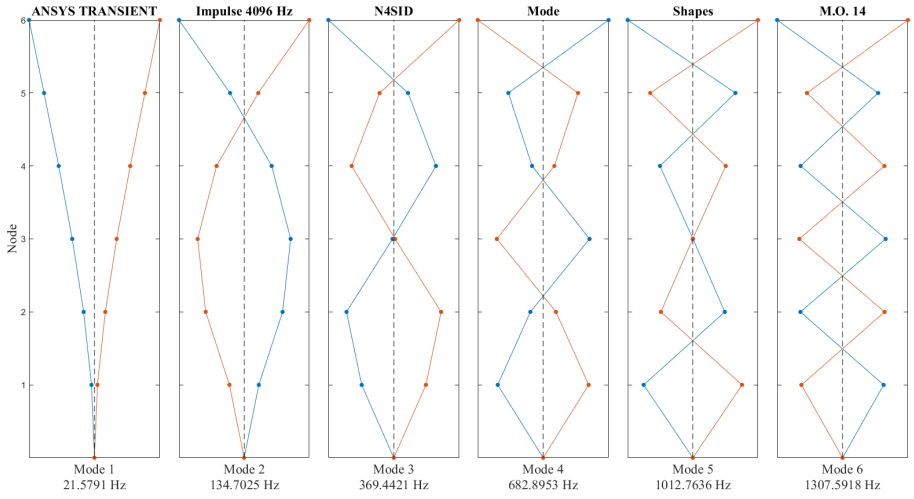

Figure C.4: Impulse Simulation 4096 Hz Mode Shapes obtained with the N4SID method.

Once the mode shapes are consistent with the results expected, the modal parameters can be extracted from the workspace environment as shown in figure C.5 below, where they are contained in the variables fn_n4 for the natural frequencies and $zeta\_n4$ for the damping ratios.

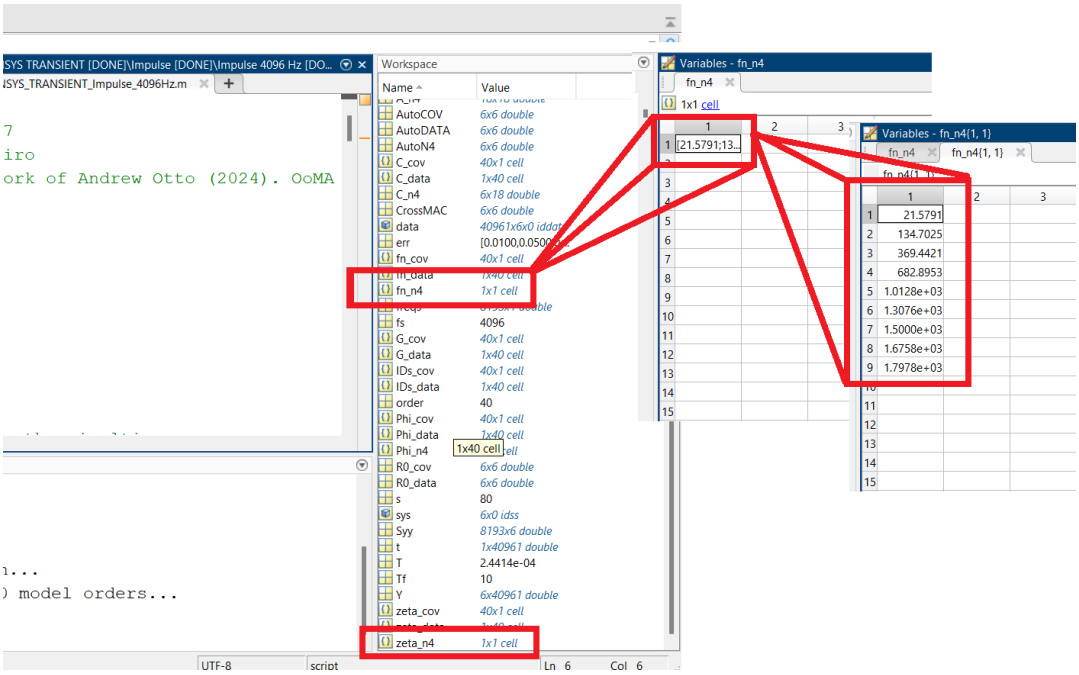

Figure C.5: The natural frequencies and damping ratios obtained with the N4SID method can be found in the workspace environment under the names fn_n4 and $zeta\_n4$ from which the values can be extracted.

C.5.2 SSI-COV

To start SSI-COV method in the OoMA toolbox, it is necessary to establish a model order for the resolution. In general higher model orders tend to yield more accurate results, however the increase in computational resources with higher model orders is not always worth the increase in accuracy, specially for initial approaches. As an initial model order, a recommended model order is of 20 as it is a good compromise between accuracy and computational resources. For *Impulse Simulation 4096 Hz* the model order used was of 40 as seen in the code below, where the variable *order* was created in the script. Along with the model order, it is necessary as well to determine the time lags that will be used in the solution. As a rule, it is recommended that the solution use twice as many time lags as the model order for identification purposes.

%Specify the order numbers wanted and then use twice as many time lags as the model order for identification purposes.

order = 40;

s = 2*order;

The second step of the SSI-COV method is create the matrices A, C, G, and R_0 needed

for the method. To do so, the function *ssicov(Y,order,s)* built-in in the OoMA toolbox is called in the script where the inputs are the output-matrix Y, the model order selected $order$ and the time lags s.

```
%Call the SSI-COV function on the output data:
[A_cov,C_cov,G_cov,R0_cov] = ssicov(Y,order,s);
```

With these matrices obtained, it is possible then to plot the stabilization diagram. This diagram shows the PSD graph of the system and the poles obtained during the solution of the system, with an × on the stable poles and dot • for unstable poles. This diagram is crucial for the SSI-COV method as it helps to identify what minimal model order is necessary to find a row with stable poles in all the suspected modes of interest, which can be inferred as the peaks in the PSD graph. The code used to plot the stabilization diagram can be seen below:

```
% Plot the stabilization diagram
figure(4)
err = [0.01,0.05,0.98];
[IDs_cov] = plotstab(A_cov,C_cov,Y,T,[],err);
title('ANSYS TRANSIENT Impulse 4096 Hz - SSI-COV Stabilization Diagram', 'fontname', 'times', 'FontSize', 14)
xlabel('Frequency [Hz]', 'fontname', 'times', 'FontSize', 14)
```

The stabilization diagram of *Impulse Simulation 4096 Hz* can be seen in figure C.6 below.

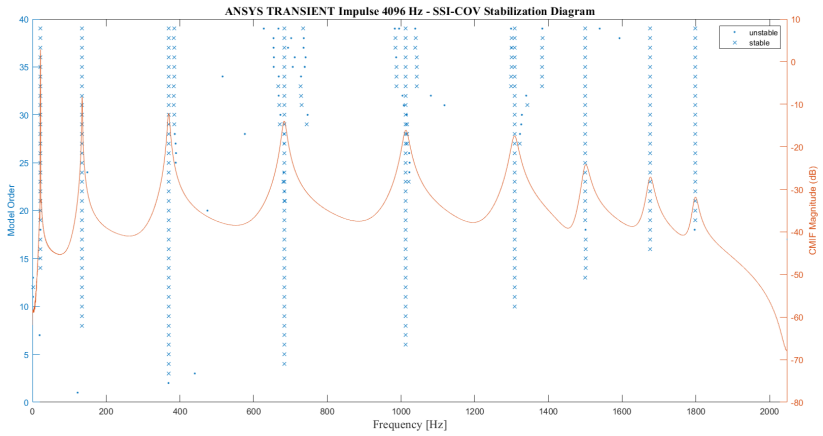

Figure C.6: In the stabilization diagram for the SSI-COV method in, it is possible to see that a model order of 14 is the minimal that yields a row with a stable pole in each one of the suspected modes of the system.

Finally, knowing the minimal model order necessary to obtain the modal parameters desired, it is possible then to plot the mode shapes. For the *Impulse Simulation 4096 Hz* the mode shapes obtained can be seen in figure C.7 below, and the natural frequencies and damping ratios can be obtained by following the same procedures as in the N4SID method as seen in figure C.8.

%Plot the mode shapes

figure(5)

[fn_cov,zeta_cov,Phi_cov] = modalparams(A_cov,C_cov,T);

plotBuildingModes(Phi_cov14(:,1:6))

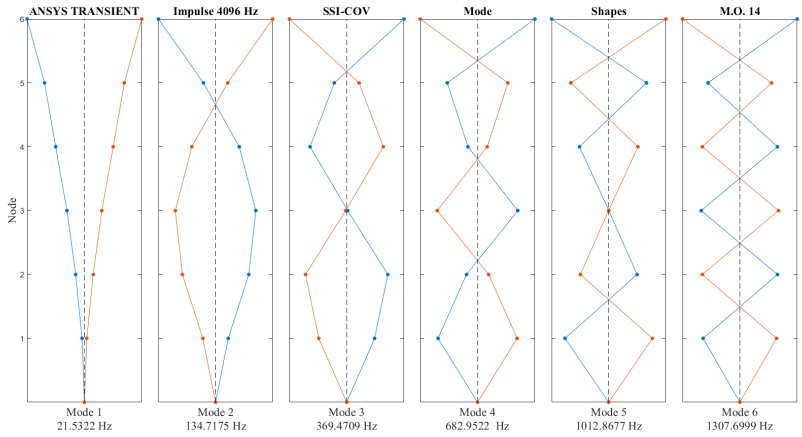

Figure C.7: SSI-COV mode shapes obtained for the Impulse Simulation 4096 Hz.

C.5.3 SSI-DATA

The SSI-DATA method follows the exact same methodology implemented in the SSI-COV method, with the only adaptations being done in the function names. The code used for this method can be seen below:

% METHOD 3: SSI-DATA

% To begin the SSI-DATA method it is necessary to stablish the maximum model order and the desired timelags. For this case, we can reuse the ones defined for the SSI-COV method. With these parameters set, the next step is to call the SSI-DATA function as follows:

[A_data, C_data, G_data, R0_data] = ssidata(Y, order, s);

% The next step is to create the stabilization diagram plot as follows:

figure(6)

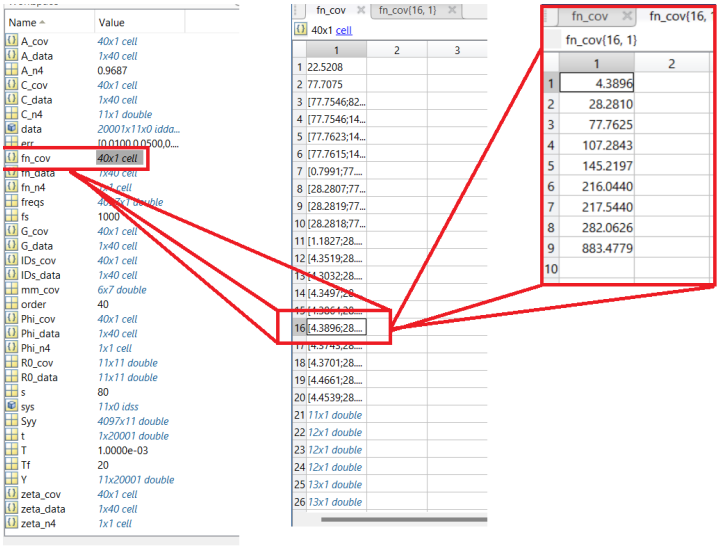

Figure C.8: The modal parameter values can be accessed in the same way done for the N4SID method. The only difference is that in the SSI-COV method it will be necessary to find the vector that corresponds to the minimal model order found.

[IDs_data] = plotstab(A_data, C_data, Y, T, [], err);

title('ANSYS TRANSIENT Impulse 4096 Hz - SSI-DATA Stabilization Diagram', 'fontname', 'times', 'FontSize', 14)

xlabel('Frequency [Hz]', 'fontname', 'times', 'FontSize', 14)

% Finally, it is possible to plot the mode shapes as shown below.

figure(7)

[fn_data, zeta_data, Phi_data] = modalparams(A_data, C_data, T);

plotBuildingModes(Phi_data14(:,1:6))

C.6 Modal Assurance Criterion (MAC)

To guarantee that the mode shapes obtained were coherent, modal assurance criterion (MAC) matrices were created to evaluate the results. Two different type of MAC analysis are available: Auto-MAC which compares the mode shapes with themselves, and Cross-MAC which compares two different sets of modes.

C.6.1 Auto-MAC

To perform the Auto-MACs of a mode shapes vector, it is possible to do it by using the MAC equation (eq. 3.29) or by using the built-in *MACMATRIX* function included in the

toolbox. The MAC matrix is created by using the command:

Auto-MAC = MACMATRIX(Phi_1,Phi_2)

Where *Phi_1,Phi_2* are the set of mode shapes to perform the the MAC. To do an Auto-MAC, the only step needed is to have both *Phi* variables as the same. The code used for creating the Auto-MAC of the N4SID method of the *Impulse Simulation 4096 Hz* can be seen below:

% MAC COMPARISON

AutoN4 = macmatrix(Phi_n41(:,1:6),Phi_n41(:,1:6));

To generate the Auto-MAC graphs, allowing for the user to visualize if there are incoherences in the mode shapes obtained with the specified method as the following code was used:

figure(8)

bar3(AutoN4)

title('ANSYS TRANSIENT Impulse 4096 Hz - N4SID Auto-MAC', 'fontname', 'times', 'FontSize', 14)

xlabel('Mode', 'fontname', 'times', 'FontSize', 14)

ylabel('Mode', 'fontname', 'times', 'FontSize', 14)

The Auto-MAC graph can be seen in figure C.9.

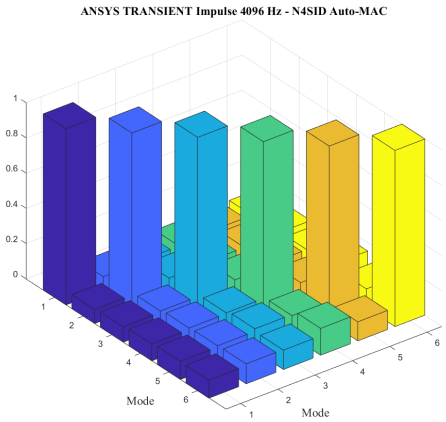

Figure C.9: Auto-MACs created for *Impulse Simulation 4096 Hz*.

C.6.2 Cross-MAC

Finally, to perform the Cross-MAC, the same command as with the Auto-MAC is necessary, with the only difference being the *Phi* variables to be evaluated as being the two

sets of modes to be analyzed. The code used to perform the Cross-MAC between the SSI-COV and SSI-DATA methods can be seen below, and the Cross-MAC can be seen in figure C.10.

```
CrossMAC = macmatrix(Phi_data14(:,1:6), Phi_cov14(:,1:6));
figure(11)
bar3(CrossMAC)
title('ANSYS TRANSIENT Impulse 4096 Hz - Cross-MAC', 'fontname', 'times', 'FontSize', 14)
xlabel('SSI-DATA Mode', 'fontname', 'times', 'FontSize', 14)
ylabel('SSI-COV Mode', 'fontname', 'times', 'FontSize', 14)
```

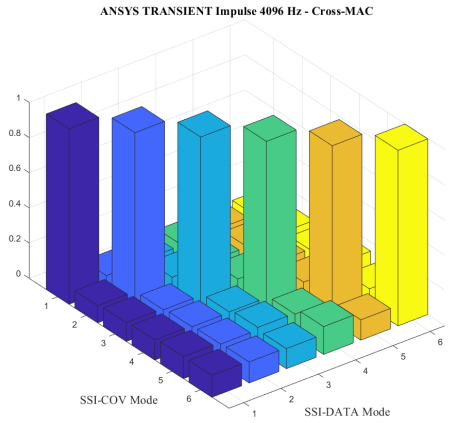

Figure C.10: Cross-MACs created for the *Impulse Simulation 4096 Hz*.

APPENDIX D

APPENDIX D: SIEMENS® SIMCENTER TESTLAB 2306® - GUIDE

The Siemens® Simcenter Testlab 2306® software is a very powerful modal analysis software capable of performing different techniques. It is possible to perform an OMA using this software in three different ways:

1. Operational Modal Analysis

2. Operational Modal Analysis Lite

3. Operational PolyMAX

This guide will focus on the ***1. Operational Modal Analysis*** and ***3. Operational PolyMAX*** methods.

The main page of Simcenter Testlab 2306 is the navigator, as seen in figure D.1. Here the work is divided into sections that can be created, deleted, and their names can be changed. This is particularly useful when a single structure is being analyzed with different sets of data.

D.1 1. Initial Setting

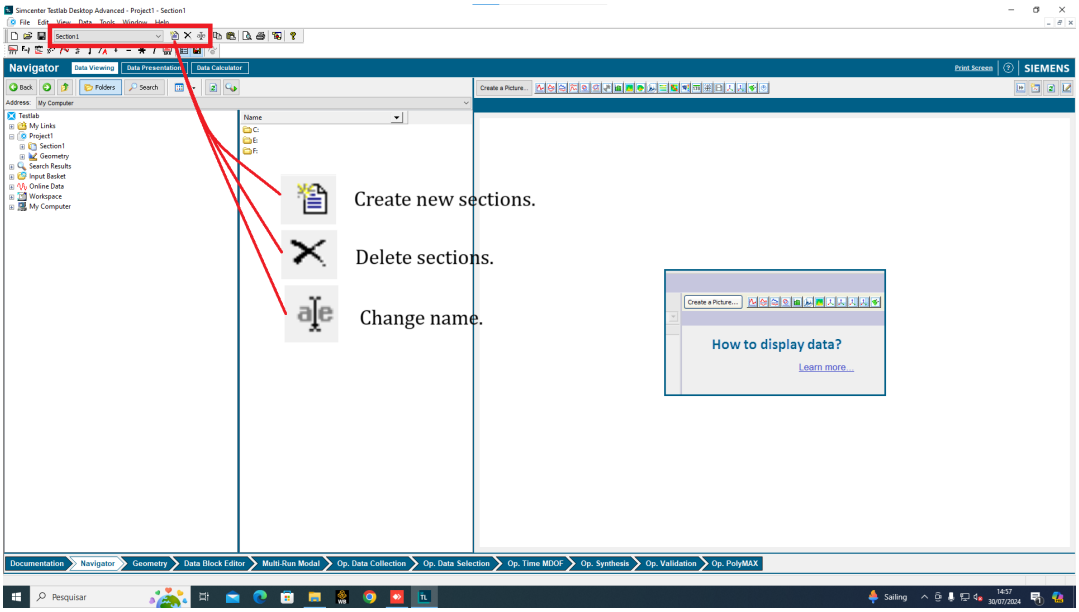

Figure D.1: Simcenter Testlab 2306® *Navigator* window.

Before performing an OMA, it is necessary to set the software. To do this, select: *Tool → Add-ins.. → Select the options: geometry, data block editor, Operational Modal Analysis and Operational PolyMAX Analysis.* This will allow to perform an OMA with the measurement from structures of interest as seen in figure D.2.

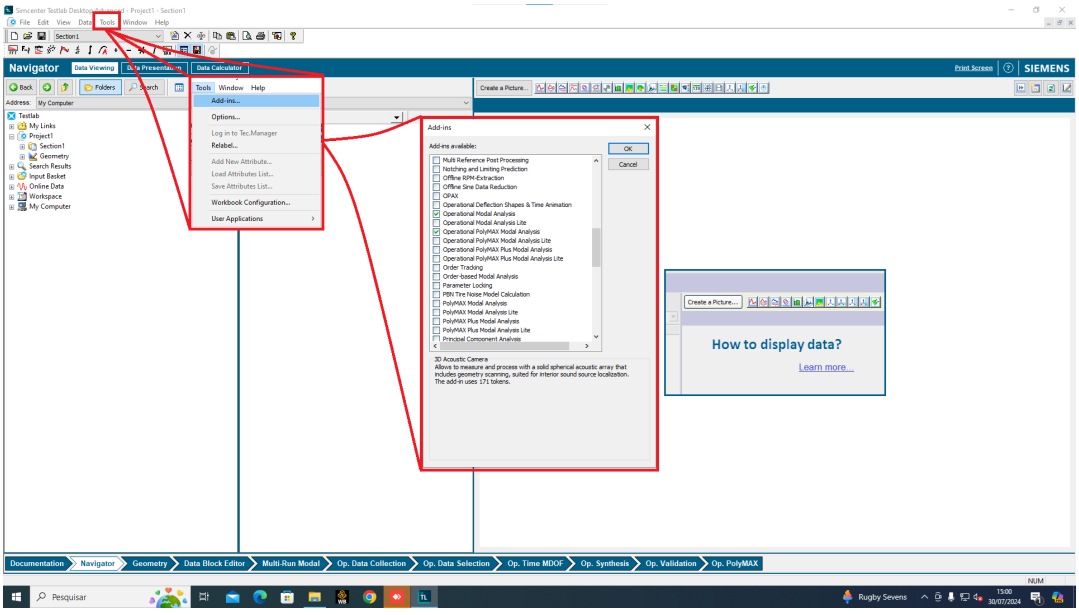

Figure D.2: Add-Ins configuration.

D.2 2. Geometry Creation

Afterward, it is recommended to create a simple geometry of the structure being analyzed. To do so, the first step is by changing the window to the geometry window in the lower toolbar. Afterwards, in the column *Component* it is necessary to assign a name for the geometry and then select in *accept table* to create this component. This can be checked in the left toolbar under the tab geometry as seen in figure D.3 where the Beam component is shown.

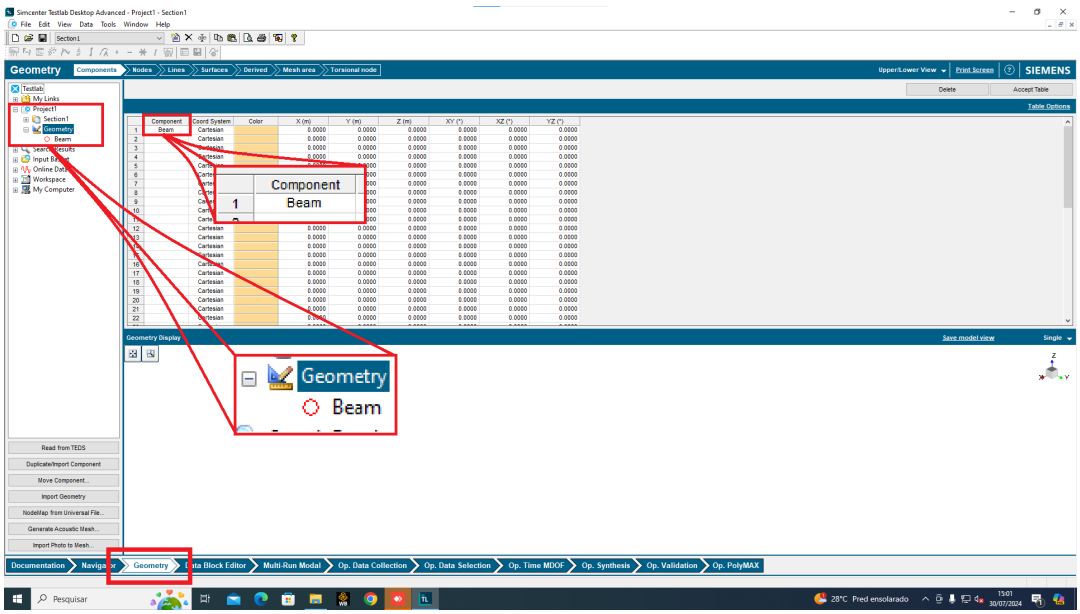

Figure D.3: Geometry creation - Components

Afterwards, the nodes for the component need to be created. It is recommended that these nodes correspond only to the measured points of the structure. After naming and defining the coordinates of all the nodes it is also necessary to click in the *Accept Table* button to create the nodes. Afterwards, the nodes defined in the table will be shown in the lower part of the window as seen in figure D.4. It is important to check that they are distributed in the expected places defined previously in the table. Finally, but **extremely important**, the column *Full name* indicates the full name with which the node is identified. This full name is fundamental as is the only way to correlate the time-signals with the nodes of the geometry created.

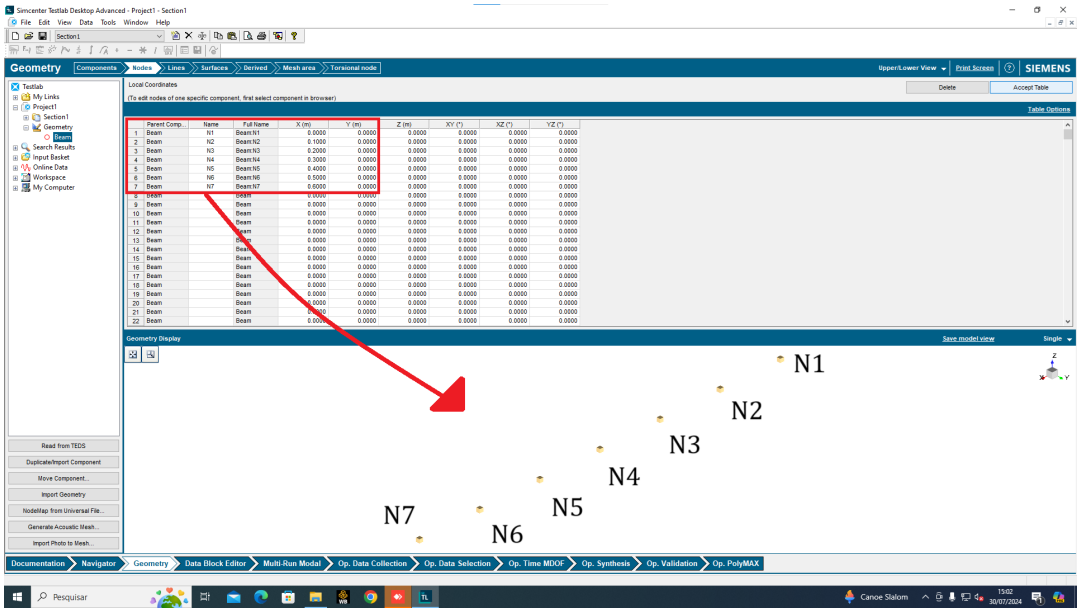

Figure D.4: Geometry creation - Nodes

To improve visualization, lines can be created by clicking between two nodes. By accepting the table the lines will be shown in the lower part of the geometry window as seen in figure D.5. The purpose of this lines is purely aesthetic and have no impact on any of the modal parameters calculated.

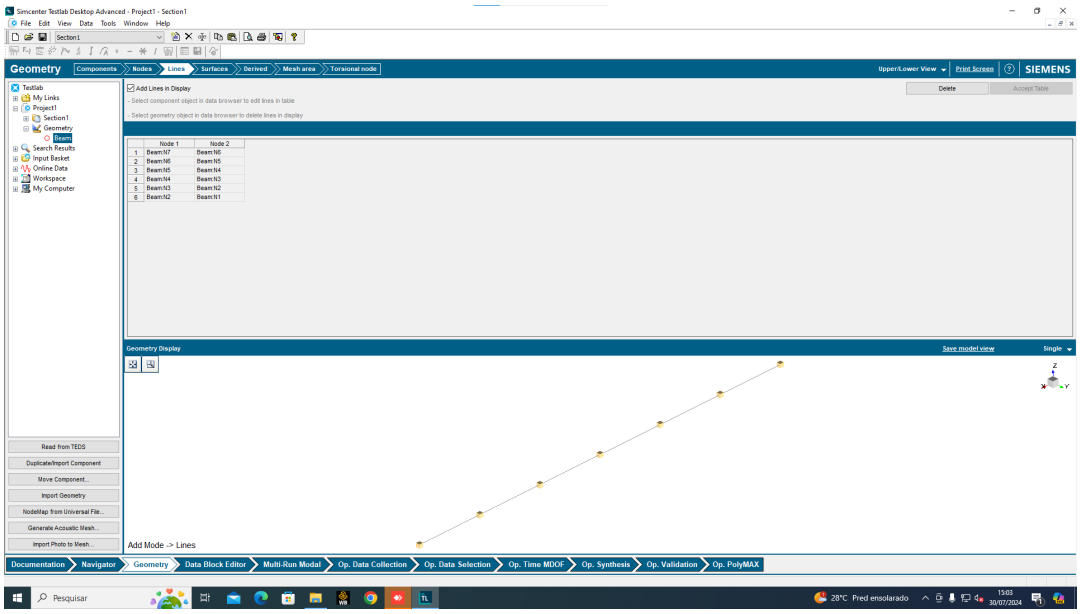

Figure D.5: Geometry creation - Lines

If the structure is not a line but rather bi-dimensional or even tri-dimensional, it is

possible to create surfaces in a similar way to the lines. There are two options for this, by using triangles which will require selecting three nodes, or squares that require four nodes.

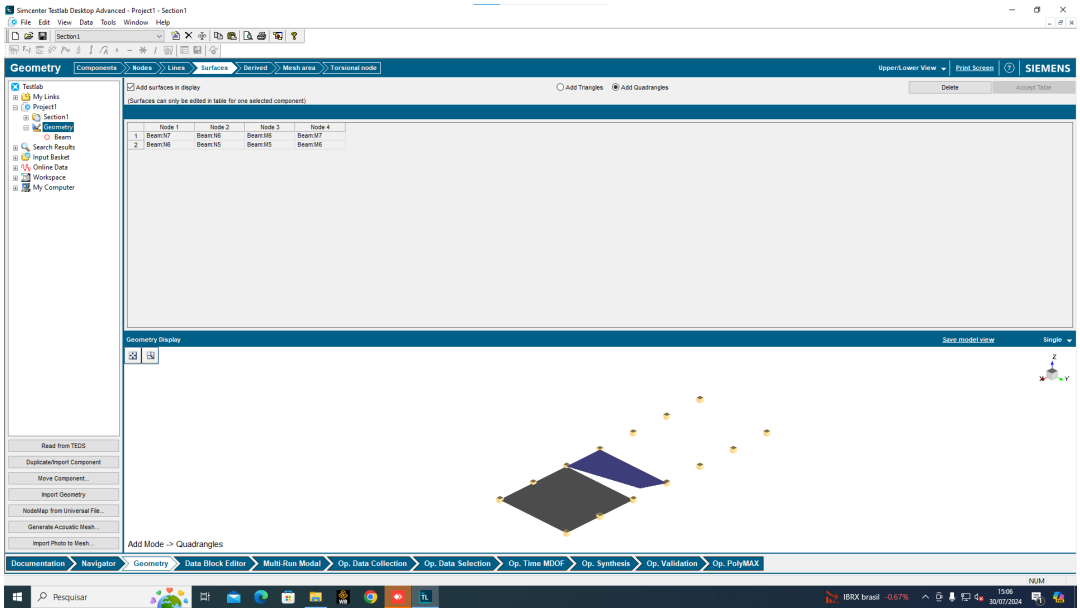

Figure D.6: Geometry creation - Surface Creation

Finally, and for aesthetic purposes as well, it is possible as well to change the color of the components to identify systems with multiple components in an easier way.

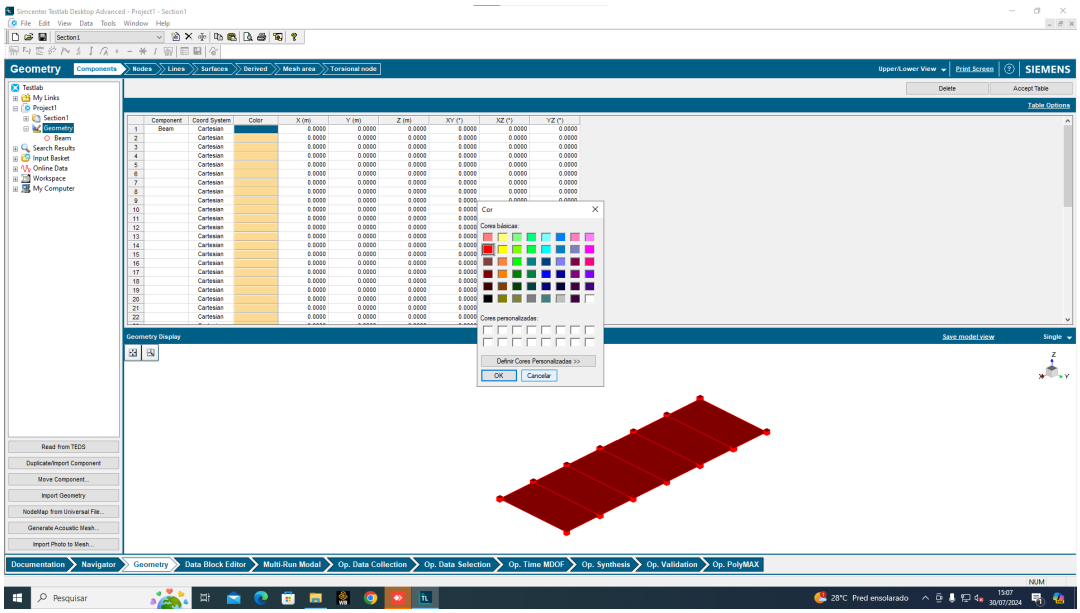

Figure D.7: Geometry creation - Component color

D.3 3. Data Import

To import the data there are two possible ways to do so. The first one is by using a UFF file containing all the time-signals measured from the system of interest. To do so, it is necessary to click on the *select block* button, from which the file must be selected. By double clicking it, it is possible to find all the individual time-signals measured as seen in figure D.8.

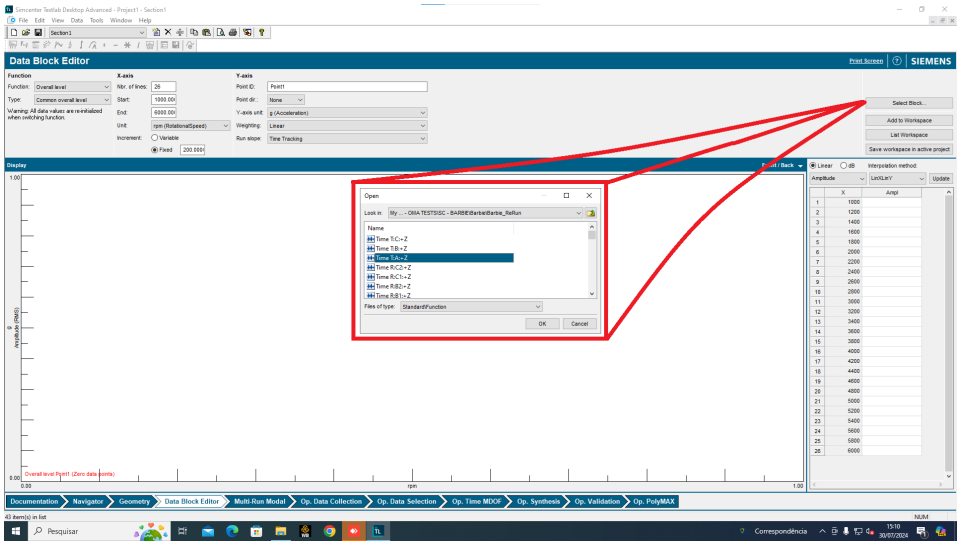

Figure D.8: Data Import - Select Block

The time-signals will have the following properties, that indicate the type of function being used, number, of lines, starting time, increment, etc. The Y-axis indicates the Point ID, its direction (+X, -X, +Y, etc.), and the unit in which it was recorded. For a proper visualization of the mode shapes, it is necessary to set all these parameters to correctly. **THE POINT ID MUST BE THE FULL NAME OF THE NODES CREATED FOR THE GEOMETRY**, otherwise the nodes will not move during the mode shape visualization. The point direction must be according to the axis system from Simcenter as well.

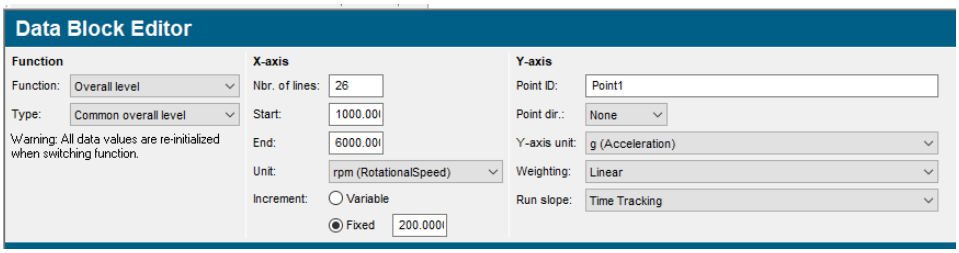

Figure D.9: Data Import - Data Block Editor

When selected, the time-signal must appear in the lower window as seen in figure D.10 below. After verifying the signal, it is necessary to add it to the workspace for its use. This is done by selecting the Add to Workspace button, and to verify that it was added it is possible to check it in the List Worspace button. The process must be repeated for all the measurements acquired and after it the button *Save as workspace in Active Project* **MUST** be selected for the data to be transferred to the current project. The second form in which the data can be imported is by pasting the measurement data directly in the right column on the data block tab, which is particularly useful if some pre-processing is required.

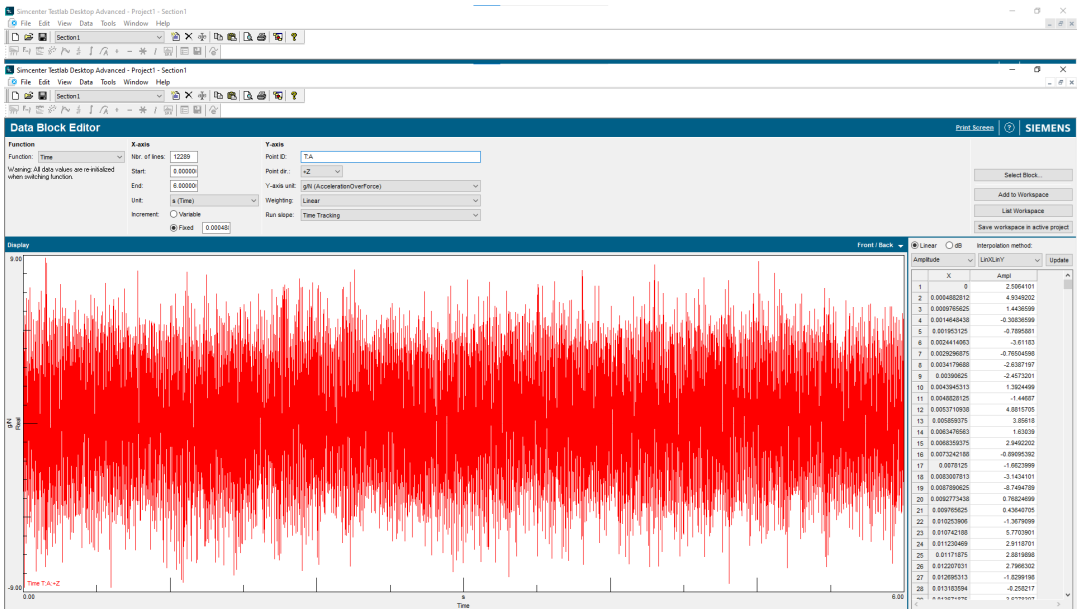

Figure D.10: Data Import - Time-signal imported

D.4 4. Data Selection

With the data in the *active section*, the next step is to import it into the *input basket*. This can be done by selecting all the time-signals in the *active section*, right click and select the *Replace in input basket*.

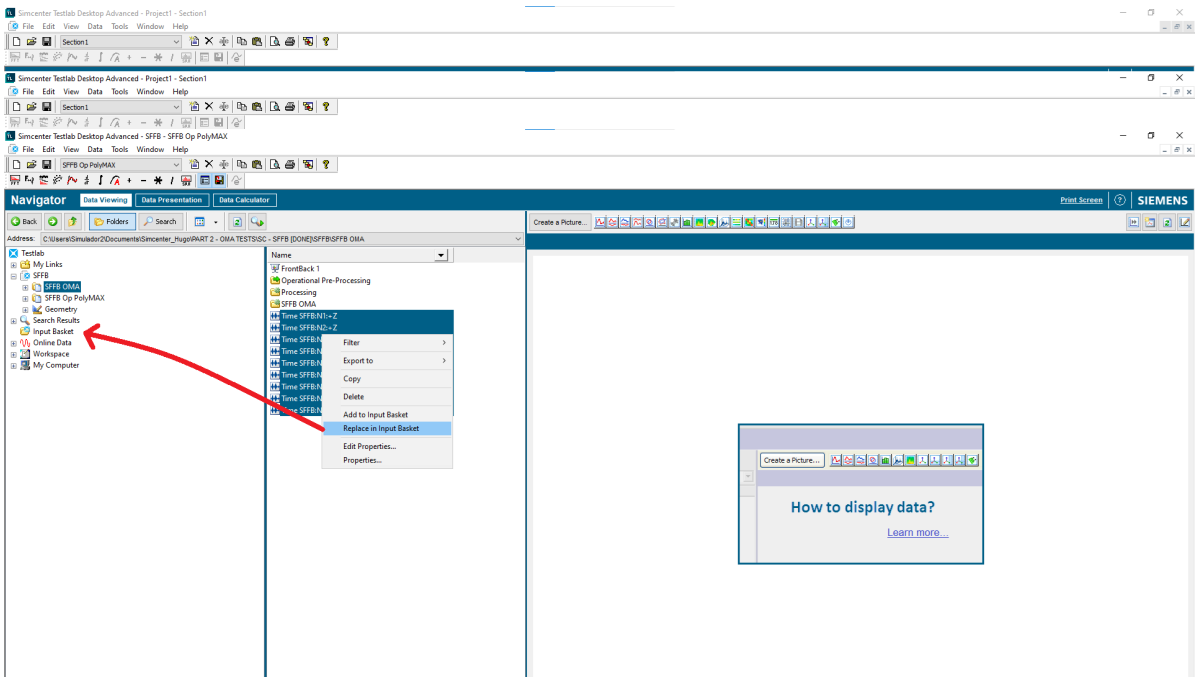

Figure D.11: Input Basket Transfer

With the time-signals in the input basket, they must appear in the Op. Data Collection tab as seen below in figure D.12. If they do not appear automatically, the button Replace must be selected for them to appear. If even after doing this they do not reappear then it is necessary to check in any mistakes were made in the previous steps. In this window, the time-signals to be used can be selected by pressing the *on*/*off* option. Reference points to create the cross-powers must also be selected, if any accelerometer was left as a reference point it must be selected here. It is also important to check the channel name to guarantee that is the same name as the nodes of the geometry and the direction.

Finally, before proceeding it is necessary to determine the number of time-lags that will be used and if any exponential window is desired. In the right-lower part of this window it will be possible to see the cross-power functions created.

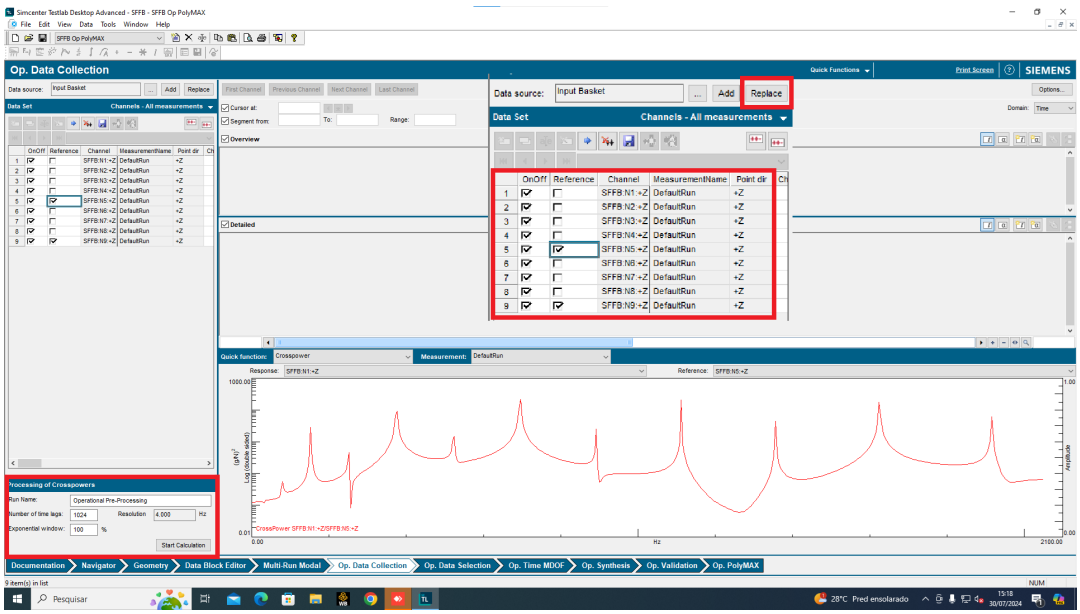

Figure D.12: Operational Data Collection

The next window is the *Op. Data Selection* window, here it is possible to create *Cross-Power sets* if wanted. The main purpose of this window is to check if all the measurements selected are valid to proceed, which can be verified by the green square next to the *status* text in the left column. If the square is red, it is necessary to check in the previous steps if any mistake was done.

Figure D.13: Operational Data Selection

The main part of the OMA add-in in the Simcenter Testlab 2306® is the ***Op. Time MDOF*** window, as seen in figure D.14. This window is divided into three main parts: Band selection, stabilization diagram and reference points. The first part, band selection, allows to select the frequency band of interest which can be done in the lower part of the window, where the minimum and maximum values to be checked in the band are set. It is recommended that this band is not intersecting any peaks nor valleys present in the cross-power. The band selection can also be made general, choosing more than one peak at the time, or can be done for every peak individually or any area in which a mode is expected, even if there is no apparent peak in the cross-power. This second method is called *narrow band* selection and is particularly useful for cases with high levels of noise or in the presence of harmonic excitations.

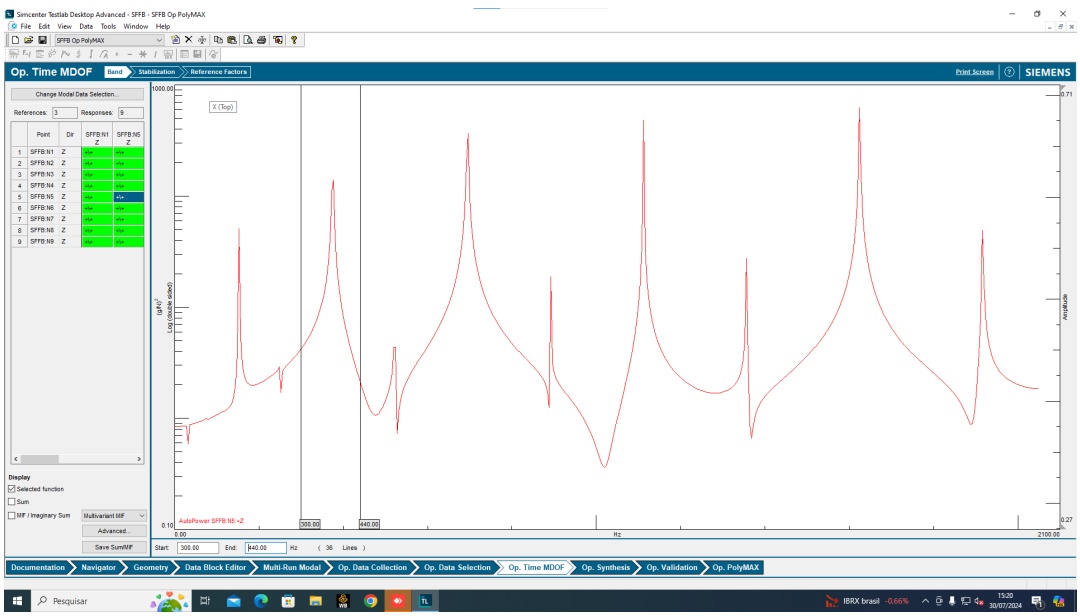

Figure D.14: Op. Time MDOF - Frequency band selection.

Once the frequency band is selected, the next step resides in the stabilization diagram. Here, it is necessary to find any columns of stable poles, denoted by the letter ***S*** that correspond to stable poles identified, indicating a possible mode. It is recommended to find for columns of stable poles as they are better indicators of actual poles. To visualize the poles easier, it is possible to zoom in an specific region by holding the left-click over the region of interest.

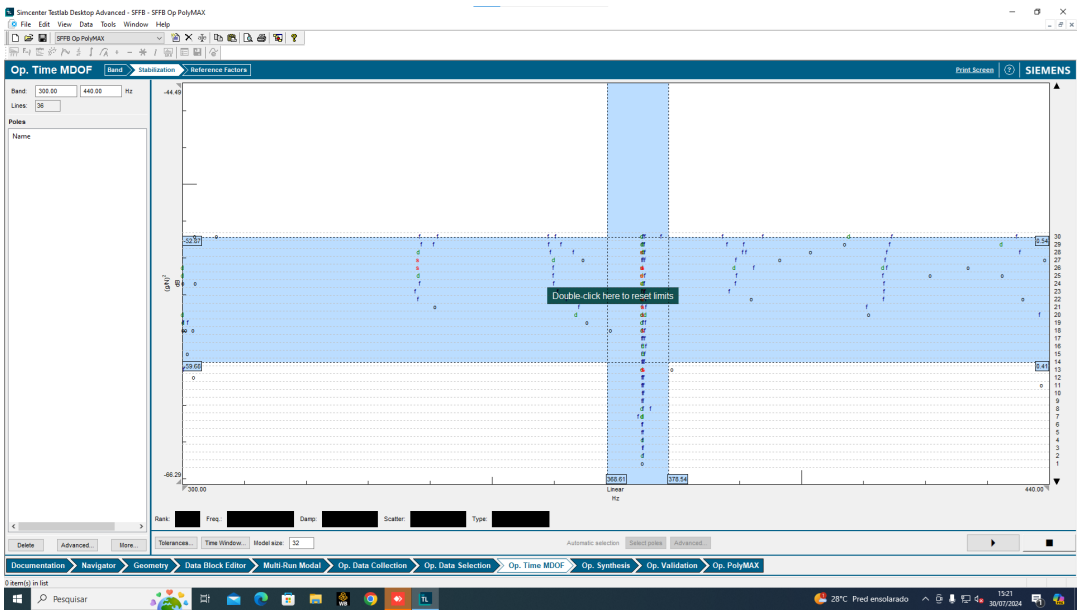

Figure D.15: Op. Time MDOF - Stabilization diagram.

Once the desired stable poles are identified, it is possible to select them by clicking on the, which will make them appear in the left column and a vertical line appear will also appear in the stabilization diagram. Previous knowledge of the structure is necessary as the best form to choose poles is to search for those with the expected natural frequency and damping ratio for the mode being identified.

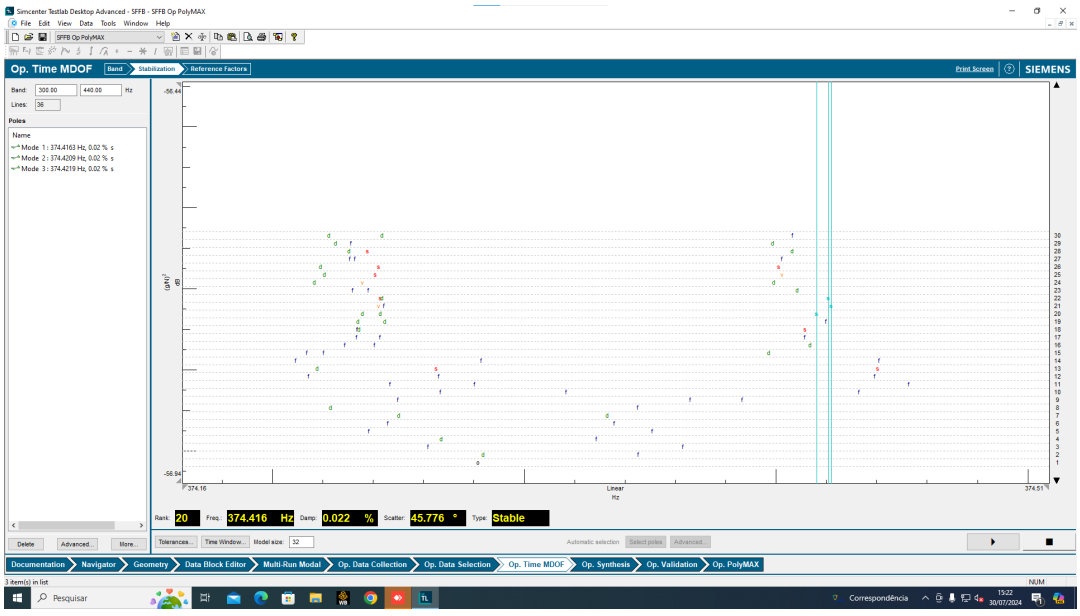

Figure D.16: Op. Time MDOF - Stabilization diagram pole selection.

The final step after choosing the stable poles is to check if they have the expected mode shapes. This is done in the *Reference Factors* tab. Where the poles to be analyzed can be selected in the upper-left column and by pressing the *Calculate* option the software will calculate their corresponding mode shapes, as seen in the lower-left column. The animated mode shape can be seen by selecting the *Display* button at the left-bottom button which will make the mode shape appear in the right window.

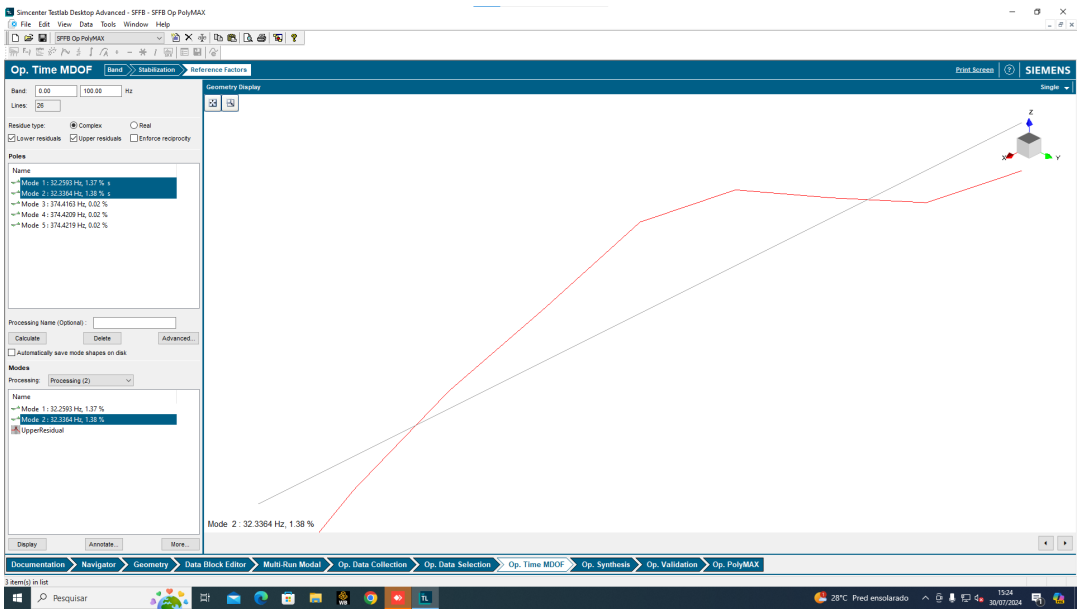

Figure D.17: Op. Time MDOF - Modal parameters verification.

If all the modal parameters have the values and mode shapes expected (or very close) it is possible then to pass to the curve adjustment section in the *Op. Synthesis* tab as seen in figure D.18. This curve is necessary to validate the data and can be used for other applications as well.

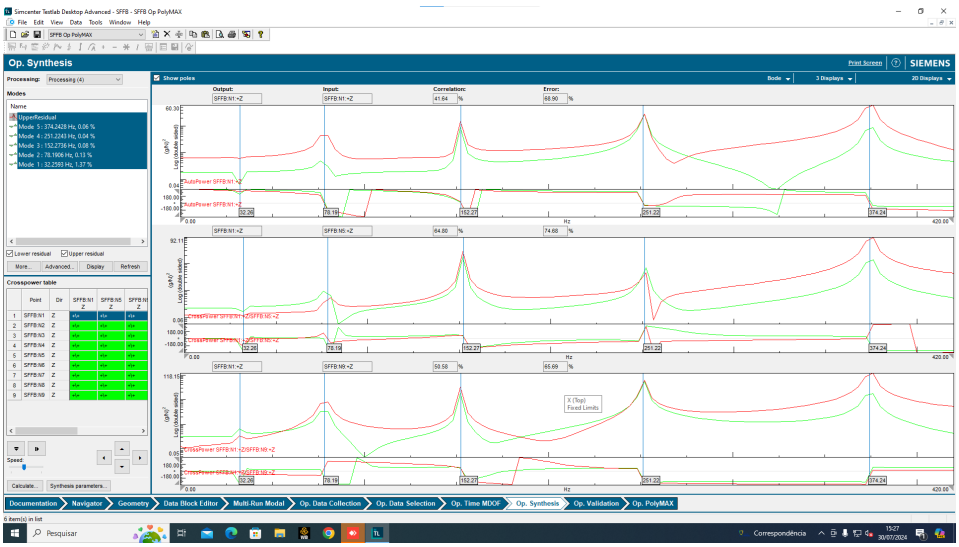

Figure D.18: Curve adjustment.

D.5 5. Data Validation

The final step is the validation of the modal parameters obtained. This can be done in the *Op. Validation* tab as seen in figure D.19. Here, the modes set will appear in the left-upper section of the window (inside the red rectangle in the image), the left-lower section will contain the options to perform an Auto-MAC with the data set obtained. The right part of the window can be adjusted to show the MAC table, MAC graph or display the mode shapes.

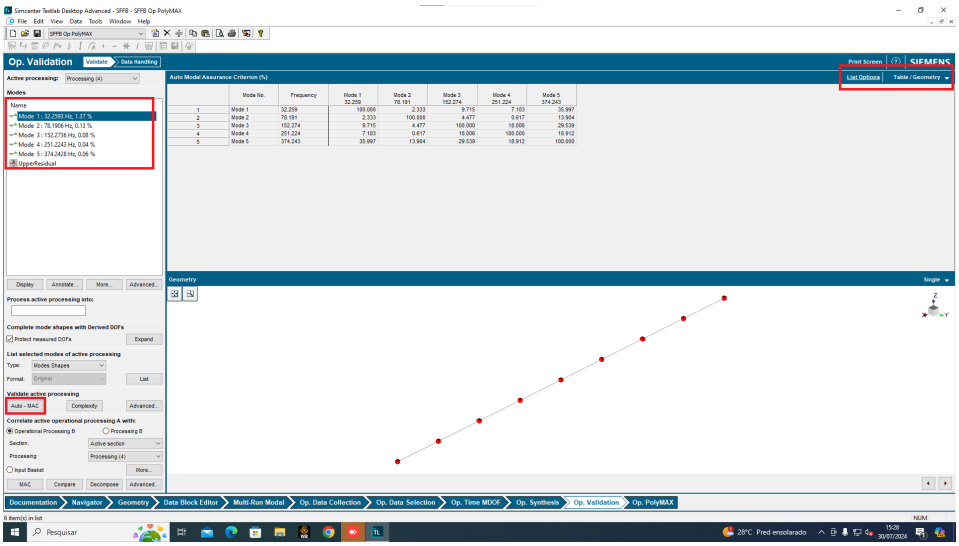

Figure D.19: OMA validation window.

Figure D.20 shows the MAC matrix created. The background colors and other customization options can be adjusted in this window.

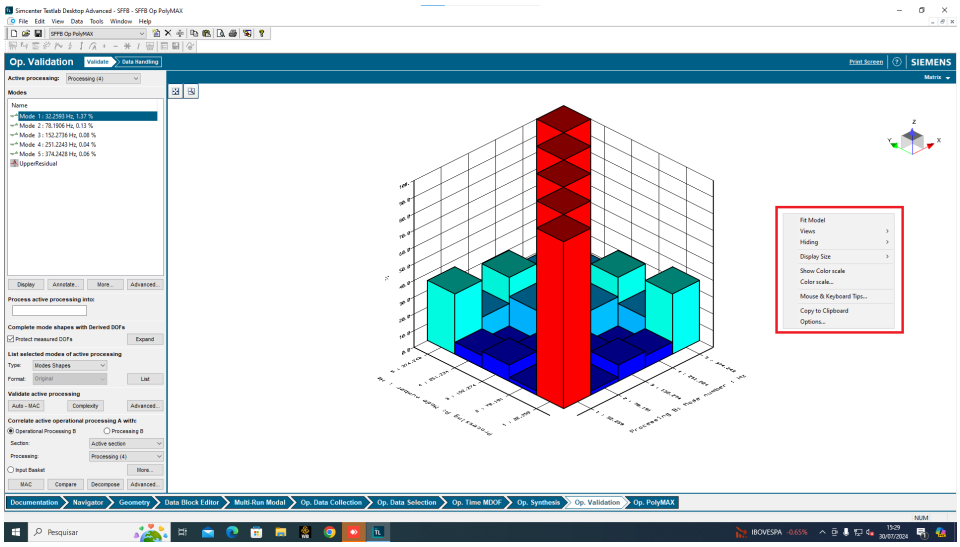

Figure D.20: OMA validation visualization options.

Figure D.21 shows a displayed mode shape. The values of the natural frequency and damping ratio can be seen in the left-lower section, which are always given in the format: Mode No: Natural frequency (Hz), Damping ratio (%) Processing Name. After verifying the MAC matrix and the mode shapes and other modal parameters, it is possible then to extract the results. The easiest form is to simply make a screenshot from which the results can be extracted.

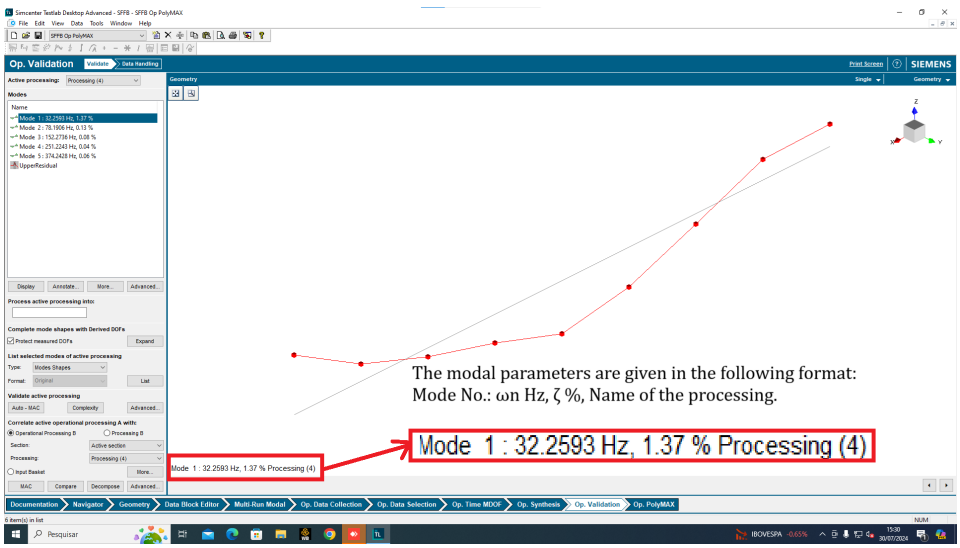

Figure D.21: OMA validation mode shapes display.

D.6 6. Operational PolyMAX

In addition to the conventional OMA, the Add-in Op. PolyMAX is also available in Simcenter Testlab 2306®. It is recommended to perform the PolyMAX after the conventional OMA. The methodology for the Op. PolyMAX is practically the same followed as for the conventional OMA, the only difference resides in the fact that while the conventional OMA uses the *Op. Time MDOF* tab, PolyMAX uses the *Op. PolyMAX* tab. In this tab, the procedure is very similar to the one followed in the *Op. Time MDOF* with the main difference being the selection of the residue type, as PolyMAX allows for real residues, as seen in figure D.22. This has some advantages and disadvantages when compared to the conventional OMA, therefore it is responsibility of the engineer performing the OMA to decide which methods is more suitable for the test. However, the recommended is to perform both to guarantee that the modal parameters obtained are reliable.

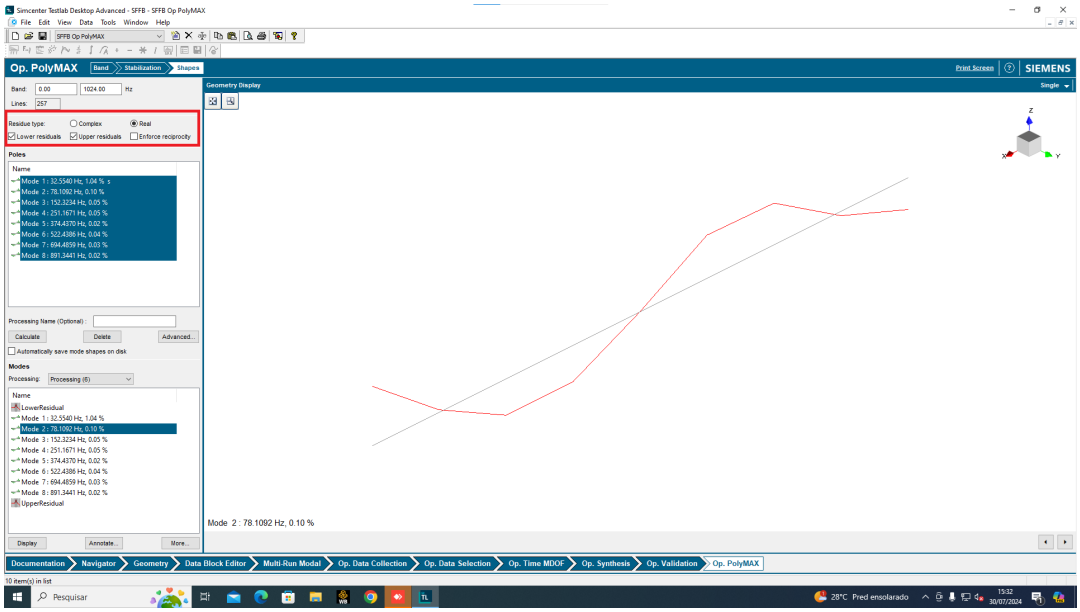

Figure D.22: Operational PolyMAX Analysis.

D.7 7. Cross-MAC

If a geometry is used for more than one test, or multiple processing were performed for the same data set, it is possible to perform a Cross-MAC between the mode shapes sets for each test as seen in figure D.23. To perform it, in the *Section* option the first mode shapes set must be selected (it is recommended for it to be the data set currently being used), and the second one can be chosen in the *Processing* option. With the mode shapes

set selected, select the *MAC* option and the MAC matrix will appear in the right side of the tab.

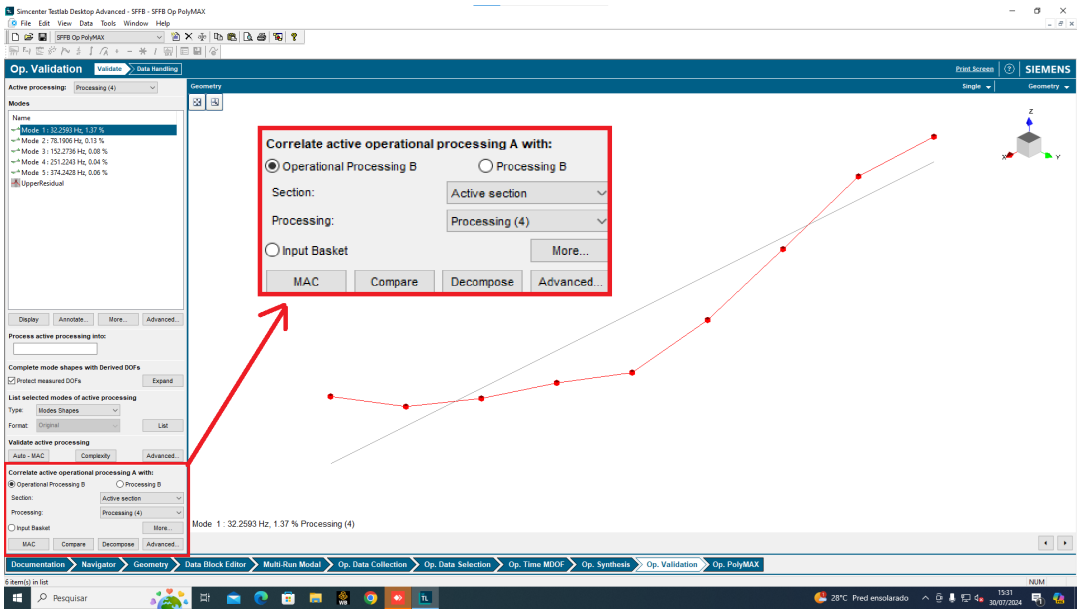

Figure D.23: Cross-MAC analysis.

APPENDIX E

APPENDIX E: COMPLETE SET OF MODE SHAPES

E.1 MATLAB® OoMA Toolbox - Mode Shapes

E.1.1 Impulse Simulations

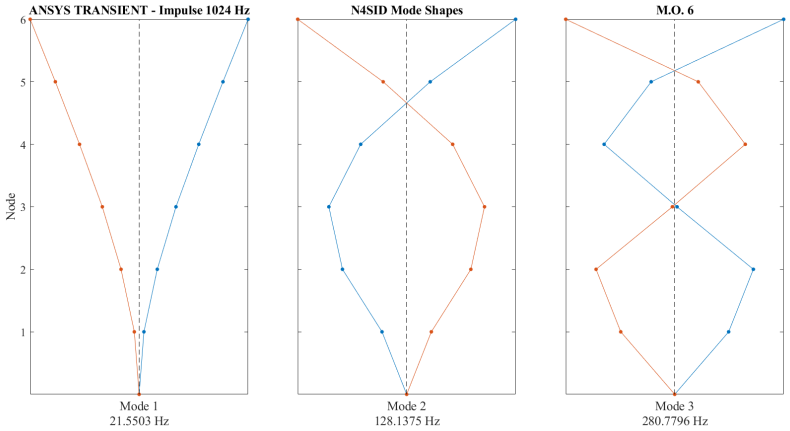

Figure E.1: Impulse Simulations 1024 Hz - Mode Shapes

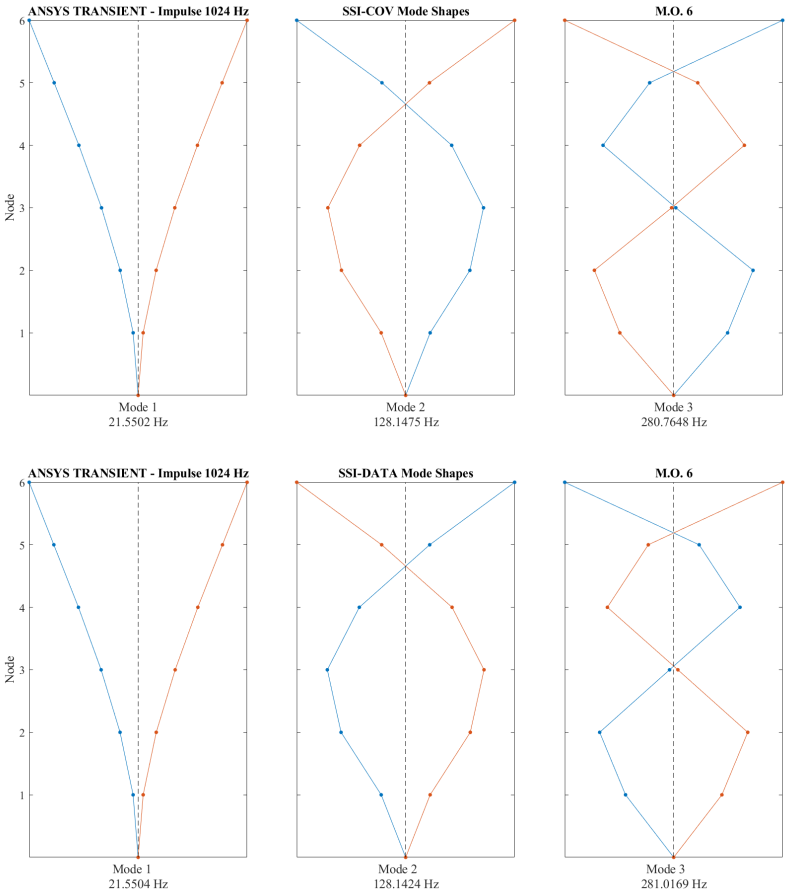

Figure E.1: Impulse Simulations 1024 Hz - Mode Shapes

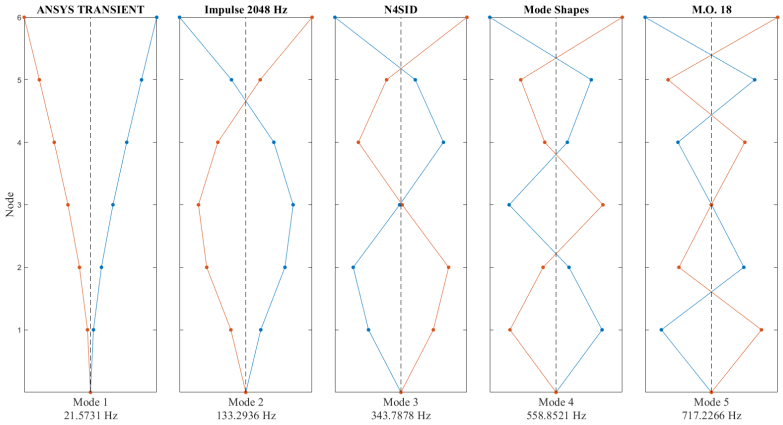

Figure E.2: Impulse Simulations 2048 Hz - Mode Shapes

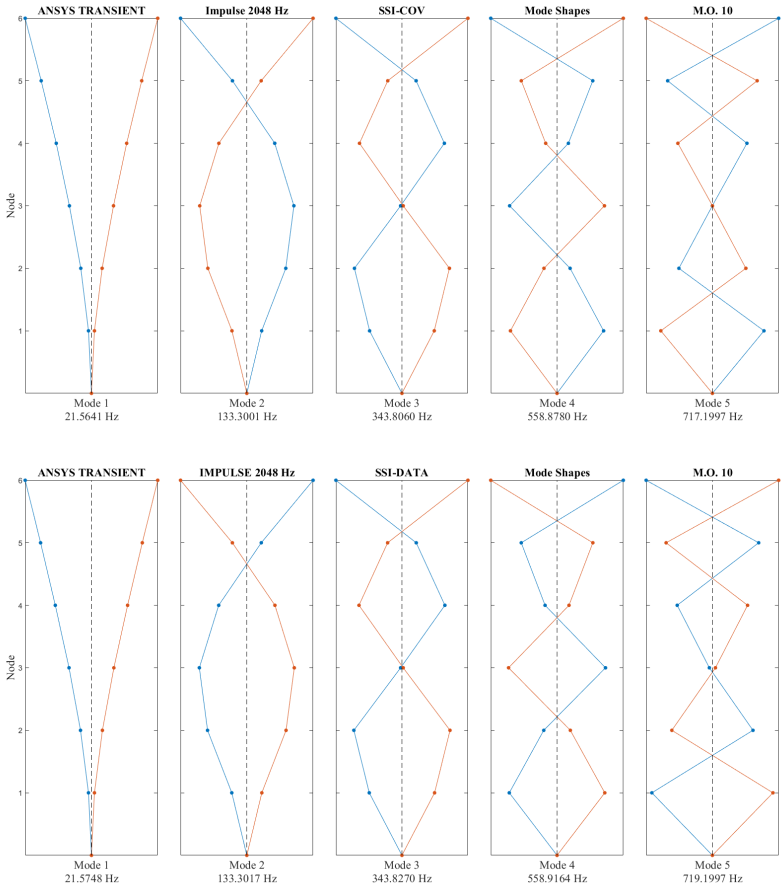

Figure E.2: Impulse Simulations 2048 Hz - Mode Shapes

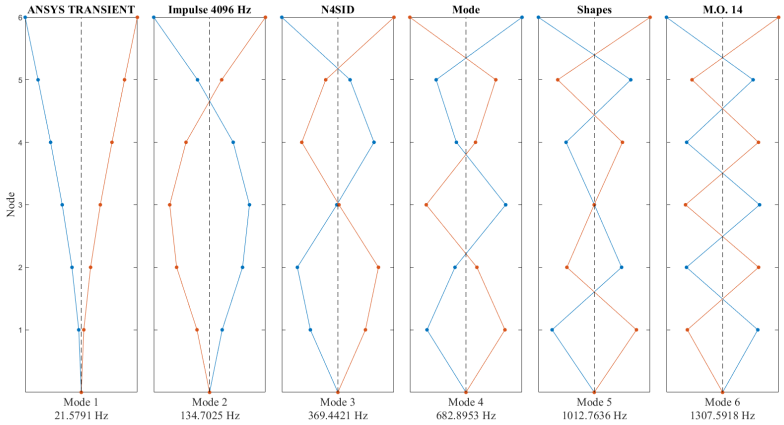

Figure E.3: Impulse Simulations 4096 Hz - Mode Shapes

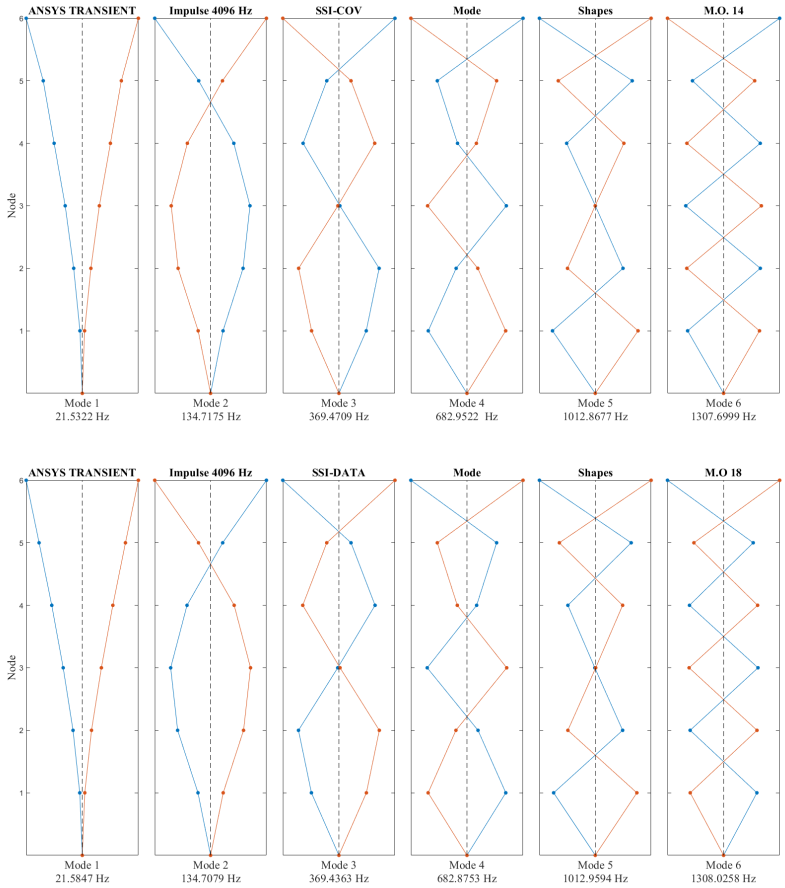

Figure E.3: Impulse Simulations 4096 Hz - Mode Shapes

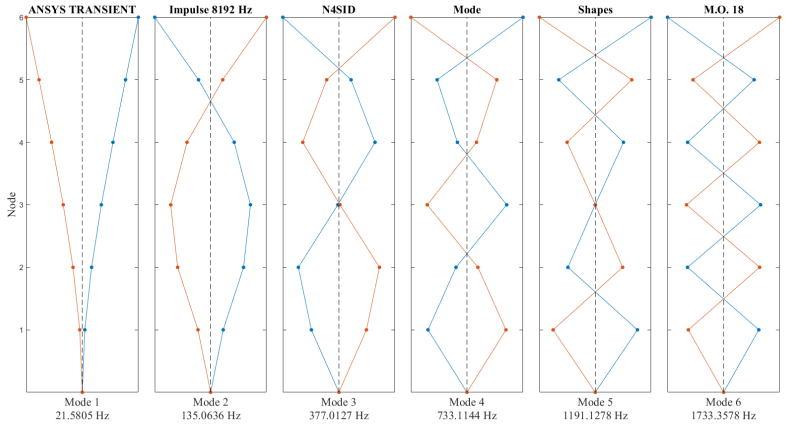

Figure E.4: Impulse Simulations 8192 Hz - Mode Shapes

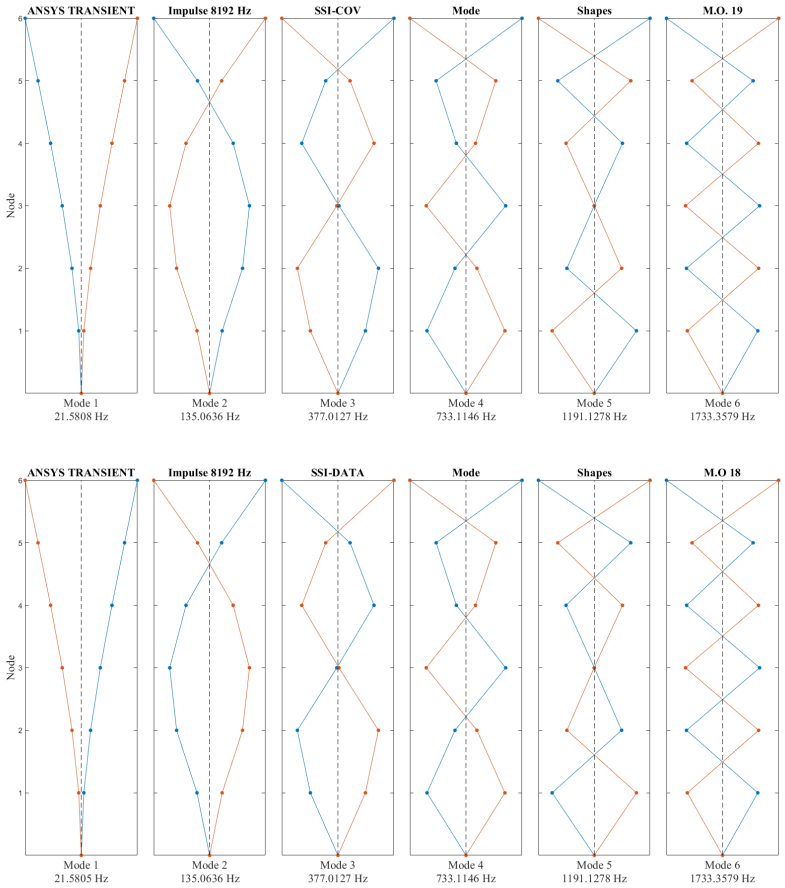

Figure E.4: Impulse Simulations 8192 Hz - Mode Shapes

E.1.2 White Noise Simulations

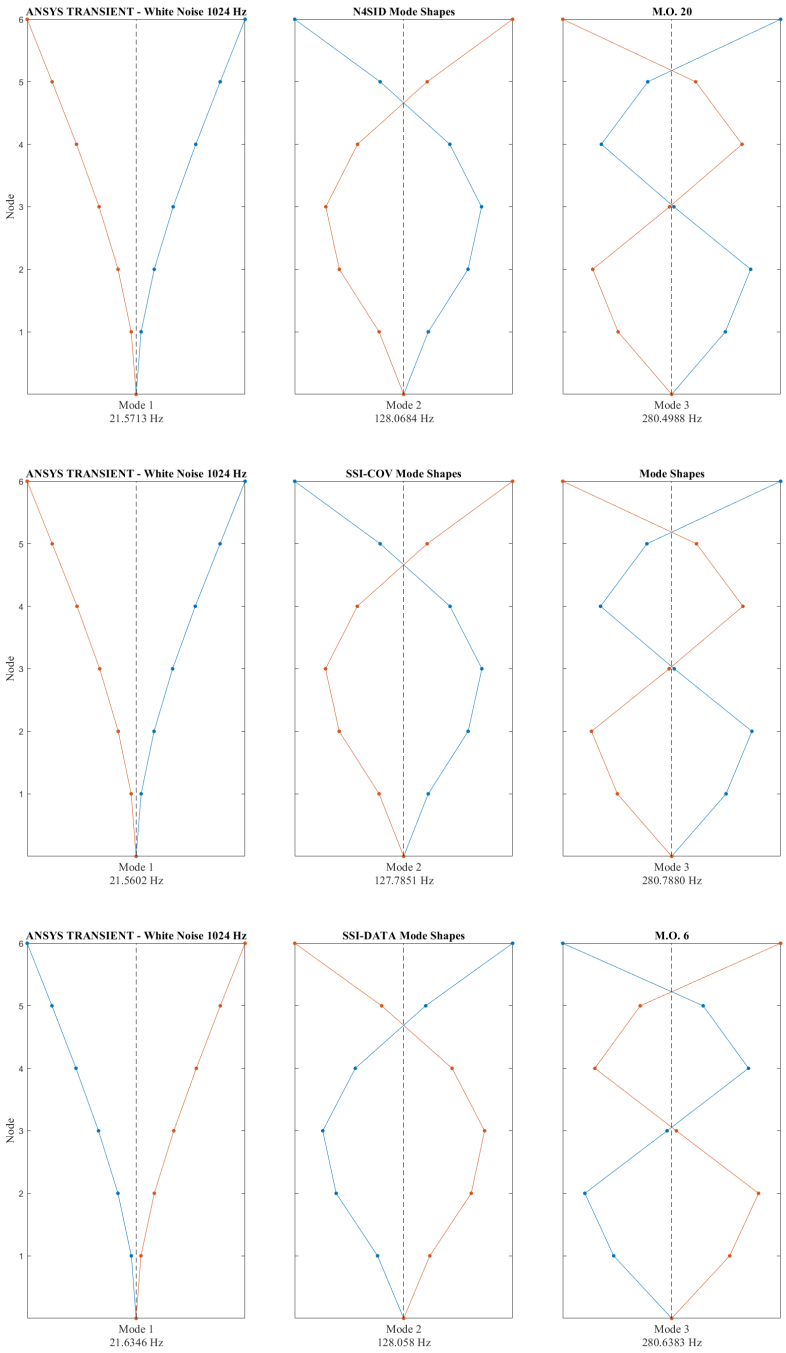

Figure E.5: White Noise 1024 Hz - Mode Shapes

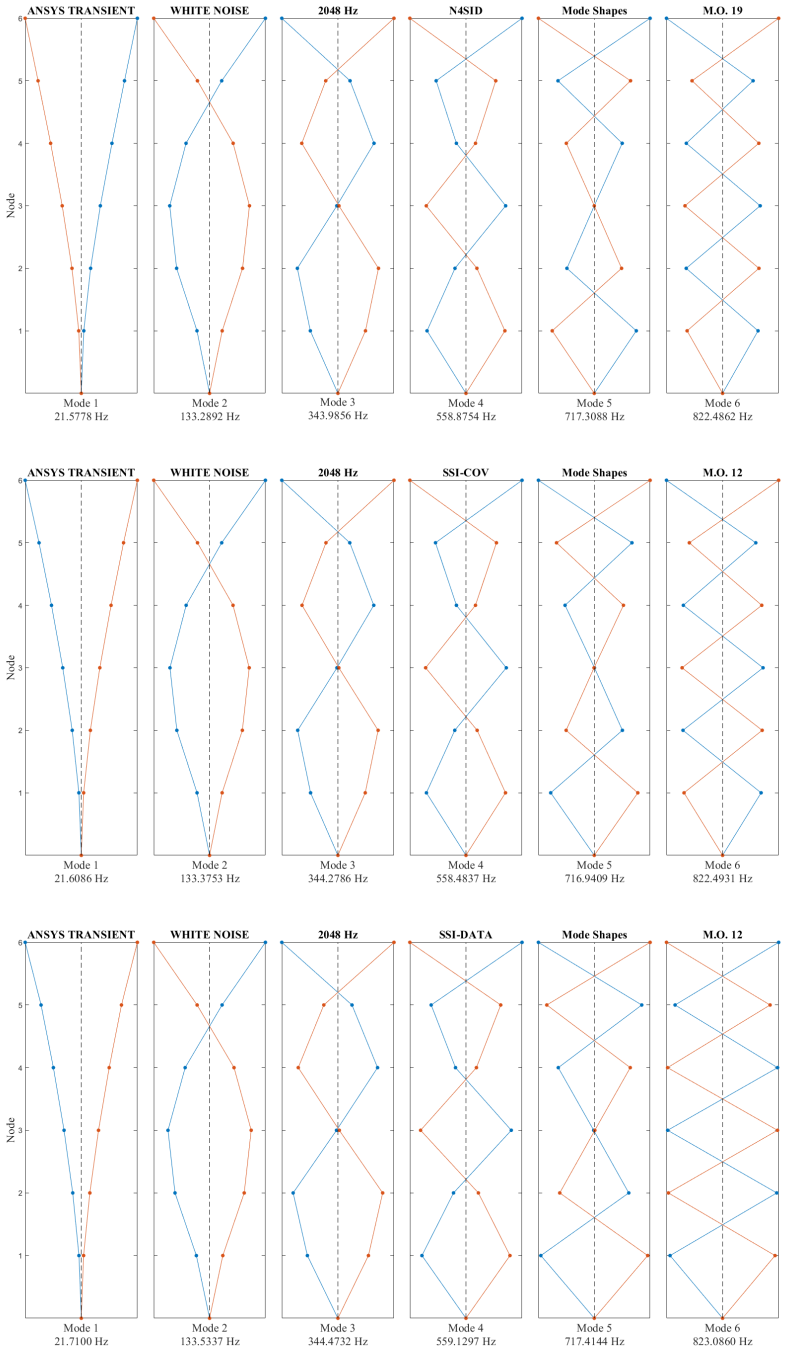

Figure E.6: White Noise 2048 Hz - Mode Shapes

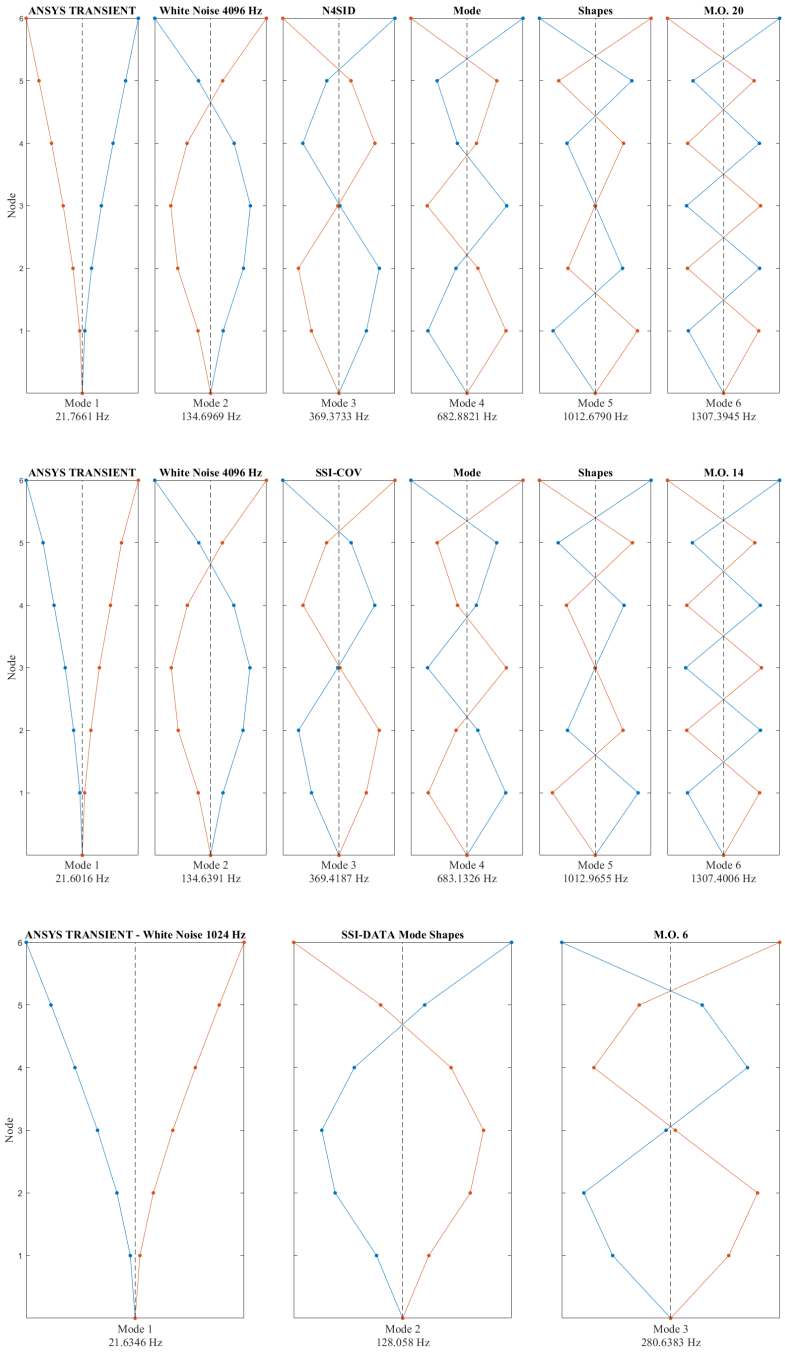

Figure E.7: White Noise 4096 Hz - Mode Shapes

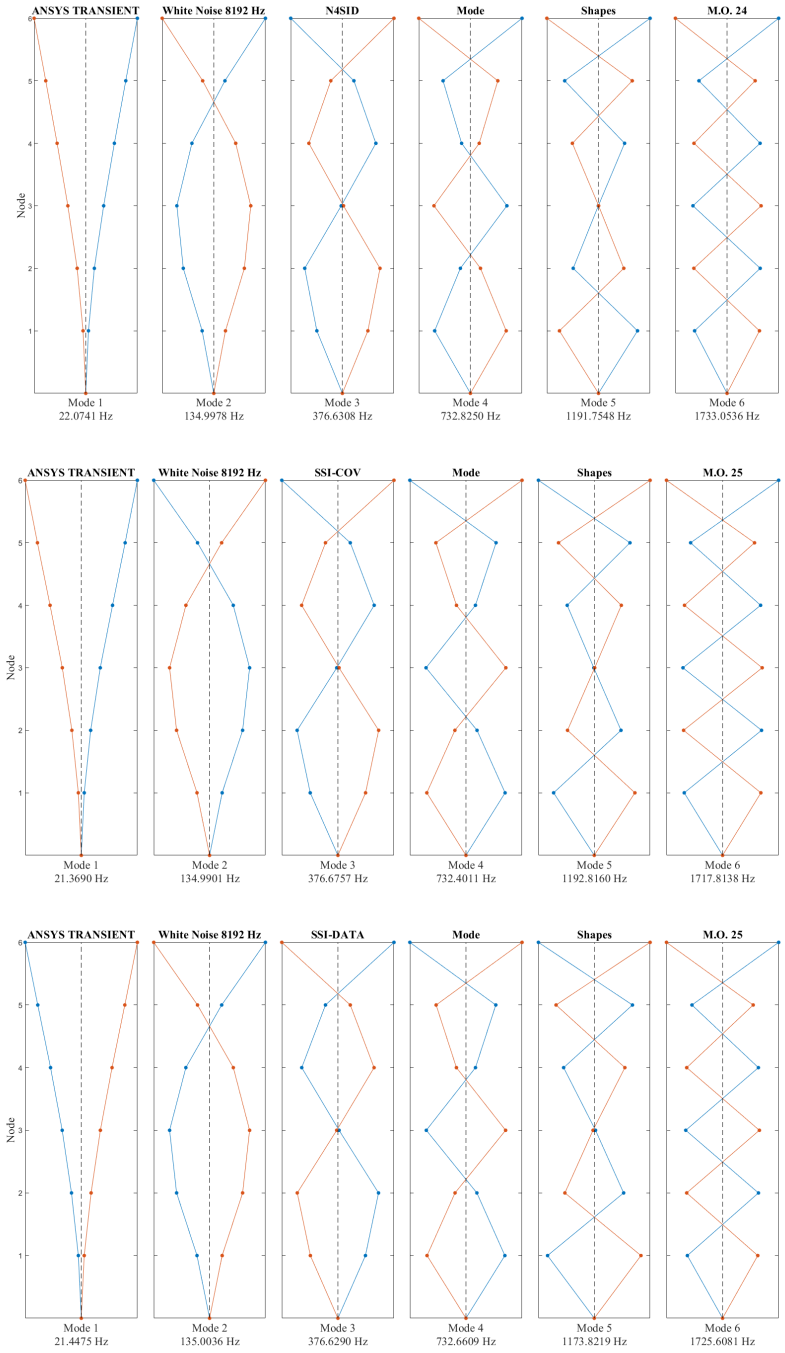

Figure E.8: White Noise 8192 Hz - Mode Shapes